# DIGITAL POSITION ERROR SIGNAL GENERATION IN MAGNETIC DISK DRIVES

Wong Wai Ee

NATIONAL UNIVERSITY OF SINGAPORE
2003

# DIGITAL POSITION ERROR SIGNAL GENERATION IN MAGNETIC DISK DRIVES

Wong Wai Ee

B. Eng. (Hons), NUS

*A THESIS SUBMITTED FOR*

*THE DEGREE OF MASTER OF ENGINEERING*

DEPARTMENT OF ELECTRICAL AND COMPUTER ENGINEERING

NATIONAL UNIVERSITY OF SINGAPORE

2003

# Acknowledgments

I would like to express my sincere appreciation for all those who have helped me through this Master thesis. Particular thanks go to my supervisor, Dr. Guo Guoxiao, for selflessly providing an open door and constructive criticism. His observations contributed a great deal to this research. I also wish to thank my other supervisors, Dr. A. Al Mamun and Mr. Ye Weichun. Dr. Mamun has been giving me opportunity to learn from him and his valuable suggestions, advises and comments. Without his help, I will not be able to complete the B.Eng Dissertation and continue on taking Master of Engineering. Mr. Ye has helped me a lot in collection of experimental data and guidance in the understanding of coding channel during my research work.

The experimental work in this thesis could not have been done without the collaboration with many people in the Data Storage Institute, Mechatronics and Micro-systems (MMS) Group. I am indebted to MMS, Senior Research Engineer, Mr. Zhang Jingliang and ex-Research Engineer, Mr. Hu Bo who had provided me much help in the implementation and experimental data collection. One of the Post Doctoral Fellow in DSI, Dr. Feng Lu has also given me much assistance in the controller design and implementation of reader servo control system on an existing spin stand for higher track density capability. Mr. Liu Jun, a Research Trainee Programme (RTP) student, has helped me a lot in converting my source code programmed under Window OS into Linux compatible format and installation of Linux OS system within a very short time frame.

I have enjoyed the time during research work at DSI, MMS group, getting to know many friends. I would like to thank my fellow graduate students who had provided support and companionship. Dr. Wu Daowei is always willing to help and give advises, especially on control practical issues when needed. Mr. Pang Chee Khiang has been a great friend who always accompanies me for lunch and tea break. Besides that, without his moral support and his teaching, I would not have been able to gain much knowledge of classical control during the study of servo engineering module and research work.

I would like to thank my husband and family for their love, support, encouragement and for their always being there to listen to me and offer advises. Without my newly-wedded husband, Chris Choy Min Chee's understanding, I would not have completed this Master thesis. Finally, I would like to dedicate this thesis to my dad, who has just passed away while I was about to finish writing this thesis.

# Abstract

Together with the extremely rapid progress of computer and information technology, the storage capacity of magnetic hard disk drives (HDDs) has been increasing tremendously at a rate of over 100% per year. Improvements in servo control algorithms, mechanical design and position error signal (PES) generation are essential to providing the continued improvement and high degree of accuracy critical for high data track density. PES, being the only output in HDD servo control system to indicate the displacement of the read/write head with respect to the track on the disk, must be accurately measured for HDDs to operate properly and reliably in any environment. Thus, the main focus of this thesis is to investigate PES generation techniques for ultra-high track density recording system with higher efficiency and accuracy.

An overview of the different PES encoding and decoding schemes is presented in this thesis. Presently, position information is encoded magnetically on the disk using 4 or 6 bursts of single-frequency amplitude servo patterns in most HDDs. To reduce servo overhead, frequency-encoded servo pattern which involves servo bursts of different frequencies written at adjacent tracks and same angular locations is studied. Digital detection techniques based on coherent detection (CD), Discrete Fourier Transform (DFT) and Fast Fourier Transform (FFT), are compared with the commonly used digital area detection technique with the addition of Finite Impulse Response (FIR) filters through simulation and experiments. DFT detection

of PES which is based on getting the fundamental frequency components of the servo pattern, is found to be less sensitive to synchronization error as compared to the single-frequency mixing signal coherent detection. In addition, it has higher noise immunity as compared to area detection.

A combination of frequency-encoded servo pattern and DFT-based decoding scheme is also implemented on the spin stand, using a separate PC-based system. PES is obtained and computed from the readback signal, which is digitized at 0.5 GS/s and DFT-based low PES computation time of less than 30 $\mu s$ has been attained. Together with the servo loop processing time, the computed PES is fed to the servo controller which updates the control output at 8.3 kHz for precise track following. Using the servo control on the spin stand, a high closed-loop servo bandwidth of 300 Hz and an improvement of 18.7% in reduction of disturbances have been achieved as compared to without servo control.

To achieve higher efficiency and accuracy of PES generation, a method of extracting the PES from the user data sector has been proposed and studied. Through the difference in frequency of the user data written at different tracks, the position of the head can also be estimated while reading the user data and the tracks can be squeezed closer together as the effect of inter-track interferences are reduced. Thus, this novel method will allow the increase of the position measurement rate, enabling the design of a higher bandwidth servo control system and higher TPI, in particular for embedded servo system.

# Contents

# List of Figures

# List of Tables

# List of Abbreviations

Unless otherwise specified, the following abbreviations are used throughout this dissertation.

| | |
|---|---|
| ADC | Analog-to-Digital Convertor |
| AWGN | Additive White Gaussian Noise |
| BAR | Bit Aspect Ratio |
| BPI | Bits Per Inch |
| CD | Coherent Detection |
| DAC | Digital-to-Analog Convertor |
| DFT | Discrete Fourier Transform |
| DSA | Dynamic Signal Analyser |
| DSP | Digital Signal Processing |
| ECC | Error Correction Code |
| FESP | Frequency-Encoded Servo Pattern |
| FFT | Fast Fourier Transform |
| FH | Flying Height |

| | |
|---|---|
| FIR | Finite Impulse Response |
| FPGA | Field Programmable Gate Array |
| FSR | Full Scale Range |
| GITOC | Group Inter-Track Orthogonal Coding |
| HDA | Head Disk Assembly |
| HDD | Hard Disk Drive |
| HDI | Head Disk Interface |
| HF | High Frequency |
| HGA | Head Gimbal Assembly |
| ID | Inner Diameter |
| IP | In Phase |
| ISI | Inter-Symbol Interference |
| LDV | Laser Doppler Vibrometer |
| LF | Low Frequency |
| LPF | Low Pass Filter |
| LTI | Linear Time-Invariant |
| LVPZT | Low Voltage Piezo Chip Translator |
| MLD | Maximum Likelihood Detector |
| MSE | Mean Square Error |
| NF | Notch Filter |
| NRRO | Non-Repeatable Run-Out |
| OD | Outer Diameter |
| OR | Orientation Ratio |

| | |
|---|---|
| OS | Operating System |
| OTC | Off-Track Capability |
| PC | Personal Computer |
| PD | Proportional-plus-Derivative |
| PES | Position Error Signal |
| PI | Proportional-plus-Integral |
| PID | Proportional-plus-Integral-plus-Derivative |
| PLL | Phase-Locked Loop |
| PMS | Patterned Media Storage |
| PRML | Partial Response Maximum Likelihood |
| PSN | Position Sensing Noise |
| PZT | Piezoelectric |
| QP | Quadrature Phase |
| RAMAC | Random Access Method of Accounting and Control |
| RPM | Revolutions Per Minute |
| RRO | Repeatable Run-Out |
| RTOS | Real Time Operating System |
| SNR | Signal-to-Noise Ratio |
| STW | Servo Track Writer |
| SSTW | Self-Servo Track Writer |
| TAA | Track Average Amplitude |
| TMR | Track Mis-Registration |
| TPI | Tracks Per Inch |
| VCM | Voice Coil Motor |

# List of Symbols

| | |
|---|---|
| $\alpha$ | Weighting factor |
| $A$ | Amplitude (V) |
| $AD$ | Area (Integral) of the servo pattern |
| $B_l$ | Bit length |
| $B_m$ | Bit interval of track $m$ |
| $C$ | Number of servo burst cycles |
| $D_F$ | DFT coefficient of frequency, $F$ |
| $DFT_{ave}$ | DFT-based position value of head position within the user data track |
| $\varepsilon$ | cross-track movement from original track center |
| E[ ] | Expected value |
| $f$ | frequency, Hz |
| $k^{th}$ | bin number in the defined window $T_w$ |
| $K$ | Number of detected dipulses |
| $K_d$ | Derivative gain |
| $K_i$ | Integral gain |

| | |
|---|---|
| $K_p$ | Proportional gain |
| $M_F$ | Amplitude of the servo signal of frequency, $F$ |
| $N$ | Number of sample points per cycle |
| $n(t)$ | Random noise signal with zero mean AWGN distribution |
| $O_{fs}$ | Offset with respect to the track center (1 unit equivalent to 1 track width) |
| $p$ | Physical width of the track |
| $PES_{ip}$ | In-phase portion of PES from quadrature servo pattern |
| $PES_{qu}$ | Quadrature phase portion of PES from quadrature servo pattern |
| $PES_{AREA}$ | PES formulation based on area detection technique and FESP |
| $PES_{CD}$ | PES formulation based on CD technique and FESP |
| $PES_{DFT}$ | PES formulation based on DFT algorithm and FESP |
| $PES_{TIME}$ | PES from time-based servo pattern |
| $p(t, T)$ | Dipulse response with transition period, $T$ |
| $r_N(\omega t)$ | Readback signal component from servo track, $N$ |
| $s(t)$ | Lorentzian model of the magnetic step response |

| | |
|---|---|
| $S(n)$ | Sampled servo signal |
| $t$ | Time |
| $T$ | Transition Period |
| $T_w$ | Period of the window |
| $v(\omega t)$ | Readback signal |
| $\omega$ | Frequency in radian/sec |
| $X_{ck}$ | Real coefficient of the spectral content |
| $X_{sk}$ | Imaginary coefficient of the spectral content |
| $\underline{X}_k$ | Spectral content of a signal |
| $Y_{ave}$ | Average DFT value of all the decoded data ($K$) within the window period ($T_w$) |

# Chapter 1

# Introduction

Magnetic Hard Disk Drives (HDDs) have been the primary means of storing information on computers since 1956 when IBM introduced Random Access Method of Accounting and Control (RAMAC), the first disk drive [44]. As opposed to semiconductor random access memory, magnetic disk drives provide long-term storage of information in the absence of electrical power, and thus providing a non-volatile storage. In this chapter, an overview of the HDD technology and the motivation for the research of PES generation techniques are presented.

## 1.1 Overview of Disk Drives Technology

HDDs have been widely used as data storage devices for computer systems. Among the various data storage devices, HDDs offer the best combination of capacity,

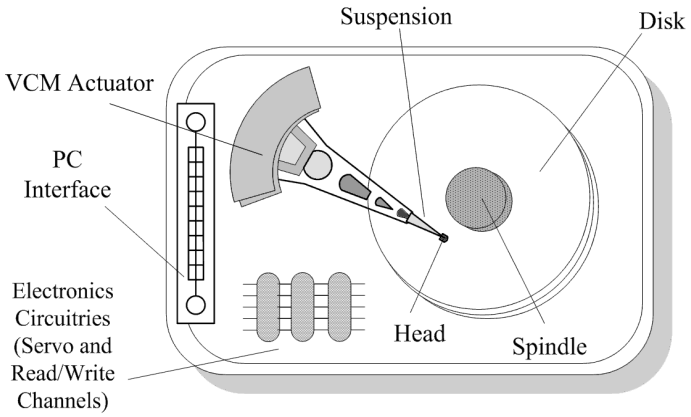


Figure 1.1: A typical hard disk drive.

speed and price to be the major storage device in a computer system. Figure 1.1 shows the general architecture of a hard disk drive. HDDs either consist of a single magnetic disk or a stack of magnetic disks, which rotate at a speed of about 3600 to 15000 RPM in most of the products today. Data are recorded on the disk using heads mounted on suspensions that are moved across the disk surfaces by a fast speed actuator. Information is recorded in circumferential tracks on the disk surfaces.

The major components in a disk drive include

1. Disks which allow the storage of data and servo information;
2. read/write heads assembly performing read or write actions on the disks;
3. Actuator assembly which contains a voice coil motor (VCM) to drive the heads;
4. Spindle motor assembly to rotate the disks at a constant speed;

5. Electronics circuitry to serve as the interface to the host computer, data read/write channel and servo controller etc;

6. Mechanical structure to provide support and cover for the spindle, actuator and electronics circuitry etc.

The first HDD (RAMAC) had only an areal density of 2 $kb/in^2$, a data rate of 70 $kb/s$ and stored 5 MB of information on fifty 24" disks [44]. From 1971 - 1991, the HDD areal density progressed at a rate of 27% per year. With the introduction of giant magnetoresistive (GMR) head and granular media technology, the areal density of HDD has been increasing at an amazing rate of more than 100% per year [61] [60] [72]. As in 2002, researchers from Read-Rite Corporation and MMC Technology have successfully demonstrated areal density of 130 $Gb/in^2$ at a track density of 213 kTPI on a spin stand platform with proprietary servo system [60]. In addition, the rotational speed of the disk is also getting higher, at above 15 k revolution per minute (RPM) [3] [12].

The primary measure of progress in hard disk drive technology has been areal density, as measured in data bits per square inch. Areal density depends on two factors, the linear density measured by the bits recorded per inch (BPI), and track density which is determined by the number of data tracks per inch (TPI). Magnetic properties, such as signal-to-noise ratio (SNR), disk coercivity and head disk interface (HDI), are improved in order to increase the bit density.

With the advancement in the technologies of media, head and signal process-

ing, the ability to fulfill the data access for higher recording density and faster data rate becomes the prerequisite for future HDDs. From the viewpoint of servo technology, precise positioning must be improved to increase track density.

In the studies of servo positioning system, position measurement provides essential information for servo loop to follow. This position information is typically encoded magnetically on the servo sectors in a hard disk drive and decoded by the head positioning servo system. To have a better understanding of how data can be read from or written on the magnetic disk, a brief discussion is given in the next section.

## 1.2 Digital Magnetic Recording Process

The basic elements of magnetic recording system are the electromagnetic read/write heads with a specially shaped ferrous core and a rotating disk with a ferromagnetic surface. To record data on the surface of a disk, current is passed through the electromagnet coils, thus generating a fringing magnetic field in only two orientations. The fringing magnetic field creates a remanent magnetization on the ferromagnetic surface, causing it to be permanently magnetized in either forward or reverse direction along the track for longitudinal recording.

Writing is the process of imparting the correct orientation of the magnetization in the magnetic medium to store the desired data. The inductive write head records bits of information by magnetizing tiny regions along concentric tracks.

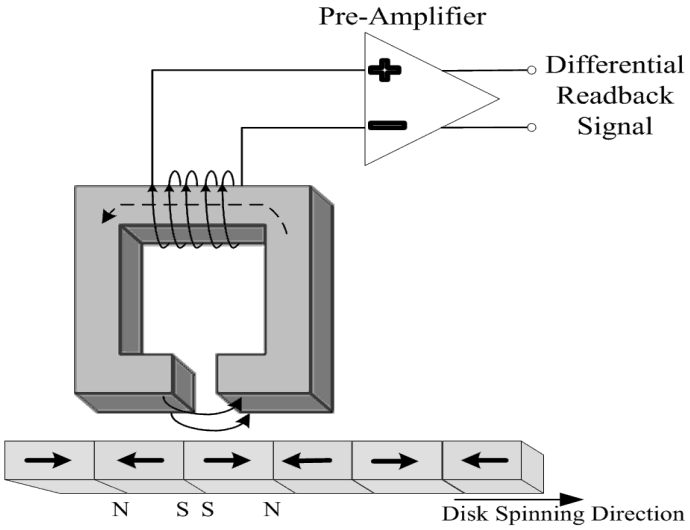


Figure 1.2: Conceptual diagram of read/write process.

The track is divided along its length into bit cells as illustrated in Figure 1.2. The bit cell boundaries are not laid physically along the track, but are determined by the timing of when the write head passes over a given location on the track. During reading, the presence of a magnetic transition or flux reversal between bits causes the magnetic orientation in the magnetoresistive (MR) or giant magnetoresistive (GMR) head sensor to change. This in turn, causes the change in the sensor's resistance. The sensor's output voltage or signal is the product of this resistance change and the read bias current [66]. This signal is amplified by low-noise electronics circuitry and sent to the HDD's data detection electronics for further processing.

To write a binary data 1 at a desired storage location, one may reverse the direction of the coil current at the time corresponding to the location of the bit cell center opposite the head gap. This current reversal writes the desired mag-

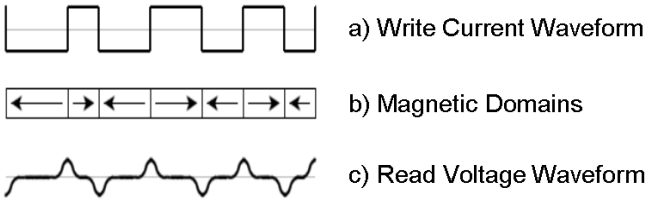


Figure 1.3: Illustrating waveforms of the read/write processes.

netization reversal at the correct location. In turn, no change in the direction of magnetization corresponds to a binary data 0. New information to be stored can be written directly over the old information. A simplified illustration of the writing process is shown in Figure 1.3. With the desired write current waveform in a), the magnetization pattern on the media will be as shown in b) and in turn, the readback signal will be similar to that illustrated in c).

The readback signal resembles that of lorentzian signal. Thus in this thesis, the periodic servo signal is modeled as lorentzian signal with additive white Gaussian noise (AWGN) for simulation [15].

At low density, peaks of the transition responses are clearly separated from one another, so it is possible to read recorded data in a simple manner by detecting these peaks. Thus the earliest data detection technique used is peak detection. However, as bits are packed more densely on the disk, it becomes harder to distinguish data from background noise or to detect separate peaks for individual transitions due to the possibility of inter-symbol interference (ISI). ISI results from the overlap of analog signal peaks streaming through the read head at increasing rates. This occurrence has traditionally been combated by encoding the data as a

stream of "symbols" as it is written, in order to separate the peaks during read operations. The problem has been that the encoding requires more than one symbol per bit, exerting a negative effect on both disk capacity and drive performance.

Thus more sophisticated detection methods are needed to resolve the issue of ISI as linear density increases. One of the the most widely used read channels is based on partial-response (PR) signalling with maximum-likelihood (ML) sequence detection, that is usually called PRML detection [62] [66]. The PRML is based on three assumptions:

1. The shape of read-back signal from an isolated transition is exactly known and determined.

2. The channel noise at the detector input is AWGN.

3. The superposition of signals from adjacent transitions is linear.

It is a method of detecting the recorded bits from the readback signal and making a determination as to the correctness of these bits. Instead of using data intense encoding to ensure accuracy, PRML compares the samples of the partial response equalized readback signal to what are "likely" using a complex trellis of possible data sequences such as Viterbi detector. The use of this "maximum likelihood" approach together with "partial response" minimizes the probability of errors in detection. This in turn allows data to be packed tighter together. The block diagram of a typical PRML system is shown in Figure 1.4.

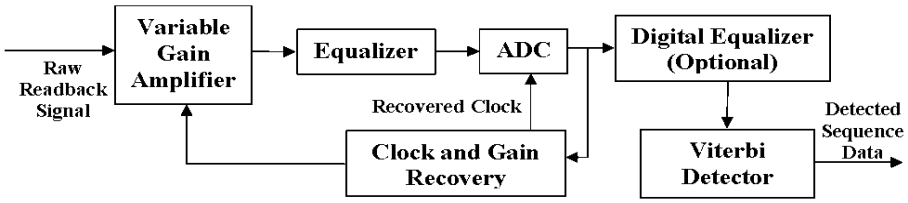


Figure 1.4: Block diagram of typical PRML system.

Besides the many variations of the PRML channel, the decision feedback equalizer (DFE) [66], a well established data detection technique in communication channels subject to ISI, has also attracted attention in the magnetic recording community. Since the focus of the thesis is on the position information detection, next, we will introduce the HDD servo system.

## 1.3 Disk Drive Servo System

The servo technology is one of the key technologies that support the disk drive industry, especially in the track recording density. It provides a means for moving a set of read/write heads in fixed radial locations over the disk surface and maintaining the heads over the center of the track from one radial location to another.

A simple conceptual block diagram of the components of a HDD servo control system is shown in Figure 1.5. The system includes the actuator, driver, PES demodulator, analog-to-digital convertor (ADC), digital-to-analog convertor (DAC) and position control subsystems. In the servo positioning system, position

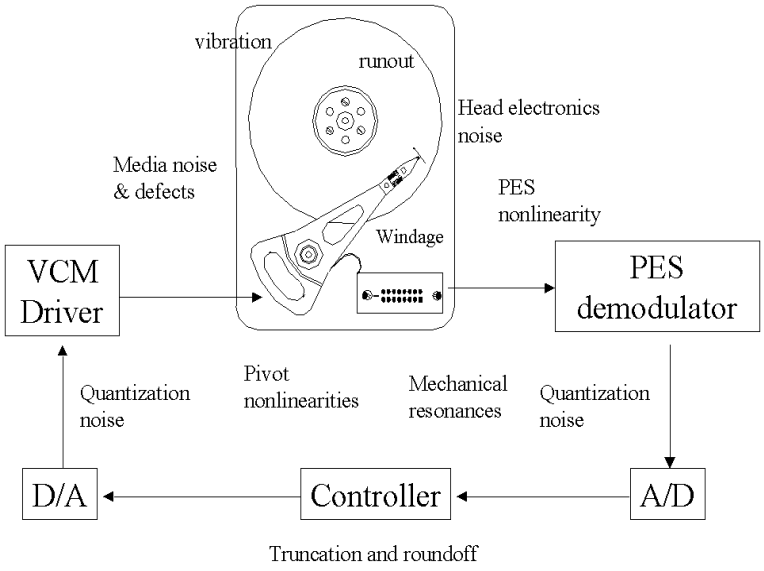


Figure 1.5: HDD servo system with external disturbances and noises.

measurement provides essential information for servo loop to follow. This position information is typically encoded magnetically on the servo sectors in a HDD and decoded by the head positioning servo system. The decoded signal, known as position error signal (PES), is proportional to the relative distance between the center of the read head and the nearest track center [57]. This PES is fed into the controller which has several modes of switching control algorithms.

The output of the servo controller is converted back to analog format via the DAC and sent to the power amplifier, which converts the desired voltage into current source, driving the actuator to set the position of read/write head.

Basically, there are two primary control objectives for the servo system:

1. Firstly, it is to move the read/write head from the current track to a target track in the shortest possible time. This process is generally referred to as seeking control.

2. The other is the track following control, which is used to maintain the head on the destination track with minimum error after seeking.

3. Since track seeking and following have completely different objectives, control switching or mode switching is essential. To facilitate a smooth switch between the two modes, an additional settling mode between seeking and following is designed to facilitate for fast settling and precise positioning.

The average seek time, defined as the time to move across 1/3 of the recorded data band and settle on a given track, is typically less than 10 ms in current high performance HDDs. The nature of the seeking servo is to force the actuator angular velocity to follow an ideal angular velocity profile that will guarantee the shortest possible seek time with minimum jerk such that the recording head arrives at the desired track at a very small angular velocity. The actuator's angular velocity is digitally estimated by an algorithm in the microprocessor that uses position error information obtained from each servo sector during the seek process. The seek mode is usually implemented as a proportional-derivative (PD) type of control with a constant monitoring of the remaining distance to the target track to minimize any unnecessary excitation of mechanical resonances in the disk drive which will

cause a mechanical ringing problem during the track following portion of the servo operation [50].

When the actuator is less than one track pitch away from the target track, the settling mode takes over from the seek mode. At this point, the settling control should guide the center of the recording head to be within a certain position error tolerance of the target track center line for a faster track following switching [70].

In the track following mode, the servo objective is to stay as close to the track center line as possible for reading and writing information. The main difficulty in this mode is caused by the various position error sources existing in the servo channel. The track mis-registration (TMR) in the case for servo, is used to measure the offset between the actual head position and the track center. The TMR during the track following mode, which is defined as three times the standard deviation ($3\sigma$) of PES, is required to be less than $10\% \sim 15\%$ of the track to track pitch in normal operation [66].

## 1.4 Motivations

Challenges arise in the designing of servo systems for high-density tracks. Data is recorded in ever-narrow tracks that must be followed with extreme precision. However, accurate positioning of the read/write heads and reducing the allowable tolerance of TMR involve an astounding feat of technology.

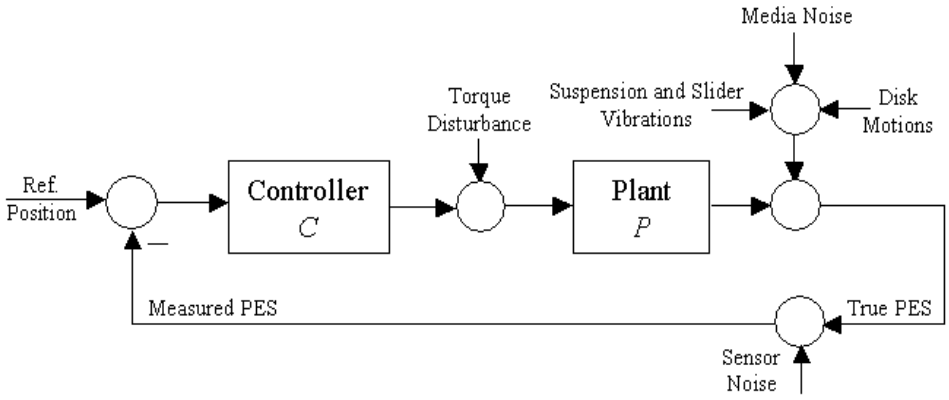


Figure 1.6: Servo block diagram with noise input sources.

As shown in Figure 1.6, the reference position is the centre of the magnetic track written on a rotating disk that the read/write heads must follow precisely within the TMR budget. The servo signal, which contains the relative position information of the head with respect to the track, is sensed by the read head and transmitted to the demodulator to process the PES. However, there are many types of disturbances and noises that cause uncertainty in the true PES. First of all, there are noises associated with the moving disk and the readback process as illustrated in Figure 1.6. These disturbances, also known as run-out errors, enter the servo loop at the same point, but with different root causes. There are two major sources of track following errors, namely repeatable run-out (RRO) and non-repeatable run-out (NRRO) errors. RRO errors are due to the motion of the disk attached to the spindle motor and typically at orders of the spindle rotational frequency. NRRO errors can be perceived as coming from other sources, like vibration

shocks, mechanical disturbances, and electrical noises which are usually random and unpredictable in nature. These include noises due to quantization in the ADC and DAC, noise from the power amplifier and windage noise. Windage noise is caused by the airflow generated as the disk spins where the air flows everywhere around the actuator arms and the magnetic head, disturbing the head position. The noise source that enters the true PES is the noise from the readback process of position information, called Position Sensing Noise (PSN). This noise can be due to the magnetic domains on the disk, the behavior of the magnetic head, the interaction of these two, or the action of the demodulator.

Therefore, among all the TMR sources, the on-track, self-introduced NRRO imposes fundamental limitations on the viability of very high TPI drives. If a drive cannot meet its TMR constraints in on-track mode and in the absence of external disturbances, certainly it will not meet them under more adverse conditions.

In summary, the on-track, self-induced TMR is mainly caused by the following noise sources in the servo channels:

1. Quantization noise of A/D converter;
2. Quantization noise of D/A converter;
3. Windage due to air-turbulence while spindle spinning;
4. Preamplifier noise;
5. Non-repeatable motions of the disk;

6. Position sensing noise;

7. Structural vibration.

Given all these potential noise sources, it is important to identify which of these are the most significant contributors to PES. With this information, the effort to improve the servo system can be focused on the more important aspects [4]. Using PES Pareto method [5][6][7], one can identify several key contributors to uncertainty in the PES of a magnetic disk drive servo system. It is found that there are apparently two main sources of baseline noise in PES. The first is windage noise, which is the turbulent wind flow generated by the spinning disks. The second major contributor is the Position Sensing Noise (PSN). Thus two distinct efforts will help to reduce the baseline power spectrum density in PES. The first effort is to study the wind flow within a disk drive to find ways to minimize the level of windage noise, which is a non-trivial task involving the study of turbulent air flows [71]. The second effort is to find ways to minimize the PSN, which can be accomplished via improving either the readback process or the demodulation process.

As stated in [28], the TPI is related to the PSN and the measured PES is the only reference input to the servo control system to indicate the current head position. Thus, the quality of position sensing is also of fundamental importance in high precision servo control systems [19].

- Firstly, the position information determines the allowable off-track limits for

read and write operations. These limits determine both performance and reliability for drive operation. Erroneous information on the actual head position can either lead to data corruption or the setting of conservative off-track capability (OTC) limit which will compromise the areal density.

- Secondly, off-track gain variations affect gain or phase margins of the servo system and error rejection characteristics. Variations in position information gain also affect settling transients following a seek command, leading to long settling times from undershooting or overshooting the target location.

- Latest collected data and theoretical models indicate that it is advantageous to have a squarer bit cell at higher densities [36][37]. It is estimated that the bit aspect ratio (BAR) will approach one-to-one in the upcoming years. Since fewer grains will be available for storing each bit, it will result in a decrease in the raw SNR and in turn a challenge for servo and data channels to operate reliably. With the increase in track density, track width is getting narrower. This leads to a lower error tolerance in the positioning of the head, higher sensitivity to media noise and inter-track interference. Advanced and efficient head positioning servo technology is needed for improved tracking capability and precise positioning to support the advancement of HDD capacities.

- Particularly for an embedded servo HDD format, the servo information is pre-written in equally spaced sectors on the disk and usually takes up about 10% of the usable magnetic recording area on a disk surface. If the amount of space reserved for the special spatial pattern (known as servo bursts) used

for servo detection can be reduced while the off-track performance does not deteriorate, an increase in the areal density or speed of retrieving data stored can be achieved.

- In addition, in recent years, the trend has been shifting from analog to digital processing of PES where it has several advantages over analog implementation [1]. Furthermore, with the same level of digital hardware currently used, real-time digital PES generation system can be incorporated together with the same hardware easily and enables reduction in the manufacturing cost.

- TMR in track following mode can be vastly reduced by designing higher servo bandwidth. However, as in embedded servo system, servo information is obtained only at regular intervals. Thus, the PES sampling rate is limited by the number of sectors available and spindle rotation speed. As a result, multi-rate control techniques have been intensively researched and applied to improve the performance of servo systems. However, more efforts are still needed to explore for practical engineering applications. Based on this observation, this thesis explores another methodology in which PES sampling rate can be increased without deteriorating the performance of spindle motor or reducing user data storage capacity.

In summary, lower PSN can help to achieve the required TMR budget. The study of PES encoding and decoding processes aims to eliminate a key contributor to uncertainty in the PES and improves the accuracy of servo control. Hence, advanced servo pattern and digital position generation techniques will be investigated

and compared in this thesis, which is the main focus of the research work.

## 1.5 Contributions and Thesis Overview

Given the importance of improving the quality of PES in future storage devices, this thesis studies the different position encoding and decoding schemes to achieve precise positioning information for servo control in systems with ultra-high track density. A combined frequency-encoded and digital demodulation scheme is proposed to replace the existing servo technology and it allows a reduction of servo overhead, increases efficiency and accuracy. The proposed scheme is also implemented and used as the feedback signal for real-time servo control on a spin stand for demonstration of higher TPI capabilities. A new track mis-registration detection strategy through estimation of head position from frequency-encoded user data, is also proposed to increase measurement accuracy and PES sampling rate, particularly for embedded servo systems.

The rest of the dissertation is organized as follows:

- Chapter 2 contains a wealth of information about position error signal generation techniques. It discusses position signal generation, different types of servo bursts patterns and detection techniques.

- Chapter 3 covers the simulations and experiments of frequency-encoded servo patterns and digital PES demodulation methods.

- Chapter 4 presents the modification and digital implementation of a real-time reader servo control together with the frequency-encoded servo pattern (FESP) and PES decoding scheme on a commercial spin stand to achieve better performance as compared to the existing servo.

- Chapter 5 outlines the methodology and testing results of the approach which enables position information to be determined while the head is reading the user data for an embedded servo system.

- Chapter 6 provides a summary of the work covered in the dissertation and proposes some new directions for future work.

# Chapter 2

# Servo Burst Patterns and Detection Techniques

Position error signal generation for magnetic disk drives has been an important component of servo-mechanism. This chapter surveys the servo patterns and the different digital demodulation methods including (1) digital area detection, (2) DFT-based detection and (3) coherent detection, particularly for the popular amplitude servo bursts pattern of single frequency.

## 2.1 Position Error Signal Generation Requirements

The motivation of this thesis is to determine an efficient way of encoding and decoding the position estimate of the head with respect to the disk. Some of the issues which affect the choice of the position error signal generation technique used, will be discussed.

### 2.1.1 Linearity

Ideally, the position error signal is a linear function of the cross-track position on the HDD. The tracking controller input is expected to be an estimate within a proportionality constant of the cross-track position. However, in practice, none of the PES generation techniques can produce a truly linear cross-track signal. This is due to the non-linear response of the MR head and the difference in the widths of the read and write elements. The use of wider write head together with narrower read head is known as "write wide read narrow" scheme, which is commonly employed, particularly in the disk drives utilizing inductive write/MR read dual-element magnetic recording heads, to reduce the negative impact of track mis-registration (TMR). In general, the width of the read head is about 60% to 70% of the width of the write element [10] [57].

A linear signal is not that important if the shape of the cross-track PES

remains the same and is invertible. Position estimate will not be affected as long as the dynamic range of the signal is enough to overcome the noise present in the system. In addition, the controller can keep track of approximately where the head is and invert the position signal to obtain the position estimate reliably. PES non-linearity can also be compensated by a self-adjusting adaptive method [21] in which a non-linear state estimator is used to match the non-linear PES. Furthermore, for coarse positioning in track seeking mode, moderate non-linearities in the cross-track PES can be tolerable. Although linearity provides simplicity to the control system design, it is not a stringent condition of a PES generation technique.

### 2.1.2 Repeatability and Consistency

It is important that the PES is repeatable and consistent from track center to track center, so that the position of the head can be determined accurately at each track. When the PES is not repeatable at the same track, then even multiple passes over the same portion of the disk by the head will be unreliable in its position estimate. If the cross-track PES shape is different in every track, it will be almost impossible for the tracking controller to precisely follow each of the track centers.

There are several factors which will influence the repeatability and consistency of the PES with respect to track center. One of the factors is the ability to write identical magnetic transitions pattern on the media, so that the resulting cross-track PES will be the same at every track. However, in reality, magnetic transitions have their own transition noise sources. These include peak jitters and amplitude

fluctuation of the individual pulses. Furthermore, the flying height (FH) of the read/write heads will also affect the magnetized signal strength. Constant FH is needed to achieve the same average magnetized signal strength throughout the reading and writing processes.

### 2.1.3 Rejection of Noise

The ability to reject noise is one of the main factors to consider for the PES demodulation technique. Better noise immunity and insensitivity to surface defects are important as SNR is getting lower and lower for higher track density recording.

### 2.1.4 Demodulation Time Delay

In addition, the delay time or computation time taken for the position measurement is one of the criteria for the selection of the demodulation technique. The data rate and the data access rate increase with the spindle speed. With the latest HDD spinning at more than 10 kRPM, servo control needs to have a bandwidth of above 2 kHz, to suppress the increased vibration and disturbances. Such a high bandwidth servo system requires PES sampling frequency to be at least about 15 kHz to 30 kHz. Thus it is crucial that PES can be computed within a smaller fraction of the sampling period so that the servo performance will not be degraded by the delay [23][67].

### 2.1.5 Servo Overhead

Another factor to consider is the servo overhead which refers to the amount of disk space taken up by the servo patterns and support bits, such as synchronization burst for automatic gain adjustment, Gray codes for track number, and fields to identify the type of tracks. Conventionally, about 10% or less of the disk surface is used for all these position information. Thus the ability to reduce the amount of disk space required without deteriorating the performance of position measurement is important.

### 2.1.6 Servo Writing or Encoding Time Requirements

With the increase in TPI, the amount of time it takes to write or encode the servo information on the increased number of tracks increases. More servo track writers (STW) are needed to meet the production demand. At the same time, the servo writing process needs to be improved to greatly reduce TMR. Thus there is a strong requirement for STWs which are of low cost and able to write quickly and efficiently.

There are different types of designs for placement of servo information on the magnetic disk. In next section, three major servo information layouts are discussed, namely, dedicated servo, embedded servo and buried servo. Focus will be on PES generation under embedded servo format, which is typically used in modern HDDs.

## 2.2 Placement of Position Information

In order to realize an ultra-high TPI, it is necessary to reduce track mis-registration by reducing the amount of position errors and improving the accuracy of writing position information on the disk media. Currently, the servo information is written on the disk by flying the head across the entire disk surface using servo track writers (STWs), self-servo track writer (SSTW) or by encoding servo information through patterned media [39]. The PES can be encoded using dedicated servo, embedded sector servo and buried servo techniques as shown in Figure 2.1. A brief review will be given next.

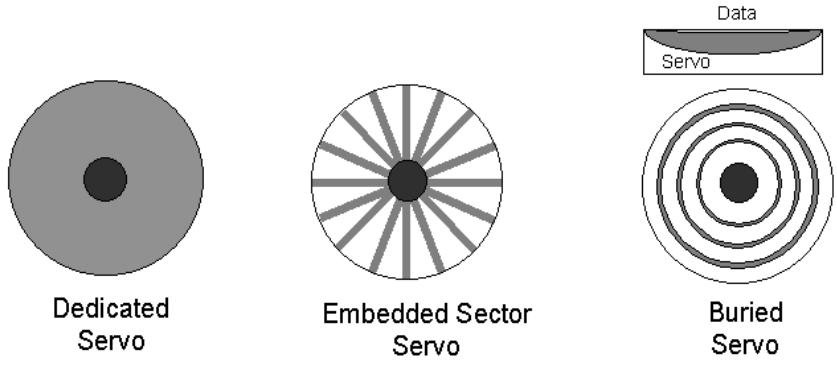


Figure 2.1: Dedicated, embedded sector and buried servo formats.

### 2.2.1 Dedicated Servo Layout

Dedicated servo is one of the earliest method to place servo information, whereby an entire surface of one disk in the disk stack is dedicated for placement of position information. The surface used for servo patterns cannot be used to store data. The

advantage of this technique is that the servo patterns are continuous around an entire revolution of the disk and so an analog, continuous-time servo system can be designed that avoids the sample rate and bandwidth limitations of any digitally sampled system.

Dedicated servo works well for systems where the amount of disk-space required to write servo information is comparable to or less than the amount of space taken up by the method of embedded sector servo, and extremely accurate positioning is not required. However, the performance will deteriorate due to thermal expansion and random vibration of the disk and head. In addition, it may also be inefficient if the number of disks in the disk stack is small. In modern HDD systems with only one to four disk platters, it is rare to find dedicated servo in actual use.

### 2.2.2 Buried Servo Layout

In buried servo, low frequency servo information is written on the magnetic media while high frequency user data are written on top of this servo information. The low frequency servo data penetrates further into the medium than the user data signal magnetization so that positioning information remains continuously available [57].

The major problem with buried servo is that it requires a thick media, or a magnetic under layer, to support the servo data of lower frequency. This constrains the optimization of media to achieve higher areal density since the media thickness

needs to be continually decreased to achieve higher linear density. In addition, the combination of low frequency servo signal with high frequency user data signal creates additional difficulty in separating both the signals. As a result, buried servo has never been used in any commercial HDD.

### 2.2.3 Embedded Servo Layout

Another method is the embedded servo or sector servo technique which would be the focus in this thesis. The servo data is recorded at regular intervals on each track forming radial sectors. The number of servo sectors will be the number of PES samples per revolution of the disk. Sector servo can avoid the thermal track shift present in a dedicated-servo system. It overcomes the limitations of dedicated servos by generating the servo information with special spatial servo data patterns recorded on each of the track sector [47]. Coarse position information can be obtained by reading the Gray-coded track addresses, whereas fine position information can be obtained from a series of spatial servo data patterns. For sector servo pattern, the same head is used for reading the servo pattern and the user data. The disadvantage of this method is that since the head has been designed to read back user data, it may not be optimized for PES generation.

### 2.2.4 Patterned Media Storage

Currently, areal density is achieved partly by reducing the grain size in the current granular magnetic media. However, beyond a certain limit, the grains will become so small as to become "superparamagnetic" [38][39]. Patterned media storage (PMS), in which a single bit of data is stored under a single patterned magnetic domain, has been proposed as an approach to break the barriers faced by conventional thin film media technology.

The advantages of PMS, in addition to the patterned bits, are that servo information can also be included in the patterned media, which allows advanced servo pattern to be easily created. In addition, the effect of track edge noise can be greatly reduced as compared to the conventional servo track writing method. However, more research is needed and the methodology is still under investigation for the manufacturing process to be cost effective.

Among the various methods mentioned, embedded servo provides the most accurate and cost-effective head positioning technique for hard disk drives. Thus, embedded servo systems are commonly used in today's HDD systems. This thesis will concentrate on the PES generation methods based on embedded servo system, which will be discussed in detail in the following sections.

## 2.3 Embedded Servo Approach

In the embedded servo approach, each disk surface includes servo track information and binary data recorded in concentric or spiral tracks in an interleaved manner and all tracks on every surface are divided into a fixed number of radial sectors as shown in Figure 2.2.

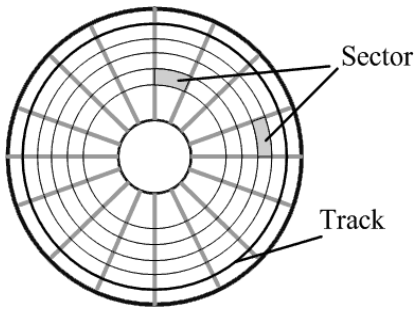


Figure 2.2: Spatial illustration of servo bursts in an embedded servo drive.

The data recorded in servo sectors must be properly positioned and encoded to generate PES signal and track number as shown in Figure 2.3. Typically, the servo fields include AGC field, servo track mark (STM), track address in Gray code and the servo bursts. The data sector includes the synchronization pattern known as preamble, followed by the user data and error correction code (ECC) for error recovery.

A Gray-coded track address is written in the servo sector of each track. Usually the tracks are numbered from outer diameter (OD) location to inner diameter (ID) location. The physical track '0' is the outermost track on a disk. Gray code has the advantage of limiting the reading error to only the adjacent track. In addition,

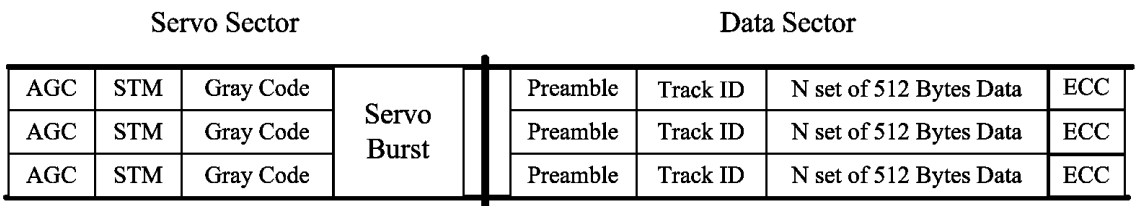


Figure 2.3: Servo data sector layout in a typical embedded servo drive.

the velocity of the actuator during seeking is bounded to ensure that the head does not move more than two tracks within the time of one Gray code frame.

Servo bursts are embedded on sector headers for the purpose of positioning the head array accurately on tracks. At high track densities, drifts in the head position with temperature and time limit servo accuracy. The read channel electronics circuitry must seek out and demodulate this information before passing it on to the servo controller.

There are many different types of patterns for servo bursts that can allow estimation of the head's position: 1) time-based servo pattern, which is commonly used in tape drive industry [42], 2) amplitude servo pattern, 3) phase-encoded servo pattern, and 4) frequency-encoded servo pattern etc. Among these patterns, amplitude servo pattern is the most popular one.

### 2.3.1 Amplitude Servo Pattern

The standard servo burst pattern in sector servo format is as shown in Figure 2.4. It provides a radial position estimate by comparing the amplitudes of signals written

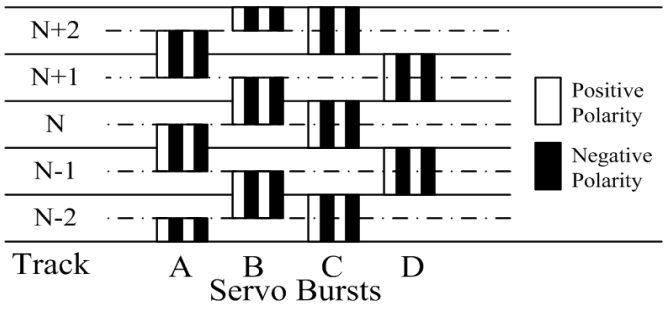


Figure 2.4: Quadrature amplitude servo pattern.

symmetrically to either side of the data track centers. The black regions are of opposite polarity to the white regions. A change from one polarity to the other would induce a pulse to be sensed by the read head. The servo burst field is divided into four separate sub-fields, A through D, which enable the PES demodulator to determine a position estimate based on the relative amplitudes of the bursts in each of the four regions.

### 2.3.2 Time-Based Pattern

Figure 2.5 shows the time-of-flight servo pattern which is popularly used in linear tape systems [13] [42] [57]. The black regions are of opposite polarity to the white regions. A change from one polarity to the other would induce a pulse to be sensed by the read head.

The position estimate is generated by measuring the time the head takes to travel from the sync pulse to the slanted transitions. The head first encounters sync pulse, and the demodulator then counts the time until the servo signal passes

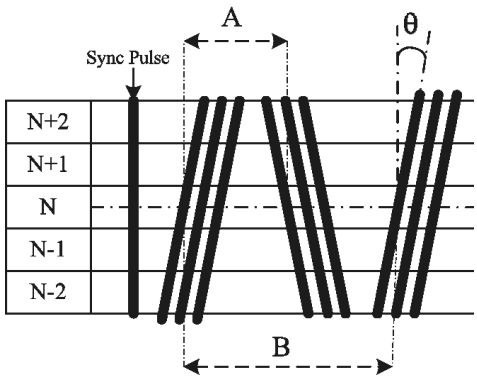


Figure 2.5: Time-of-flight servo pattern.

a threshold value when passing over the burst. This count in turn can be used to determine the amount that the head is offset from the track center. The position formula can be written as

$$PES_{TIME} = \frac{B_l \sum_i a_i}{2tan\theta \sum_i b_i} \tag{2.1}$$

where $a_i$ and $b_i$ are the time intervals measured and $B_l$ is the written length of $b_i$.

### 2.3.3 Phase-Encoded Servo Pattern

Phase servo pattern can be used for encoding position information. For examples, there are bi-phase servo format as discussed in [41] and format with three distinct phase differences at $120^o$ offset in adjacent tracks which enable position information to be decoded [35].

As an example, a dual-phase ($180^o$ out of phase) pattern which is also known as null servo pattern, is shown in Figure 2.6, where the black and white patches in the servo fields 'A' and 'B' correspond to opposite magnetic polarities. Adjacent

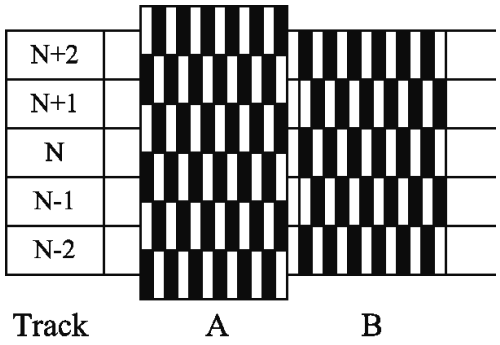


Figure 2.6: Quadrature null pattern.

tracks are written $180^o$ out of phase. If the head is on the center of the data track, the interferences from each adjacent servo track will cancel each other out and the readback signal will be ideally of zero amplitude. As the head drifts to either direction of the track center, the readback signal will increase in proportion to the head position till the offset is about or larger than the width of the read sensor. This saturation is due to the "write wide read narrow" scheme. For linearity purpose, quadrature servo field 'B' is also provided across the track. Hence when the head is moving off-track, the PES will be either positive or negative depending on the position with respect to the track center. The approach used by amplitude-based servo demodulation can be used similarly in this case.

### 2.3.4 Frequency-Encoded Servo Pattern

Since the servo pattern can be created by alternating transitions on the magnetic media, this generates a periodic signal [51]. Thus, another variation of generating the position error signal is based on frequency of the written servo pattern [10] [59].

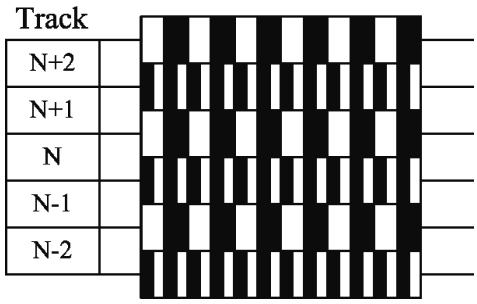


Figure 2.7: Dual frequency servo pattern.

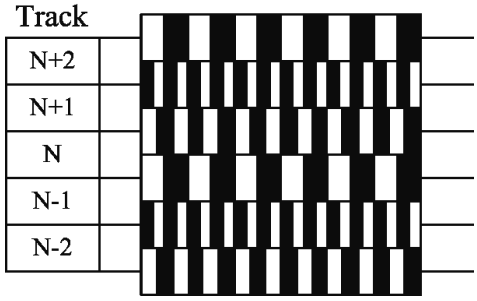


Figure 2.8: Triple-frequency servo pattern.

Figure 2.7 shows the dual frequency servo pattern, and the triple-frequency servo pattern is as shown in Figure 2.8. The black and white regions in the servo fields correspond to opposite magnetic polarities. The difference in the duration/length of magnetization or alternating transitions will result in different frequency servo signal.

The head position is estimated based on the strengths of the different frequency components that the readback signal contains. When the servo head is positioned over the intersection of the tracks 'N' and 'N+1', the signal strengths of the two frequency components should ideally be equal. Usually, matched filters are used in the servo demodulation process for frequency-encoded servo signal to

extract the desired frequency components.

In this thesis, digital demodulation techniques for frequency-based PES generation will be the focus of the research. However, to have a better understanding of the demodulation process, a survey of the different demodulation techniques for the popular amplitude servo pattern is presented. With some modifications, the digital detection techniques for the amplitude servo patterns can also be applied to the frequency-encoded servo patterns.

## 2.4 PES Formulation of Amplitude Servo Pattern

The most popular servo pattern is the amplitude servo pattern [62]. A typical servo waveform written on a disk surface is shown in Figure 2.9. For illustration purpose, each of the blocks A, B, C, and D is considered to be consisting of just two magnetic transitions on the media. As a result, a pair of pulses with opposite polarity (dibit or dipulse) is produced when a head moves over any one block. The patterns A, B, C, and D are separated from each other by equal distance in the down-track direction. The patterns A and B are placed at alternate positions in the cross-track direction, and patterns C and D are also similarly placed. The pair A/B is in quadrature with the pair C/D.

The servo pattern provides radial position estimates by comparing the am-

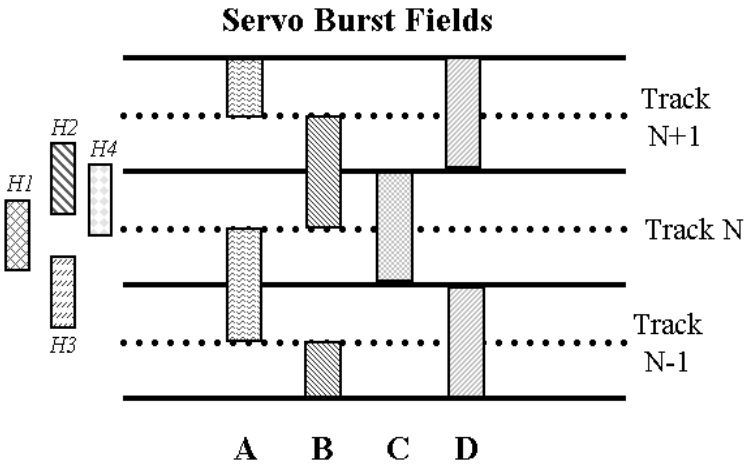


Figure 2.9: Servo pattern magnetized on the disk surface of an HDD.

plitudes of signals written symmetrically to either side of the data track centers. When the head is on track center, A and B fields are of half amplitude strength, and one of C or D field is at the full value and the other is at zero strength. Each field may contain a series of bursts depending on the accuracy needed and manufacturers' specification.

In Figure 2.9, there are several heads in the cross-track direction for illustration. For example, at position $H1$, the head is exactly along the center of track 'N'. $H2$ is at an off-track location towards the track 'N+1', and $H3$ is off-track towards track 'N-1' etc. For position $H1$, the head senses no flux from the transitions of servo pattern 'D'. It can sense the flux from other three pairs of transitions. However, amplitude will be larger for the pattern 'C' than those from patterns 'A' and 'B'. For an ideal situation, the head will sense equal amplitude for patterns 'A' and 'B' when on track center. Figure 2.10 shows some of the resultant servo signals read from different locations.

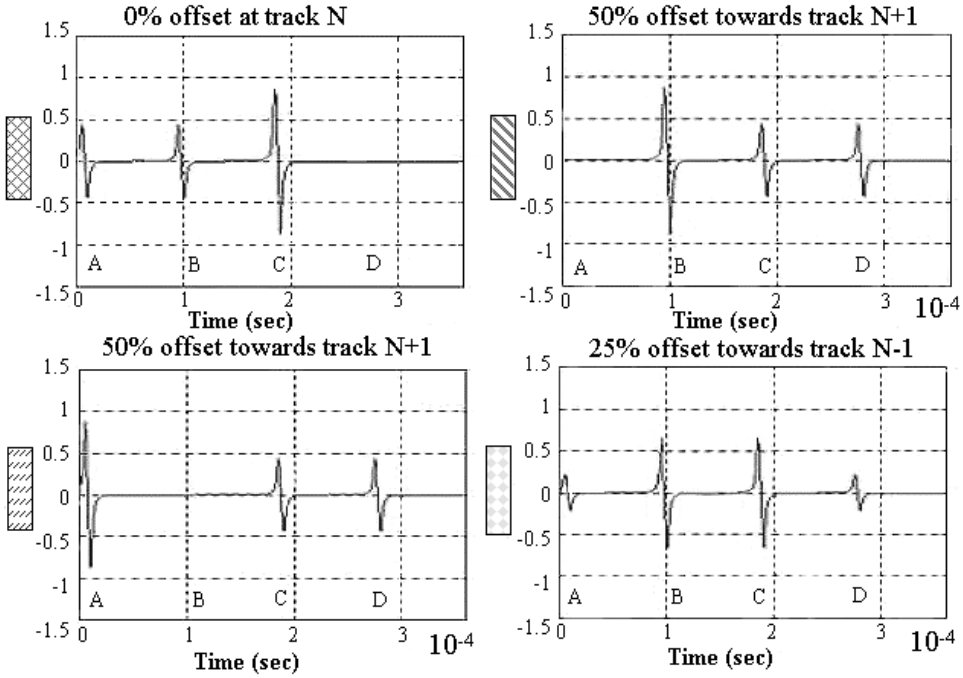


Figure 2.10: Readback signal waveforms for the different read head positions.

The readback signal $v(\omega t)$, where $\omega$ is the speed of the transitions in radian, is sensed by the head at a radial offset from track N and it is a linear combination of the signals from its adjacent tracks. Let $r_N(\omega t)$ be the readback signal from the head directly on servo track 'N' and $\varepsilon$ be the amount of variation from the track width $p$. Then,

$$v(\omega t) = (\frac{p-\varepsilon}{p}) r_N(\omega t) + (\frac{\varepsilon}{p}) r_{N-1}(\omega t), \tag{2.2}$$

for cross-movement towards "N-1" direction and

$$v(\omega t) = (\frac{p-\varepsilon}{p}) r_N(\omega t) + (\frac{\varepsilon}{p}) r_{N+1}(\omega t), \tag{2.3}$$

for cross-movement towards 'N+1' direction. The cross-track response of the head sensitivity function is assumed to be ideally zero (without noise) outside the phys-

ical width $p$ and unity otherwise, for linearity.

The PES is a function of the head's radial position, extending from ID to OD. The basic computation of the PES is based on amplitude variations. The amplitudes for all the four servo patterns are detected and the following two signals are derived as

$$PES_{ip}(\omega t) = \frac{v_A(\omega t) - v_B(\omega t)}{v_A(\omega t) + v_B(\omega t)}, \tag{2.4}$$

$$PES_{qu}(\omega t) = \frac{v_C(\omega t) - v_D(\omega t)}{v_C(\omega t) + v_D(\omega t)}. \tag{2.5}$$

The two signals derived above vary linearly within a track width. The signals are plotted as a function of cross-track position in Figure 2.11. The signal $PES_{ip}(\omega t)$ has zero amplitude at the center of each track, and is called in-phase position error signal. The signal $PES_{qu}(\omega t)$ is called the quadrature position error signal and has zero magnitude at mid-point between two tracks.

In practice, the cross-track PES is not a triangular function of radial displacement. PES tends to saturate at the peaks due to the characteristics of MR head and difference in the read and write heads' width [44] as illustrated in Figure 2.11 by the dotted line. In addition, the head sensitivity function is also related to several parameters, like the gap between the magnetic head, the FH of the head, spacing of the medium from the head etc. Thus, in order to improve linearity and reduce sensitivity to disk surface effects, quadrature technique is employed. The signals are obtained from two sets of patterns, which, when demodulated, produce position error signals that are quadrature to each other. By taking the linear por-

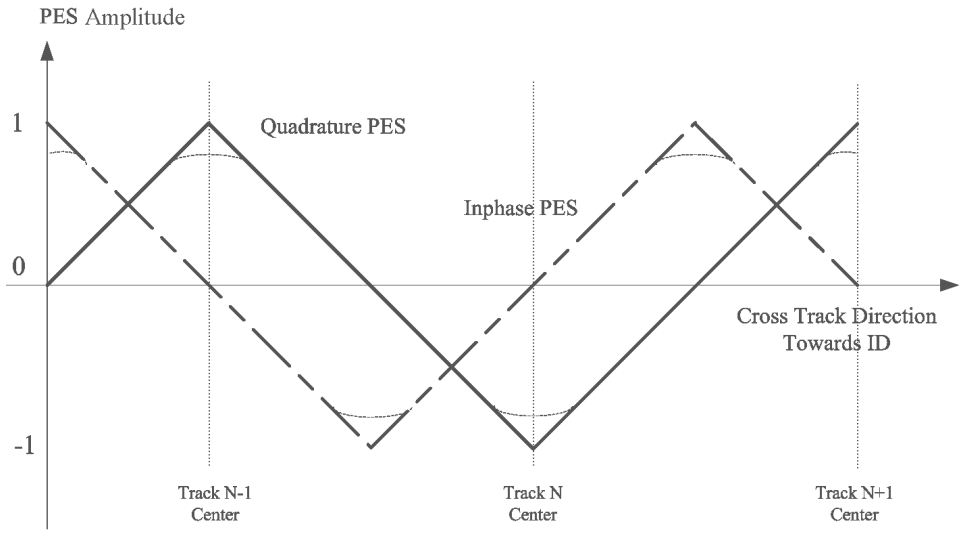


Figure 2.11: In-phase and quadrature PES as a function of off-track distance.

tion of the cross-track PES using the quadrature layout, a more accurate position error signal can be derived. Thus, the quadrature layout is used for identifying the linear part of slope.

For the peak detection technique, relying on the amplitude of a single pulse makes the system susceptible to noise and dropouts. Thus a series of transitions are normally used for each of the servo pattern. For better noise immunity and insensitivity to surface defects, averaging of several pulses would make the demodulation more robust.

A commonly used averaging process for disk drive is the Area Demodulation. An example is shown in Figure 2.12, which is taken from [27]. The readback servo signal is rectified by a full-wave rectifier to get all positive pulses. Four logic windows are generated to define the four servo burst fields, namely 'A', 'B', 'C'

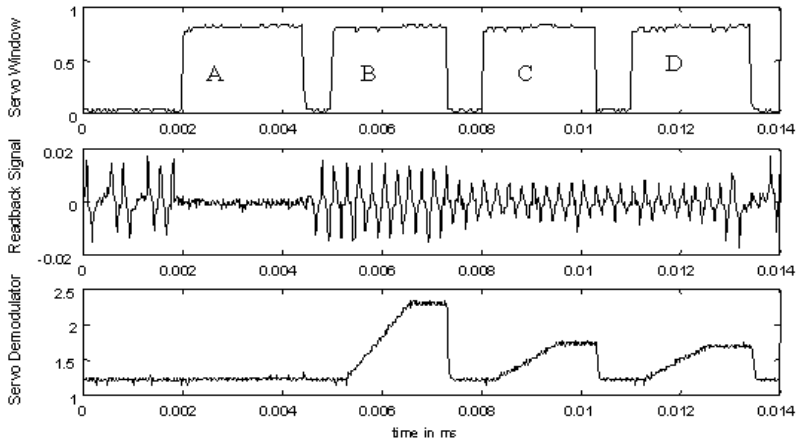


Figure 2.12: Readback servo signal and resultant area detection output.

and 'D'. The rectified pulses of the servo fields are used to charge the capacitor in each of the four windows. Once the pre-defined number of pulses have charged the capacitor, the voltage is latched to a Sample and Hold amplifier and the capacitor is discharged to zero before the next window opens. Four separate Sample and Hold amplifiers are used to store each of the servo fields' integral voltages and an Analog to Digital Converter (ADC) converts these voltages to 4 binary numbers each representing the strength of each servo fields. Thus the in-phase PES is generated by the difference between the integral of the rectified 'A' and 'B' servo burts and the quadrature PES is determined by the difference between the integral of the rectified 'C' and 'D' bursts.

## 2.5 Digital PES Detection on Amplitude Servo Pattern

With the rapid progress of digital technologies and availability of highly integrated digital and linear circuits, digital control and demodulation became feasible in the recent years [17] [56].

Both control and detection algorithms have lately been switched from analog to digital schemes. The following subsections describe several digital demodulation techniques for amplitude based PES generation method. The digital demodulation techniques discussed here work well for the amplitude or null servo patterns of single frequency.

### 2.5.1 Digital Area Demodulation

A digital implementation of the burst demodulator must contend with sampling and ADC quantization effects. One technique which adapts well to digital implementation is area detection [17], where it is ideally insensitive to the starting delay or phase of the burst waveform.

Figure 2.13 shows the block diagram of a typical area detector. The readback servo signal is of very small amplitude. Thus a pre-amplifier is needed and after automatic gain adjustment, the readback signal is filtered to reduce aliasing effects and reject undesirable signal components such as inter-track interference and high

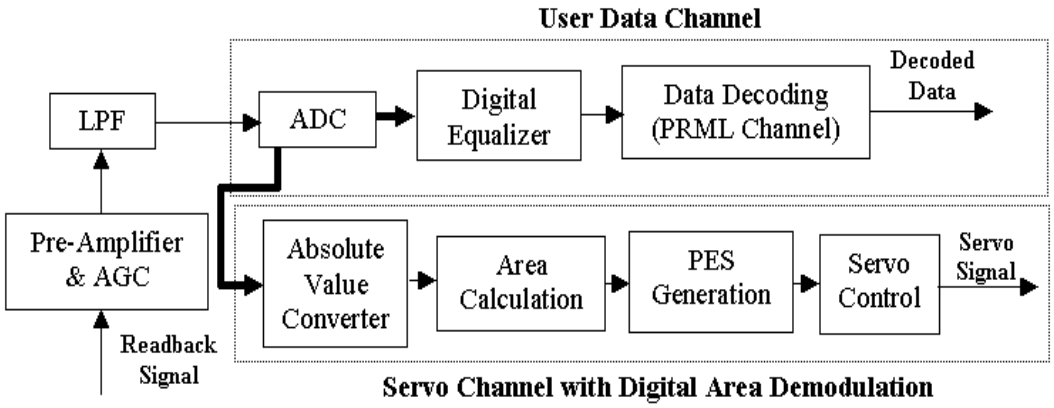


Figure 2.13: Block diagram of a digital area detection based PES demodulator.

frequency noise. Since the input to the read channel is analog in nature, any digital processing should be preceded by an analog-to-digital converter (ADC). Thus, both the servo and data channels can share the same ADC as the servo and user data fields are time-multiplexed in embedded servo system [53]. In servo channel, the digitized samples are rectified by an absolute value logic circuit which inverts the signs of the negative numbers. Following which, the rectified samples are summed in an accumulator and the accumulator adds a predetermined number of samples to fix the integration window to an integer number of periods of the burst waveform. The following equation is used to calculate the area,

$$AD = \sum_{n=1}^{N} \sum_{c=1}^{C} |X_{cn}|, \tag{2.6}$$

where $AD$ represents the area, $N$ represents the number of sample points per cycle, $C$ being the number of cycles of the burst and $X_{cn}$ represents the sampled values. The PES can be derived from the difference between the areas of burst $AD_A$ and burst $AD_B$ as shown in (2.7) which is similar to the amplitude detection (2.4). In addition, the equation is divided by the sum of the areas in order to achieve

normalization.

$$PES_{AREA} = \frac{(AD_A - AD_B)}{(AD_A + AD_B)}. \tag{2.7}$$

To get better noise immunity, another method is by mixing the servo burst signal with an idealized model of the dibit response and integrating over a finite, integral number of periods of the waveform which is the process of demodulation [2]. In general, there are two types of demodulation techniques, namely coherent demodulation, where it is a synchronous operation, and non-coherent demodulation. Each will be briefly introduced next.

### 2.5.2 Discrete Fourier Transform Detection Technique

For non-coherent demodulation, it involves passing of the modulated signal through some memoryless non-linear operator. Several simple circuits can serve as the non-linear operator, such as a full-wave rectifier, and requiring no synchronization with the mixing signal. The non-linear operator has the effect of splitting the signal energy into bands among the multiple harmonics of the carrier signal. The filter operation will then choose one or some of the harmonic bands. If the baseband harmonic is chosen, the signal will be effectively demodulated. One of the non-coherent demodulation techniques uses a method based on the Fourier series rules to extract the position error signal [9] [12], since the encoded position signal utilizes a periodic signal.

For digital signal processing, the continuous-time signal must be bandlimited

to less than half the sampling rate to avoid aliasing upon sampling as stated by Nyquist sampling theorem [43]. In this detection scheme, demodulation of servo relies on the use of discrete Fourier transform (DFT) which takes a discrete time series of N equally-spaced samples of the signal, and transforms into frequency domain. Thus, the formula for calculating the spectral content, $\underline{X}_k$, of a signal from a set of N equal-spaced samples of the signal, $x(n)$, is given by

$$\underline{X}_k = \frac{1}{N}\sum_{n=0}^{N-1} x(n)e^{-j2\pi k(n/N)}. \tag{2.8}$$

The coefficient $\underline{X}_k$ can be expressed as a complex number since

$$e^{j\omega n} = \cos(\omega n) + j\sin(\omega n). \tag{2.9}$$

Hence, the complex exponential of (2.8) can be broken down into its real and imaginary components. Equation (2.9) can be written as

$$\begin{aligned}\underline{X}_k &= \frac{1}{N}\sum_{n=0}^{N-1}[cos(k2\pi\frac{n}{N} - jsin(k2\pi\frac{n}{N})] \\ &= \frac{1}{N}[\sum_{n=0}^{N-1} x_n cos(k2\pi\frac{n}{N}) - j\sum_{n=0}^{N-1} x_n sin(k2\pi\frac{n}{N})] \\ &= X_{ck} + jX_{sk}. \end{aligned} \tag{2.10}$$

Thus, if we take only N data points (one cycle of burst), the magnitude of this complex number at frequency component $k = 1$ will represents the coefficient of the fundamental frequency of the servo burst. If we consider 2N points (two cycles of burst), then the frequency of the burst can be deduced from twice that of the fundamental frequency. Henceforth, the magnitudes of the first and second servo burst signals in servo fields A and B can be obtained and the position error signal

will be the difference between magnitude information of the first and second servo burst signals.

However, DFT is a highly computational intensive algorithm for getting the frequency spectrum of the signal. Thus the Fast Fourier Transform (FFT), which allows the DFT of a sampled signal to be obtained rapidly and efficiently can be used. Direct computation of DFT is inefficient primarily because it does not exploit the symmetry and periodicity properties of the phase factor. DFT computations are in the order of $N^2$ where N is the number of data points in the data sequence, while FFT computations are in the order of $Nlog_2N$. Hence, using FFT reduces the number of computations by a significant amount.

**Fast Fourier Transform PES Demodulation**

There are many FFT algorithms available, based on different approaches. There is the Radix-2, Radix-4, Split-Radix etc [49]. The FFT code used for simulation is based on the MATLAB function which is developed by M. Frigo and S.G. Johnson, named as "Fastest Fourier Transform in the West" (FFTW) [24].

Consider the Radix-2 Cooley-Tukey algorithm [20] where it requires $3 \times N \times log_2(N)$ multiplies. For a 1024 point FFT, this amounts to $30,720$ adds and $20,480$ multiplies for a total of $51,200$ arithmetic operations. In contrast, each DFT output frequency requires $4 \times N = 4096$ multiplies and $4 \times N - 1 = 4095$ adds for a total of 8191 arithmetic operations. Thus, if more than $51,200/8191 = 6.25$ of the 1024 potential DFT outputs are needed, it is more efficient to use an FFT algorithm to

compute all 1024 outputs and throw away the unwanted ones.

The dramatic reduction in computational load makes the FFT algorithms more efficient, even when only a few output frequencies of DFT need to be computed. There are a variety of FFT algorithms available and research on the efficiency of the FFT algorithms can be found in [26]. The method of obtaining the PES is the same as that of DFT-based algorithm, in which the servo readback signal is converted to frequency domain using FFT and the amplitude of the single frequency servo pattern is extracted. Following this, the PES is calculated by taking the difference between the two amplitudes.

However as the DFT/FFT is used to approximate the Fourier transform of a continuous time process, there exist some inherent problems in this approach. There are three possible phenomena that result in errors between the computed and the desired transform [43]. These three phenomena are (a) aliasing, (b) leakage, and (c) the picket-fence effect.

(a) Aliasing. Error occurs when the sampling frequency of analog-to-digital conversion is lower than twice the highest frequency contained in the signal (Nyquist frequency). The only solution to the aliasing problem is to ensure that the sampling rate is high enough to avoid any spectral overlap, or to use an anti-aliasing filter.

(b) Leakage. This problem arises because of the practical requirement that the observation of the signal is limited to a finite interval. The process of terminating

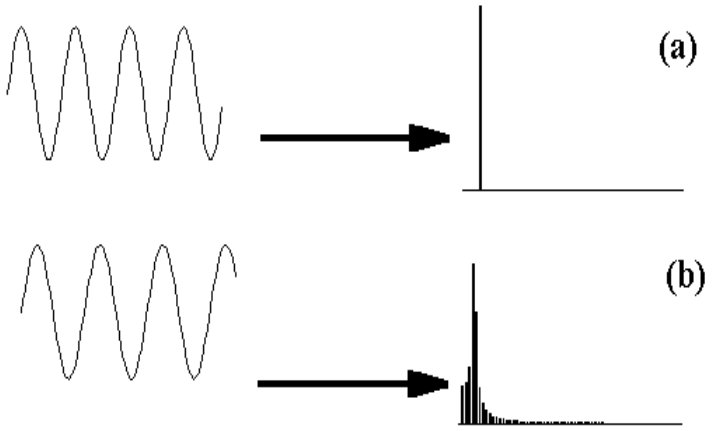


Figure 2.14: Frequency spectrum of (a) complete periodic signal (b) incomplete periodic signal.

the signal after a finite number of terms is equivalent to multiplying the signal by a window function. The net effect is a distortion of the spectrum. There is a spreading or leakage of the spectral components away from the correct frequency, resulting in an undesirable modification of the total spectrum.

From the power spectrum in Figure 2.14, it can be seen that there is a "broading" effect if the periodic waveform is not taken as whole. In the case of using sinewave to model the readback servo signal, leakage is not a big problem, since it is easy to distinguish the major component of the signal. The problem is the closeness of the signal frequencies and not the number of periods within the window. Since, the readback servo signal has odd harmonics components, this leakage will affect the resultant PES greatly.

The leakage effect cannot always be isolated from the aliasing effect because

leakage may also lead to aliasing. Since leakage results in a spreading of the spectrum, the upper frequency may move beyond the Nyquist frequency and aliasing may then result.

(c) Picket-Fence Effect. This effect is produced by the inability of the algorithm to observe the spectrum as a continuous function, since computation of the spectrum is limited to integer multiples of the fundamental frequency $F$ (reciprocal of the sample length). Observation of the spectrum with the algorithm is analogous to looking at it through a sort of "picket-fence", since the exact behavior can only be observed at discrete points. The major peak of a particular component can lie between two of the discrete transform lines, and the peak of this component might not be detected without some additional processing.

One procedure for reducing the picket-fence effect is to vary the number of points in a time period by adding zeros at the end of the original record, while maintaining the original record intact. This process artificially changes the period, which in turn changes the locations of the spectral lines without altering the continuous form of the original spectrum. In this manner, spectral components originally hidden from view can be shifted to points where they can be observed.

### Simplified DFT-based PES Demodulation

Execution time taken by the PES demodulator is one of the important criteria, which may limit the sampling rate required for the design of higher servo bandwidth and speed performance. Thus an optimized DFT algorithm that can reduce

the execution time is needed for more efficiency. The servo signal of single amplitude servo pattern consists of only one frequency at any one time. Henceforth, instead of using the conventional Fourier transform algorithm to find the whole frequency spectrum of the servo signal at servo fields A and B, the PES can also be obtained by getting only the fundamental frequency component of the amplitude servo pattern at servo fields A and B. In this way, the amount of computation can be greatly reduced.

The cosine/sine coefficient calculation of PES method [9] starts by recording the servo burst signals in servo fields A and B alternately in the radial direction. The readback signals are digitally sampled at a frequency of at least twice greater than the servo burst signal frequency. Magnitude of each frequency component can be obtained from the sample values by calculating the cosine and sine coefficients (see (2.10)) of signal components having a frequency identical with the servo burst signal frequency.

The magnitudes of the servo burst signals in servo fields A and B are obtained through the square roots of the sums of the squares of the respective cosine coefficients and sine coefficients. The position error signal will be the difference between magnitude information of the first servo burst signal and the magnitude information of the second servo burst signal.

For simplicity, this cosine coefficient/sine coefficient calculation of the PES will be referred to as simplified DFT or DFT-based PES detection throughout the thesis. Next, the coherent demodulation technique is presented.

### 2.5.3 Coherent Demodulation Techniques

For coherent demodulation [2], rather than passing the modulated signal through a non-linear element, the modulated signal is mixed with another signal. The mixing signal that is being used is of the same frequency and phase as the carrier signal. The algorithm uses a mixing signal that is composed only of a weighted sum of the harmonics of the dibit carrier frequency to achieve improvement in filtering of broadband noise. Any periodic signal can be decomposed into the sum of harmonics of the fundamental frequency as

$$m(t) \quad = \quad A_0 + \sum_{n=1}^{\infty} (A_n cos(n\omega t) + B_n sin(n\omega t)), \tag{2.11}$$

where

$$A_k = \frac{1}{\pi} \int_0^{2\pi} m(t) cos(k\omega t) d(\omega t), \tag{2.12}$$

$$B_k = \frac{1}{\pi} \int_0^{2\pi} m(t) sin(k\omega t) d(\omega t), \tag{2.13}$$

$$A_0 = \frac{1}{\pi} \int_0^{2\pi} m(t) d(\omega t), \tag{2.14}$$

where $A_k$ represents the cosine coefficient, $B_k$ represents the sine coefficient and $k$ represents the $k^{th}$ harmonic content.

The main idea of this scheme as stated by Abramovitch [2] is to mix the readback servo signal with a customizable set of harmonics of the noise-free dibit signal. The mixing signal is assumed to be the readback signal from the single

burst field with no noise or distortion, signal starting at zero, repeating at each new dibit and terminating at zero.

The readback servo signal $r(t)$ can be analyzed using Fourier series. Due to the symmetric properties of $r(t)$ where the signal has a zero dc value and is odd, it can be written as

$$r(t) = \sum_{k=1}^{\infty} B_k sin(k\omega t). \tag{2.15}$$

Next, considering only a two harmonics readback signal and assuming that $n(t)$ is a zero-mean AWGN signal,

$$r(t) = A_0(r_1 sin(\omega t) + r_2 sin(3\omega t)) + n(t), \tag{2.16}$$

with a single sinusoidal mixing signal

$$m(t) = sin(\omega t), \tag{2.17}$$

yields

$$m(t)r(t) = \frac{A_0}{2}[r_1(1 - cos2\omega t) + r_2(cos2\omega t - cos4\omega t)] + sin(\omega t)n(t). \tag{2.18}$$

By integrating the mixed signal for an integral number of periods of the signal, we get

$$\frac{1}{MT}\int_0^{MT} m(t)r(t)dt = \frac{A_0 r_1}{2} + \frac{1}{MT}\int_0^{MT} sin(\omega t)n(t)dt. \tag{2.19}$$

The expected value of the second term in (2.19) can be equated to zero. Thus,

$$E[\frac{1}{MT}\int_0^{MT} m(t)r(t)dt] = \frac{A_0 r_1}{2}. \tag{2.20}$$

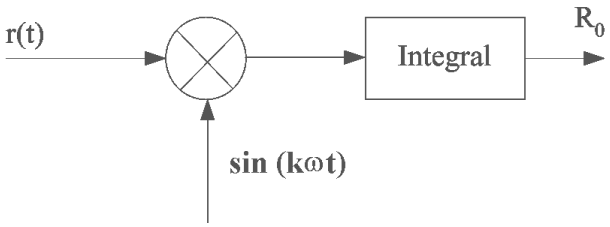


Figure 2.15: Coherent detection method.

Hence, by integrating the product of $r(t)$ and $m(t)$, the relative amplitude of the servo signal can be computed. Any individual harmonic can be chosen to be demodulated. In this case, only a single custom mixing signal is generated, which contains the desired harmonics to be demodulated. Thus the demodulation system can be optimized with respect to the presence of a wide variety of non-idealities, like transition noise. The method that have been discussed so far, uses sinewave as the mixing signal for digital demodulation [11]. However, if synchronization of the data becomes an issue, we can mix with sine and cosine components separately and extract the amplitude of the burst signal by taking the square root of the sum of squares of the two individual results. This is also known as the simplified DFT method as discussed in Section 2.5.2.

Figure 2.15 and Figure 2.16 show the block diagrams of the coherent detection method and simplified DFT detection method respectively. For coherent detection, the signal amplitude is obtained after integrating the product of the readback signal $r(t)$ and $sin(kwt)$. In the case of DFT-based method, the signal magnitude $A$ of $r(t)$ at $k^{th}$ frequency harmonic is obtained as

$$X_k = \sqrt{X_{ck}^2 + X_{sk}^2}. \tag{2.21}$$

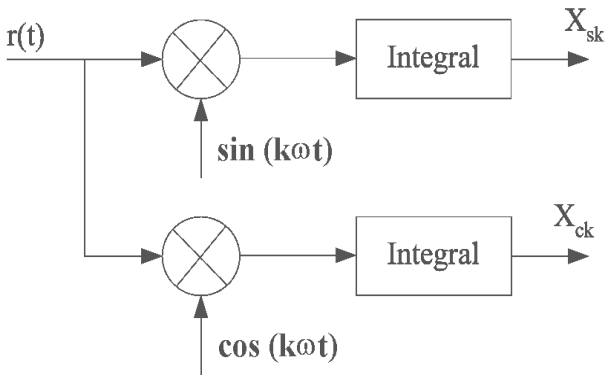


Figure 2.16: Simplified DFT detection method.

## 2.6 Summary

This chapter reviewed the different ways of position information emplacement, namely dedicated, buried, embedded servo and patterned media. Different servo burst patterns are also discussed, namely amplitude, time-based, phase encoded and frequency-encoded servo bursts. Digital PES demodulation schemes including digital area detection, non-coherent simplified DFT detection and coherent detection for the popular amplitude servo pattern are reviewed.

Frequency-encoded servo pattern is chosen to be the focus of this research, where servo burst overhead can be reduced and track mis-registration in either direction can be easily detected. The performance of these demodulation techniques for FESP will be analyzed in the next chapter.

# Chapter 3

# Digital PES Detection of Frequency-Encoded Servo Pattern

In this chapter, servo patterns of different frequencies for the servo burst fields are simulated and experimental data of frequency servo format is collected to evaluate the performance of digital demodulation techniques. The digital detection techniques that we compared are 1) area detection using 2 digital notch filters, 2) coherent detection, and 3) DFT-based detection techniques.

## 3.1 Servo Pattern Layout and Simulation

There are many different servo patterns suitable for retrieving PES which have been discussed in the previous chapter. In Sacks' thesis [57], comparison between

phase, null and amplitude servo patterns is made. Phase and null PES generation methods have been shown to perform better than amplitude servo pattern in terms of additive noise. However, the effect of transition noise on the amplitude servo pattern is less as compared to the phase and null servo patterns. Signal space technique, which is popular in digital communications system, can be used to design estimators for different head positioning formats and to measure their performance. As discussed in [52], it was found that among amplitude, continuous phase, quantized phase and frequency servo pattern formats, the continuous phase method offers the best performance in terms of SNR, followed by quantized phase and frequency formats which are of equal performance. As for amplitude servo format, it is the worse of all.

Although phase-encoded servo pattern format is deemed to be superior in terms of signal-to-noise ratio (SNR), difficulties in actual writing of different phases exist. In fact, a major concern with the time-based or phase methods is the capability to accurately write the servo pattern. In hard disk drives, it is difficult to record a periodic pattern that changes the phase linearly with radial position. Precise positioning and timing are required by the servo writer to write this pattern. The effect of discretization and overwrite in the writing pattern would be of major concern to the operation of the demodulator in generating a good PES. Furthermore, to achieve continuous phase format, read head must be infinitely small, which is not possible in practice [52].

Thus frequency-encoded servo scheme is proposed for the servo pattern layout

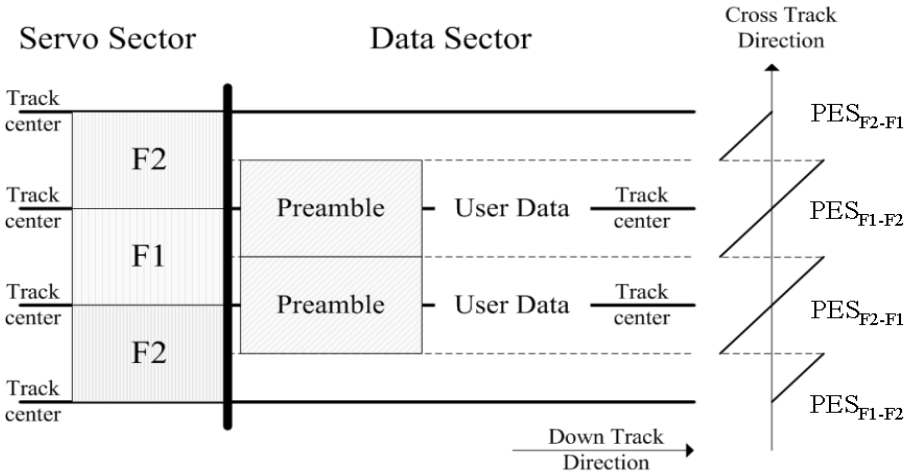


Figure 3.1: Dual frequency-encoded servo layout.

in this research work. This allows the possibility of placing them at the same angular location. In turn, servo overhead can be reduced, allowing for more user data storage [10][14]. To determine the direction of the positioning error, we used servo burst patterns with different frequencies in adjacent servo tracks as shown in Figure 3.2, instead of the dual frequency servo burst pattern as shown in Figure 3.1, in our study.

In this way, the direction of the head with respect to the desired track can be easily determined from the different frequency components of the readback servo signal.

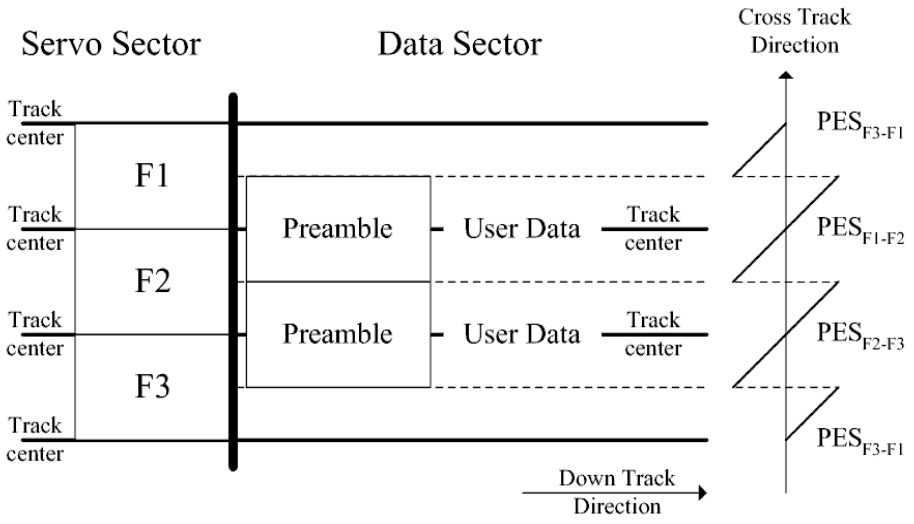


Figure 3.2: Multiple frequency-encoded servo layout.

### 3.1.1 Lorentzian Model of Servo Signal

The read head senses transitions in the direction of magnetization, which corresponds to a step signal in the write current. The magnetic recording channel response can be characterized by step response $s(t)$, which can be modeled by the Lorentzian function [15],

$$s(t) = \frac{1}{1 + (\frac{2t}{PW_{50}})^2} \tag{3.1}$$

where $PW_{50}$ is the pulse width at which the amplitude is at fifty percent of the peak value.

It is also generally assumed that a servo channel is a linear time-invariant (LTI) system and that individual pulses can be combined together through linear superposition. If a bit stream is written consecutively to the disk, the read head will produce a transition response whenever a transition in magnetization occurs.

The step response is considered equal to 0.5 times the transition response. As a result, the read signal can be considered as the superposition of the channel step responses, each corresponding to a change (-1 to +1 or +1 to -1) in the channel input. Thus a readback signal can be modeled as

$$s(t) = \sum_k x_k p(t - kT, T) + n(t) \tag{3.2}$$

where

$$p(t, T) = s(t) - s(t - T) \tag{3.3}$$

is the servo pulse response which depends on the transition period $T$, $n(t)$ is the AWGN whose mean is zero and the power density spectrum is constant for all frequency and is simulated using the MATLAB function $AWGN$ [64]. A range of reasonable SNR from 20dB to 30dB is used [63] and the peak amplitude for the servo burst is taken to be 1. The respective sigma for the AWGN is calculated using the following equation

$$SNR(dB) = 10log(\sigma_X^2/\sigma_N^2) \tag{3.4}$$

where $\sigma_X^2 = 1/\sqrt{2}$ = root-mean-square value of burst, $\sigma_N^2$ = variance of noise.

In addition, an analog-to-digital converter (ADC) block is needed in actual digital demodulation process to convert the analog signal to digital representation. Quantization errors due to digitization will occur and reduce the performance of the digital implementation of the servo burst demodulator. Thus in the simulation, the digitization error is simulated by using a MATLAB function $floor$,

$$X_{sampled} = \frac{floor(\frac{2^{(N-1)}2x}{FSR} + 0.5)}{2^N} FSR, \tag{3.5}$$

where $x$ is the analog signal value, $N$ is the digitization level which is set to be 8-bit and Full Scale Range (FSR) is set to be 0.5 V ($\pm$ 0.25 V) assuming that the analog readback signal is of amplitude $\pm$0.2 V range. Henceforth, conventional

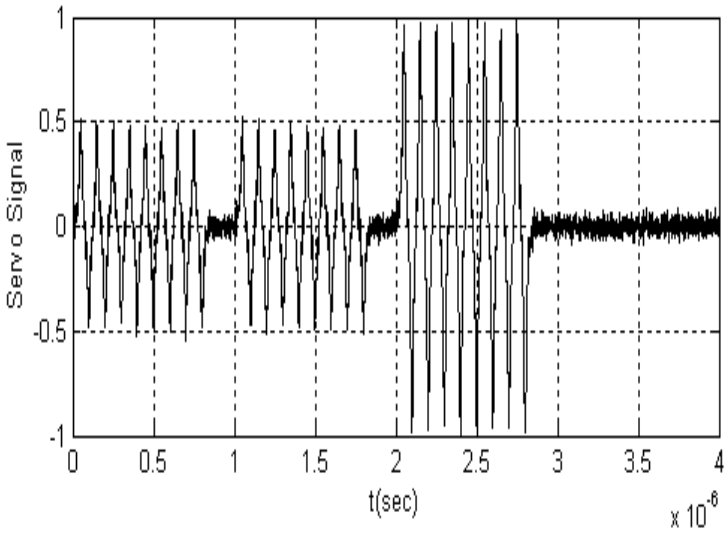


Figure 3.3: Simulated conventional amplitude servo signal

single frequency quadrature amplitude servo signal with SNR of 20 dB is simulated and shown in Figure 3.3.

### 3.1.2 Simulated Frequency-Encoded Servo Signal

For the FESP proposed, the quadrature format of this pattern is assumed and simulated according to the servo layout as shown in Figure 3.4.

When the read head moves from servo track F1 to servo track F2, the signal amplitude of servo track F2 will be increasing while that of track F1 will be de-

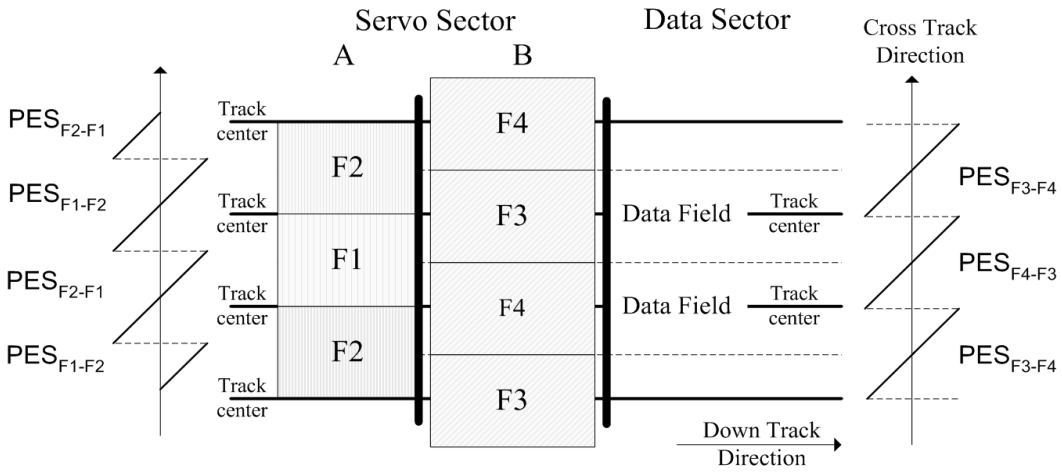


Figure 3.4: Quadrature dual frequency servo pattern.

creasing, and similarly for the case of quadrature pattern F3 and F4 [10] [57]. The readback signal between $\pm 50\%$ offset of the data track center using two different frequency servo patterns can then be simulated as

$$r(t) = A_{F1} g(t, T_1) + A_{F2} g(t, T_2) + n(t), \tag{3.6}$$

and for quadrature servo pattern,

$$r(t) = A_{F3} g(t, T_3) + A_{F4} g(t, T_4) + n(t), \tag{3.7}$$

where $A_{F1}$, $A_{F2}$, $A_{F3}$ and $A_{F4}$ are the amplitudes of the corresponding periodic servo patterns of frequencies $F1$, $F2$, $F3$ and $F4$ respectively. Function $g(t, T)$ represents the series of Lorentzian pulses for transition interval $T = PW_{50}/D$, where $PW_{50}$ is chosen to be 50 ns based on the parameters obtained from the head and media used for the experiment and $D$ is the transition density, defining the

number of bits stored on a single pulse. Thus the servo frequency $F_n$ is equal to the inverse of the two transition intervals $T_n$ where n = 1,2,3...

Assuming that the servo bursts are equally spaced and the mixing signals are accurately phase-locked to the servo signal, the amplitude of the servo signal is related to the variation of the head's position from the track center as discussed in Section 2.4 with the peak amplitude = 1.

Thus, for track $N$ which is odd,

$$A_{F1} = O_{fs} + 0.5; \tag{3.8}$$

$$A_{F2} = |O_{fs} - 0.5|; \tag{3.9}$$

$$A_{F3} = 1 - |O_{fs}|; \tag{3.10}$$

$$A_{F4} = |O_{fs}|. \tag{3.11}$$

For track $N$ which is even,

$$A_{F1} = |O_{fs} - 0.5|; \tag{3.12}$$

$$A_{F2} = O_{fs} + 0.5; \tag{3.13}$$

$$A_{F3} = |O_{fs}|; \tag{3.14}$$

$$A_{F4} = 1 - |O_{fs}|. \tag{3.15}$$

Since the resultant PES for the in-phase and quadrature PES are the same except for a 90 degree phase shift, our simulation and experimental results will only focus on one of them, that is, only the results for servo pattern of frequencies F1 and F2 are presented and quadrature servo frequencies F3 and F4 will be ignored.

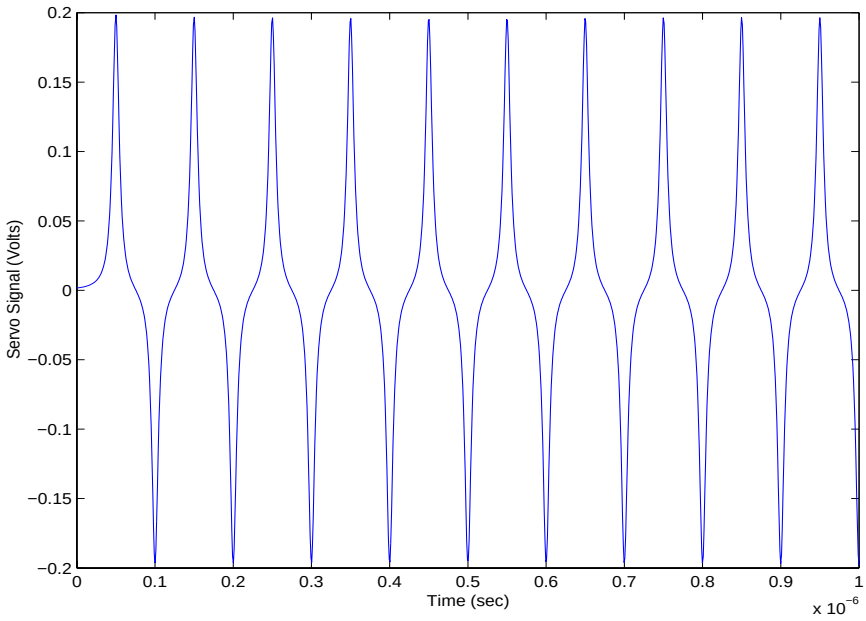


Figure 3.5: Simulated servo signal with read head entirely over the 10 MHz track.

Based on superposition theorem and (3.6), the simulated servo signal at the center of the data track is assumed to be an equal addition of the servo signal of frequency 10 MHz in Figure 3.5 and the servo signal of frequency 20 MHz as in Figure 3.6. Figure 3.7 shows an example of the readback servo signal when the read head is at the center of the two servo frequencies. The simulated servo signal of the servo pattern with frequency of 1:3 where servo track 1 is 10 MHz and servo track 2 is 30 MHz is also plotted and as shown in Figure 3.8.

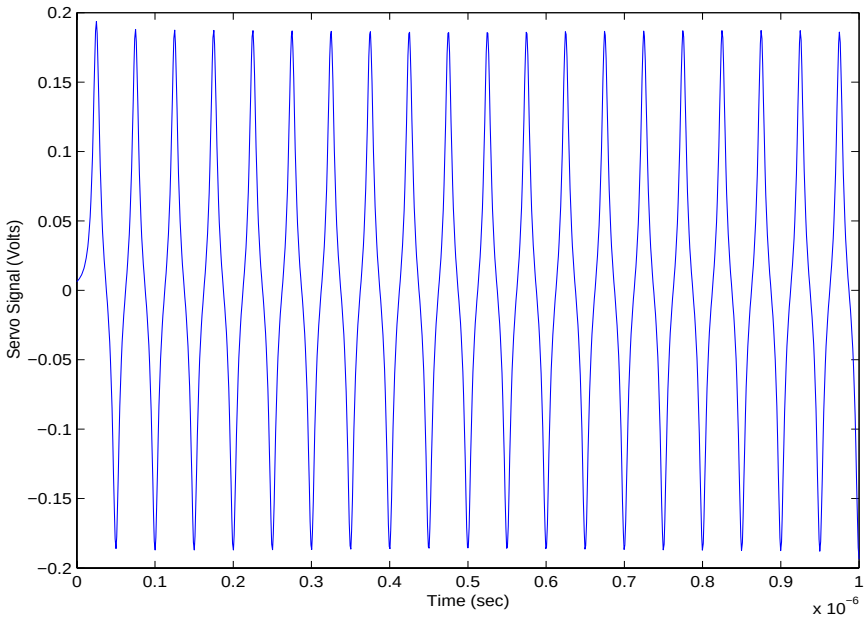


Figure 3.6: Simulated servo signal with read head entirely over the 20 MHz track.

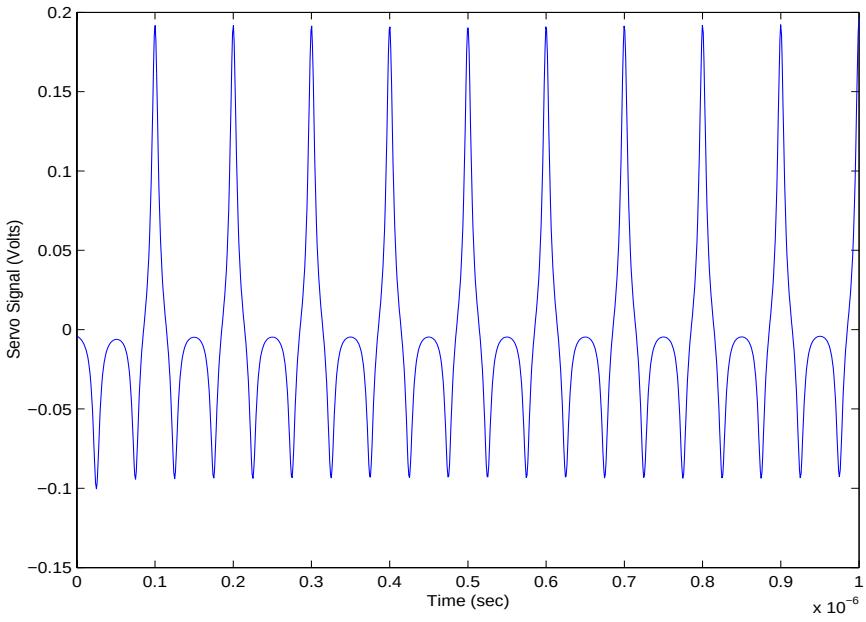


Figure 3.7: Simulated servo signal of frequency ratio 1:2 with read head at track center.

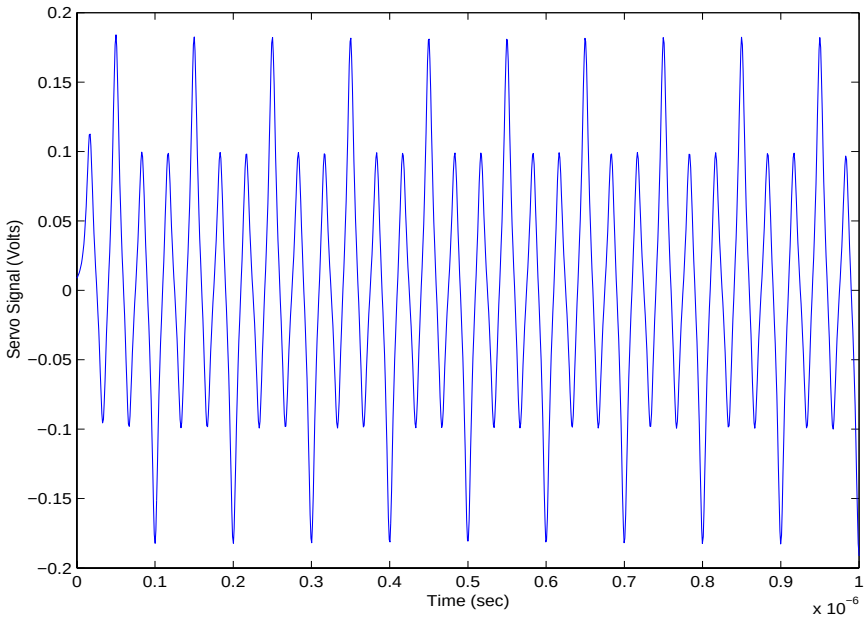


Figure 3.8: Simulated servo signal of frequency ratio 1:3 with read head at track center.

## 3.2 Digital Demodulation Methods

With the proposed FESP, suitable detection scheme is needed to demodulate the position signal. Area, coherent demodulation and DFT-based demodulation algorithms for single frequency amplitude servo pattern are presented in previous chapter. These algorithms can be modified with some adjustments and used for the decoding of PES from the FESP.

### 3.2.1 Digital Area Demodulation

Digital area demodulation is currently used in modern HDDs [2][10] and the algorithm is as presented in the previous chapter. In the case for demodulation of dual frequency servo pattern, filters are incorporated to extract the desired frequency components. The filter block consists of 2 digital bandpass filters, whereby both filters F1 and F2 are designed such that they reject all frequency components outside the frequencies they are built for. The digital filters used are specifically Finite Impulse Response (FIR) filters [63]. This type of filter is stable as it has only zeros and no poles. Furthermore, FIR system can be easily designed to have exactly linear phase with respect to frequency. Such system only results in a delayed response and no distortion.

There are a number of ways to design an FIR filter, such as windowing, frequency sampling and weighted Chebyshev approximation [43]. The filter responses are created by defining the desired pass-band, which are used to compute the coefficients. Finally the coefficients are tapered at the ends by multiplying them by a windowing function. The purpose of the window function is to sacrifice the steep skirts for a more uniform large attenuation in the stop-band. If the window function is omitted, sidelobes from the Gibbs phenomenon in the stop-band are relatively large. Several windowing functions have been tried as in [63]. Kaiser windowing is used in our FIR filter design, which has an adjustable parameter, $\beta$, to control the trade-off between a steep transition region and lower sidelobe levels and the MATLAB function (*kaiserord*) provides the estimation of the order value

$N$ and $\beta$ required to meet a frequency-selective filter specification. The output filter is given by

$$\begin{aligned} y(n) &= \sum_m h(m)x(n-m) \\ &= h(0)x(n) + h(1)x(n-1) + ... + h(N-1)x(n-N+1) \end{aligned} \quad (3.16)$$

where $x(n-m)$ represents the input (readback) signal samples and $h(m)$ represents the length $N$ filter coefficients. Let the filtered servo signal for field F1 be $y_{F1}(n)$ and the filtered servo signal for field F2 be $y_{F2}(n)$. The filtered data are then provided to the accumulators (3.18) and (3.18) respectively and the PES function is derived from the normalized differences which is similar to the case for single frequency PES formulation (2.7) in Section 2.5.1:

$$|AD_{F1}| = \sum |y_{F1}(n)|, \quad (3.17)$$

$$|AD_{F2}| = \sum |y_{F2}(n)|, \quad (3.18)$$

$$PES_{AREA} = \frac{(|AD_{F1}| - |AD_{F2}|)}{(|AD_{F1}| + |AD_{F2}|)}. \quad (3.19)$$

The simulated dual frequency servo pattern is chosen to be 10 MHz and 20 MHz. The specifications of the desired filters are as shown in Table 3.1. The frequency spectrums of the designed FIR filters at 10 MHz and 20 MHz are shown in Figure 3.9.

Table 3.1: Filter Specifications

| Filter Spec. | F1 (10 MHz) | F2 (20 MHz) |
|---|---|---|
| Stop Band 1 (MHz) | 7 | 17 |
| Pass Band 1 (MHz) | 9 | 19 |
| Pass Band 2 (MHz) | 11 | 21 |
| Stop Band 2 (MHz) | 13 | 23 |

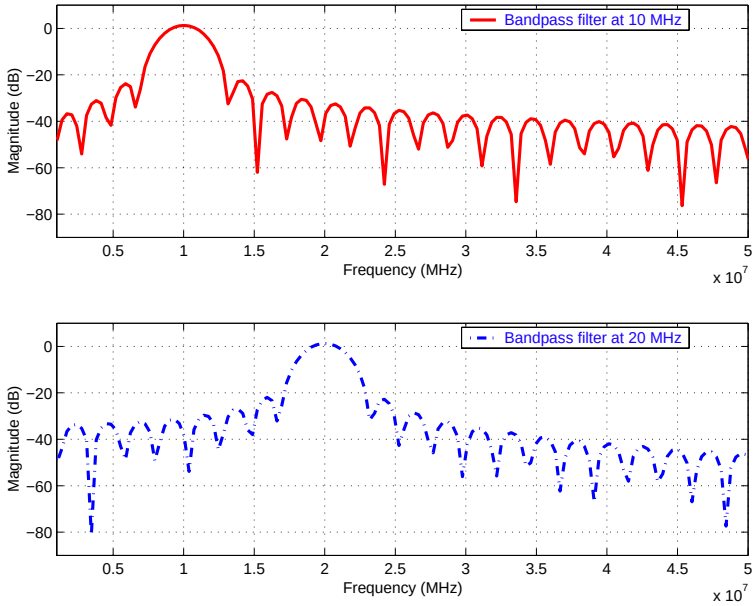


Figure 3.9: Frequency responses of FIR bandpass filters for fields F1 (10 MHz) and F2 (20 MHz).

### 3.2.2 Coherent Demodulation

For FESP, the main idea is to use frequency selectivity algorithm to extract the desired information. One way is by using matched filter demodulators to extract the

individual frequency components from the frequency-encoded servo signal [14][18].

Since the servo signal has a periodic property, we can also choose to demodulate or ignore any individual harmonic by coherent demodulation as discussed in Chapter 2. In this simulation, the mixing signals, $M_{x1}$ and $M_{x2}$ for the coherent detection are chosen to be sine waves of 10 MHz and 20 MHz, which are the same as the two frequencies that the servo burst patterns are simulated [10] [11].

$$M_{x1}(n) = sin(2\pi f_{s1} t_1 n) \tag{3.20}$$

$$M_{x2}(n) = sin(2\pi f_{s2} t_2 n) \tag{3.21}$$

The sampling intervals $t_1$ and $t_2$ for $M_{x1}$ and $M_{x2}$ are selected to be 0.01 $\mu$s and 5 ns respectively, so as to result in $N = 10$ sampling points per cycle for computation.

$$C_{D1} = \sum_{n=1}^{N*C} S_1(n) \times M_{x1}(n) \tag{3.22}$$

$$C_{D2} = \sum_{n=1}^{N*C} S_2(n) \times M_{x2}(n) \tag{3.23}$$

where $C$ is the number of complete cycles of the servo bursts taken for computation and $S_1(n)$ and $S_2(n)$ are the sampled servo data at sampling intervals $t_1$ and $t_2$ respectively according to $N$ sampling points.

### 3.2.3 Simplified DFT-based PES Demodulation

By getting the sine and cosine coefficients of the servo pattern's fundamental frequency, the variation of the head position with respect to the track offset can be detected as discussed in Section 2.5.2. Assuming that the readback process is linear

and the read sensor is narrower than the track width, the readback servo signal is a linear combination of the series of dipulses with two major frequency components at any one time for the case of FESP. A simplified method of DFT algorithm can be used to extract the amplitude of each of these frequency components and generate PES, by extracting only the respective fundamental frequency of each servo frequency.

The estimated amplitude of servo burst of frequency F1 is

$$\begin{aligned} B_1 &= \sum_{n=1}^{N*C} S_1(n) e^{-j2\pi(n-1)/N}, \\ &= \sum_{n=1}^{N*C} S_1(n) cos(2\pi \frac{n-1}{N}) - j \sum_{n=1}^{N*p} S_1(n) sin(2\pi \frac{n-1}{N}), \\ &= B_{1real} - jB_{1img}, \\ |B_1| &= \sqrt{(B_{1real})^2 + (B_{1img})^2}, \end{aligned} \tag{3.24}$$

and the estimated amplitude of servo burst of frequency F2 is

$$\begin{aligned} B_2 &= \sum_{n=1}^{N*C} S_2(n) e^{-j2\pi(n-1)/N}, \\ &= \sum_{n=1}^{N*C} S_2(n) cos(2\pi \frac{n-1}{N}) - j \sum_{n=1}^{N*p} S_2(n) sin(2\pi \frac{n-1}{N}), \\ &= B_{2real} - jB_{2img}, \\ |B_2| &= \sqrt{(B_{2real})^2 + (B_{2img})^2}, \end{aligned} \tag{3.25}$$

where $S_1(n)$ and $S_2(n)$ are the re-sampled servo signals according to N sampling points per cycle ($C$) of the servo burst frequencies F1 and F2, respectively. The normalized coefficients are determined as

$$|B_{n1}| = \frac{|B_1|}{|B_1| + |B_2|}, \tag{3.26}$$

and

$$|B_{n2}| = \frac{|B_2|}{|B_1| + |B_2|}. \tag{3.27}$$

Similar to the previous demodulation techniques, the position error can be computed as

$$PES_{DFT} = \frac{|B_{n1}| - |B_{n2}|}{|B_{n1}| + |B_{n2}|} \tag{3.28}$$

where $PES_{DFT}$ is the measured off-track result with respect to the center of the servo track.

## 3.3 Simulation Results of Digital PES Generation

Based on the modified digital PES demodulation algorithms for the FESP discussed in the previous section, the resultant PES are computed using MATLAB. Simulation of 21 sets of servo signals from -50% to +50% of the track in an interval of 5% are recorded. The ideal $PES_{ip}$ and $PES_{qp}$ functions across the tracks using equations (3.24) - (3.28), are as shown in Figure 3.10.

In this thesis, the MATLAB $FFT$ function is used for the simulation which is based on the FFTW library [24].

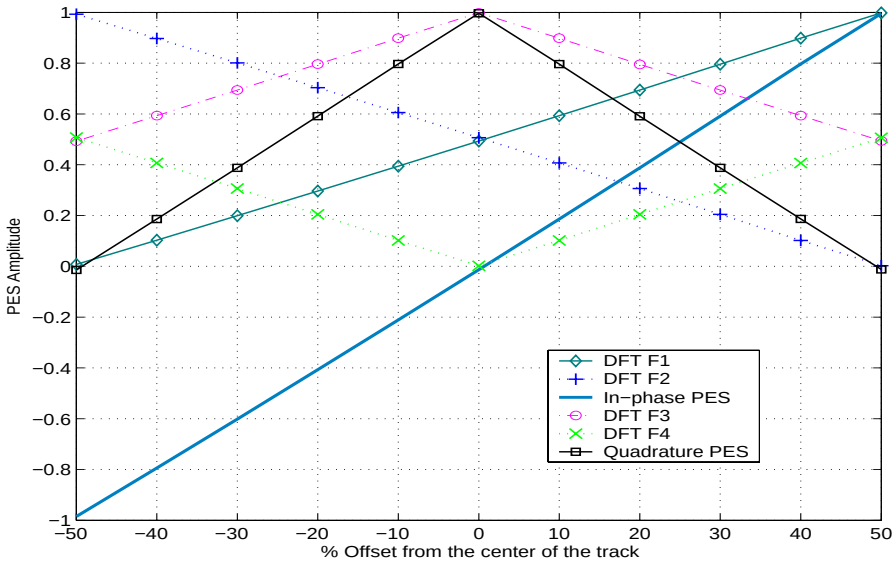


Figure 3.10: Ideal in-phase and quadrature PES for quadrature frequency-encoded servo pattern.

### 3.3.1 PES Linearity and Synchronization Error

Figure 3.11 shows the corresponding PES results from the simulated lorentzian servo signals using MATLAB $FFT$ function.

The frequencies of the servo patterns are 10 MHz and 20 MHz. However, from the simulation results, the resultant PES is not a linear function. This is due to the leakage of the spectral components away from the correct frequency, resulting in an undesirable modification of the total spectrum.

One solution is to multiply the sampled signals by a window function (called 'windowing') to suppress glitches and so avoid the broadening of the frequency spectrum caused by the glitches [40]. To illustrate the effect of windowing, the

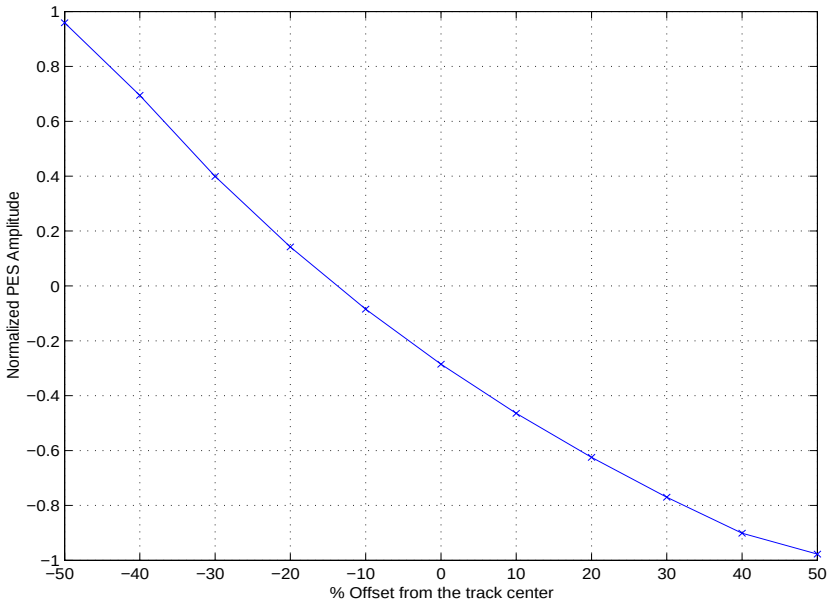


Figure 3.11: Resultant PES from FFT computation for 1024 points at 1 GS/s.

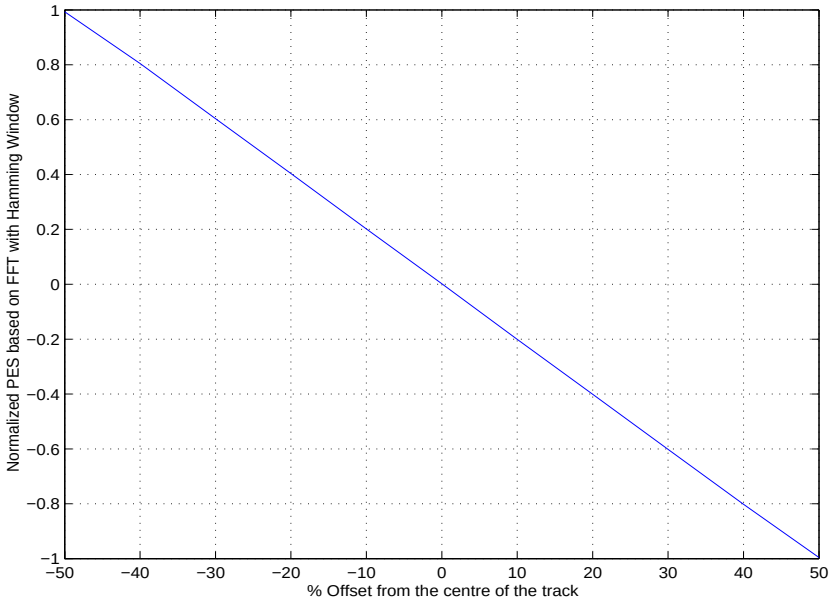


Figure 3.12: Resultant PES from FFT computation with Hamming window for 1024 points at 1 GS/s.

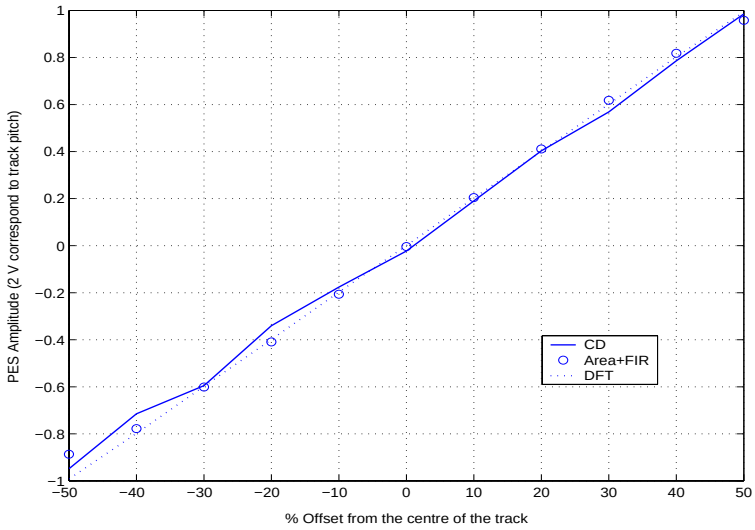


Figure 3.13: Simulated PES generation of dual frequency servo pattern with synchronization error (solid line - coherent detection, circle - FIR filter with area detection and dotted line - simplified DFT-based detection).

analysis is repeated using a hamming window as in Figure 3.12. With windowing, the linearity of the resultant PES is greatly improved.

When a random synchronization error is added to the computation of PES detection scheme, by computing the servo signal at different points of the sampled data, it can be seen from Figure 3.13 that there is slight non-linearity for CD technique. Besides the advantages of better noise immunity, immunity to baseline shift, thermal asperities, and baseline popping effect [2] [69], in the simulation, it was found that different combination of the dual servo pattern in terms of frequency ratio and phase-shift, will result in different quality of the PES. For CD method, the mixing signal must be precisely synchronized with the modulated signal, oth-

erwise significant error will occur. In reality, there is difficulty in actual writing of synchronized servo pattern. The error is about 0.4% for coherent demodulation as compared to the simplified DFT method by getting the sine and cosine coefficients of the fundamental servo frequency.

The result shows similar PES for all the different digital demodulation techniques as in the case of the conventional quadrature servo demodulation with the DFT algorithm producing the most linear PES function of all.

### 3.3.2 Demodulation Noise

A study on the effect of SNR is performed, where AWGN is added to simulate the servo signal at a SNR range from 5 dB to 30 dB with sigma, $\sigma = 1$ and mean = 0. The calculated errors between the resultant PES and ideal PES (without noise) are based on the average of 10 times from 21 servo data sets ranging from -50% to +50% offset from the track center. Different methods of digitization algorithms like DFT/FFT with and without windowing are investigated. From Figure 3.14, FFT without windowing has larger error as compared to FFT-based PES generation with windowing from 15 dB onwards.

The FFT algorithm with hamming window and simplified DFT have the minimum error of all, for SNR above 15 dB as shown in Figure 3.14. The simplified DFT algorithm based on individual fundamental servo frequency, does not suffer from the leakage effect and has higher noise immunity.

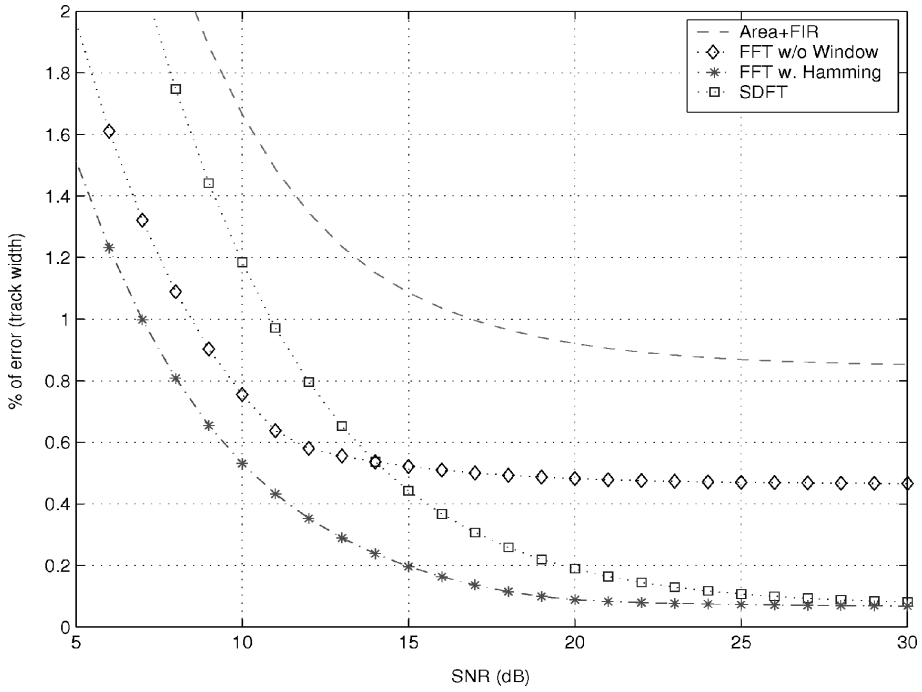


Figure 3.14: PES $\sigma$ error versus SNR based on simplified DFT, FFT, FFT with Hamming window and area detection techniques.

Table 3.2: Comparison of PES generation error

| Detection Method | Mean (% of track) | Variance (% of track) |
|---|---|---|
| Area + FIR | 0.7902 | 0.0896 |
| FFT w/o Window | 0.5091 | 0.0701 |
| FFT w Hamming Window | 0.0846 | 0.0248 |
| Simplified DFT | 0.0730 | 0.0071 |

Table 3.2 shows the mean and variance of PES error based on the various methods of detection. The error is calculated based on the PES values at the track center for an average of 1000 times. The simplified DFT has the least error, followed by the FFT with windowing, in this case Hamming window, FFT without windowing, and the last of all, the area detection detection with high-order FIR filters as can be seen from Table 3.2. Simplified DFT-based demodulation method is found to be superior as compared to the conventional amplitude demodulation scheme for decreasing the narrow track edge effect and adjacent pattern jitter effect.

### 3.3.3 Coding Efficiency

The requirements of processing power and computation time are as critical as the accuracy of obtaining the head position. These factors usually affect the decision of the manufacturers and the feasibility of any PES scheme adopted.

Assuming dual frequency servo pattern of 80 sample points, a comparison in terms of the number of complex additions and multiplications is tabulated in Table 3.3. For FFT radix-2 without windowing, the sampled data points are padded with zeros to increase the length to 128 points. In the case of the simplified DFT-based computation of PES from dual frequency servo pattern, only complete cycles of each servo fields are captured and the magnitude of the fundamental frequency component of each servo frequency pattern are computed for efficiency.

Thus as can be seen, the amount of data points needed for the simplified DFT

Table 3.3: Number of computations for 80 sample points

| Detection Method | No. of Complex Additions | No. of Complex Multiplications | No. of Square Root Function |
|---|---|---|---|
| FFT Radix-2 w/o windowing | 506 | 253 | 80 |
| Conventional DFT | 6320 | 6400 | 80 |
| Simplified DFT | 160 | 160 | 2 |

computation is greatly reduced by at least 97% and 37% as compared to getting the whole range of frequency components using conventional DFT and Radix-2 FFT algorithms, respectively. Although FFT method is less computational intensive than the conventional DFT method, additional windowing is needed to reduce the leakage error and zeros padding may be needed to perform the computation, which will increase the computation complexity.

From the simulation results, it can be seen that when synchronization becomes an issue, the DFT method is superior as compared to coherent detection in minimizing the effect of phase-shift. In addition, by computing only the magnitude of the fundamental frequency of the servo pattern, the coding is more efficient as compared to using the conventional DFT or FFT methods. Furthermore, the sine and cosine coefficients can be computed and stored or a look-up table could be used as an approximation to further reduce the unnecessary computation time

for practical application. The PES obtained with the simplified DFT-based PES detection technique is found to be more robust and more effective in rejection of noise.

In this thesis, the simplified DFT-based PES detection technique will be investigated and implemented to study the feasibility of this scheme.

## 3.4 Experimental Investigation

Experimental investigations are carried out to verify the simulation results. Different frequency servo patterns are written on a spin stand. Both discrete Fourier transform and coherent detection methods are then performed on the servo burst signal data collected off-line to generate the position error signal.

### 3.4.1 Experimental Setup

An experiment is performed on the $Guzik^{TM}$ spin-stand (Model : S-1701B) [29] using a 2.5" disk and an MR head to verify the feasibility of the proposed dual frequency servo pattern. The readback servo signal is collected off-line using the Lecroy digital oscilloscope. This Guzik spin stand together with Read-Write Analyzer (RWA 2585S) and Lucent read/write channel are also used for the support of reader servo implementation as in Chapter 4. The Guzik spin stand system and the screenshot of its operating program (WITE32) are as shown in Figure 3.15 and

Figure 3.16, respectively.

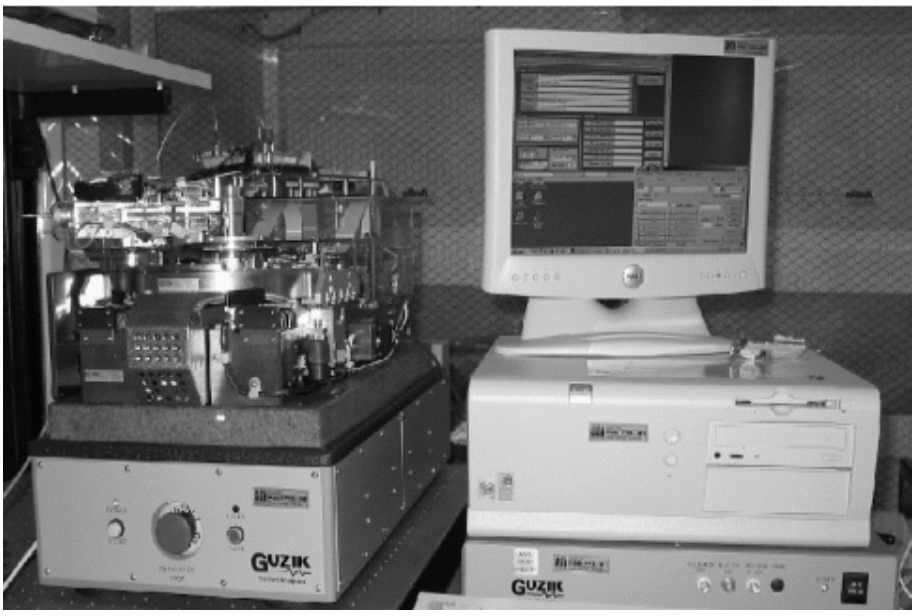


Figure 3.15: Guzik S-1701B micro-positioning spin stand.

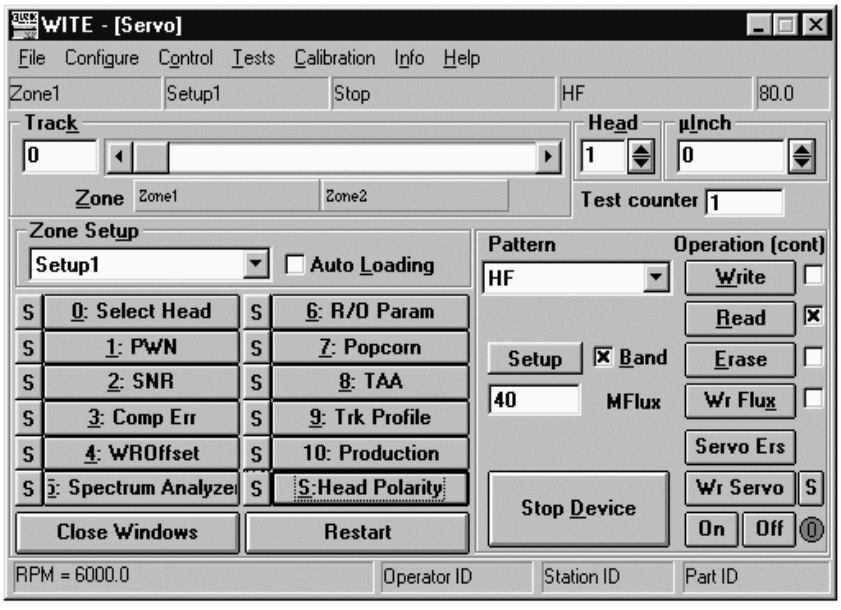


Figure 3.16: Screenshot of WITE32 - GUI program for Guzik spin stand.

As the write head is typically wider than the read head, a partial erasure method is used to write a narrower track width. The first track is written at an alternating magnetization of frequency F1 and the track width is initially about the width of the write head. Next, the head is positioned off-track which is about the width of the read head and an alternating magnetization at frequency F2 is written on the media. A portion of the first track will be overwritten to the point where the first track width is approximately about the width of the read head. The subsequent tracks are written in the same way at a different frequency. In this way, the track pitch can be narrower up to about the width of the read head.

Five tracks are written with different frequencies servo pattern. The width of the writing element is about 0.42 $\mu m$ and the width of the reader sensor is about 0.25 $\mu m$. The ease of decoding the multiple frequencies servo patterns, will pave the way for higher track density. Using a partial erasure servo writing method, the tracks are written at 100 kTPI (track pitch = 0.254 $\mu m$). However, due to the limitation of the width of the read head available during the experiment, satisfactory results can only be obtained for up to about 100 kTPI after which the effect of adjacent tracks become significant [65].

### 3.4.2 Comparison of PES Detection Techniques

The readback servo signals at different cross track position are monitored and saved using the Lecroy digital scope at an interval 5% offset for a total of 41 sets of data. Figure 3.17 shows the readback signal when the head is along the centre of the

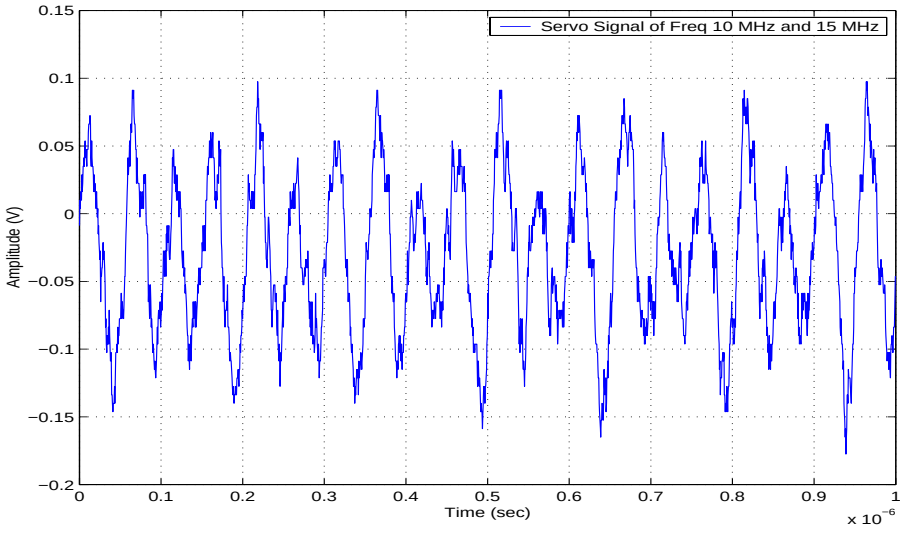


Figure 3.17: Readback servo signal at center of 10 MHz and 15 MHz servo bursts.

dual frequency servo pattern. Following this, the PES is calculated off-line, using (2.8) - (2.9), with 8 cycles of servo bursts taken for computation. Figure 3.18 shows the frequency strength of servo signal across the track and the resultant PES.

From Figure 3.17 where the servo frequencies are of ratio 1:1.5, the readback signal seems to be slightly noisy. This could be due to the writing inaccuracy or external noise due to defects from media or electronics circuitry. However, this does not affect or reduce the performance of the resultant cross-track PES computed as can be seen from Figure 3.18.

Other set of servo pattern with different dual frequency ratio have also been written. The readback servo signal at the center of 10 MHz and 20 MHz servo fields is shown in Figure 3.19. Its resultant PES across the tracks is shown in

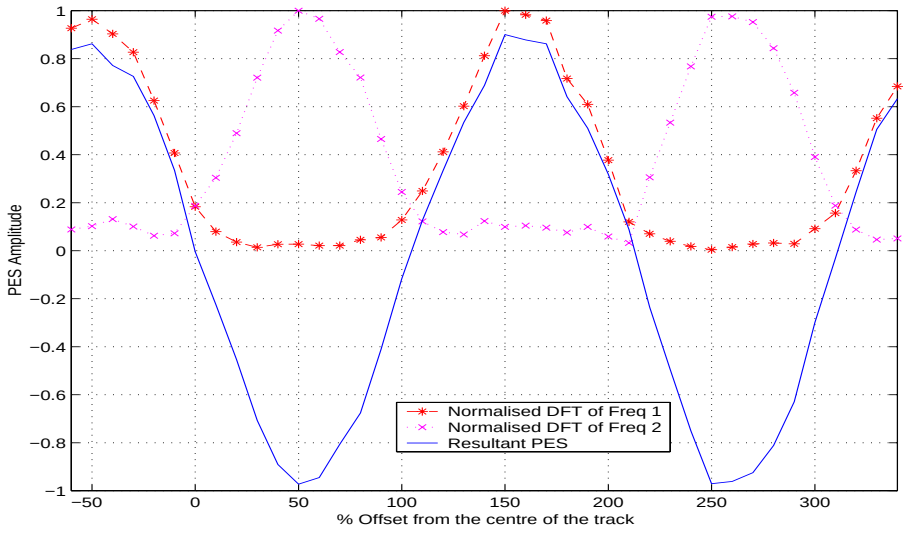


Figure 3.18: Resultant simplified DFT-based PES of servo frequency pattern (ratio 1:1.5).

Figure 3.20. The experimental servo signal in Figure 3.19 resembles the simulated servo signal at track center with frequency components of 10 MHz and 20 MHz in Figure 3.7 except for slight distortion. This could be due to the following factors. Firstly, the tracks on the disk surface are circular and thus, there is a slight skew angle between the head and the data track. In the experiment, the skew angle is assumed to be 0 by writing the tracks at around the middle diameter (MD) location. Secondly, in the experiment, no clock head is available for the writing of the servo patterns. In addition, the simulations do not take into account the effect of write-read offset error [66].

So far, the experimental result shows satisfactory PES for frequency ratios of 1.5 and 2. In addition, the simulated servo signals are also found to be comparable

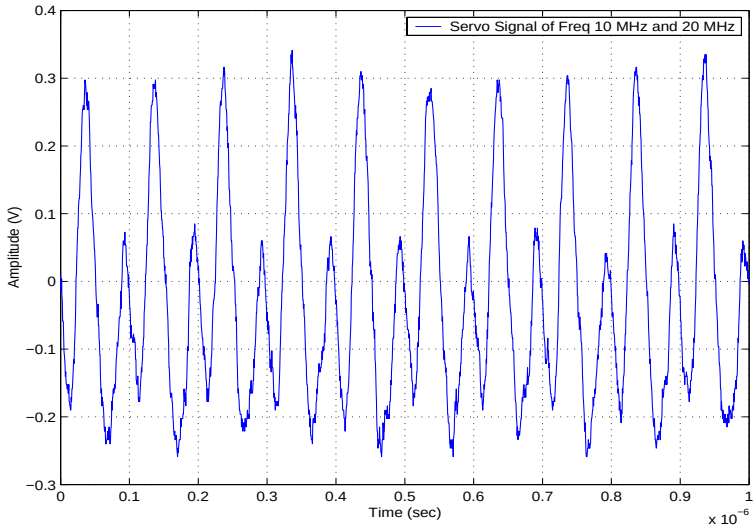


Figure 3.19: Readback servo signal at center of 10 MHz and 20 MHz servo bursts.

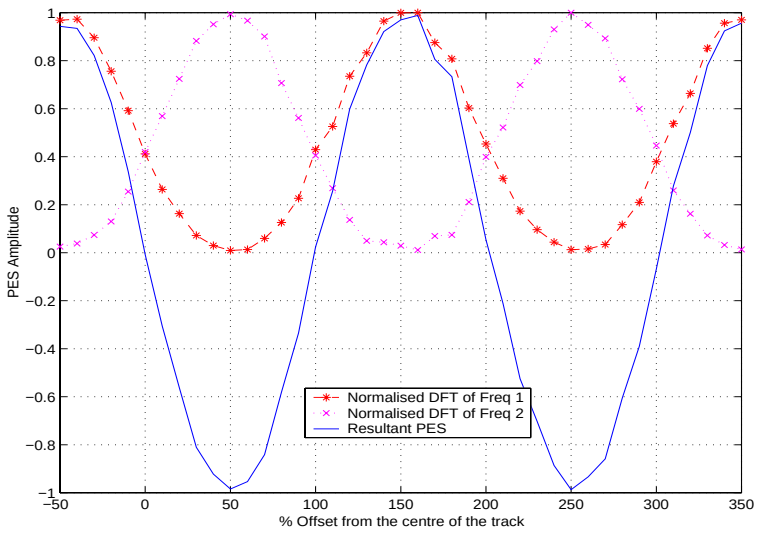


Figure 3.20: Resultant DFT-based PES of servo frequency pattern (ratio 1:2).

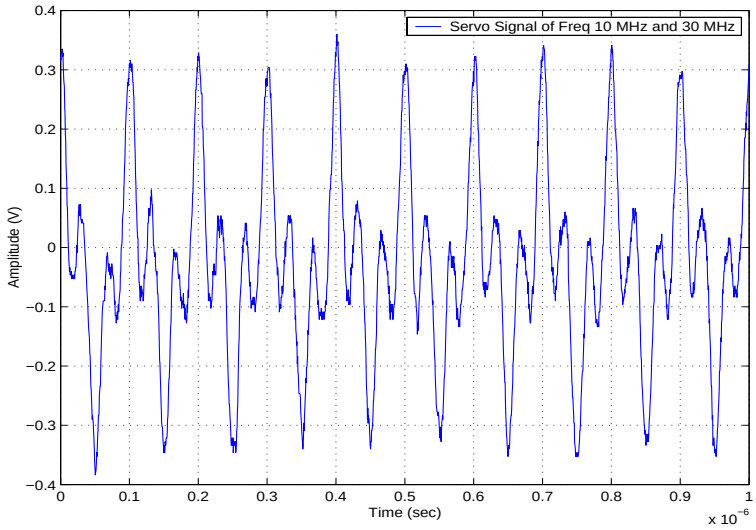


Figure 3.21: Readback servo signal at center of 10 MHz and 30 MHz servo bursts.

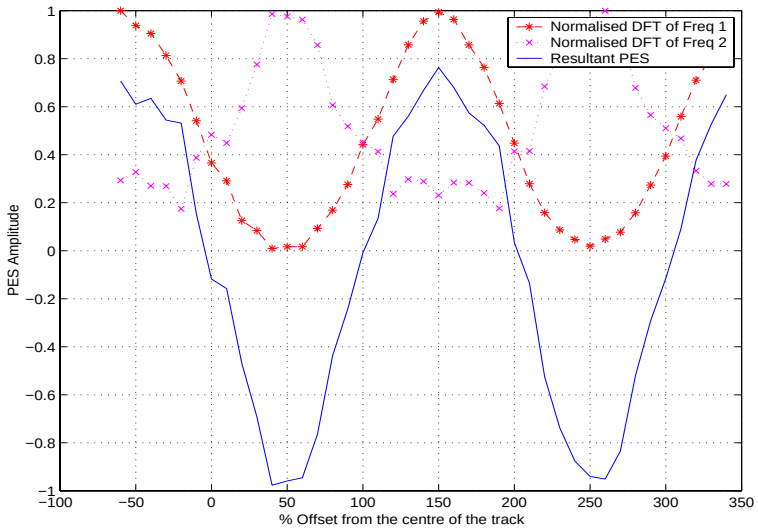


Figure 3.22: Resultant DFT-based PES of servo frequency pattern (ratio 1:3).

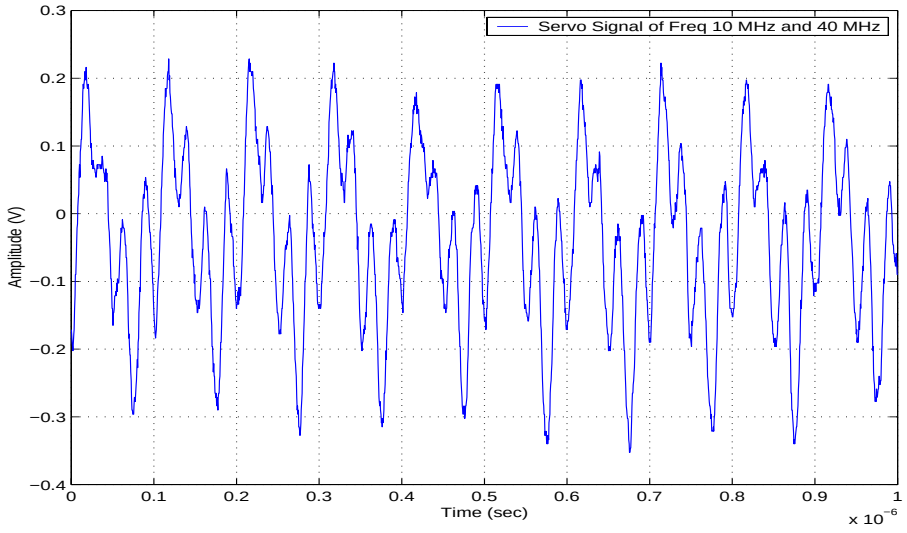


Figure 3.23: Readback servo signal at center of 10 MHz and 40 MHz servo pattern.

to the actual servo signals. However, with servo pattern of dual frequency 10 MHz and 30 MHz, the positive and negative peaks within the resultant PES profile are not symmetrical as can be seen from Figure 3.22. With servo pattern of frequency 10 MHz and 40 MHz, the resultant PES profile as can be seen in Figure 3.24, does not have the asymmetry effect. These results verified the existence of odd harmonics components of the readback signal [66]. In other words, the spectrum of the readback signal contains the frequencies $nf$ for $n$ = 1,3,5,.... Thus, to avoid inaccurate computation of the servo bursts, the frequency of the servo pattern chosen, should not be of any odd harmonics of the lowest frequency servo pattern.

Besides the dual frequency servo pattern written, three servo patterns of frequencies where F1 = 6 MHz, F2 = 8 MHz and F3 = 10 MHz are also created as illustrated in 3.2. The cross-track PES profiles between F1 and F2, F2 and F3

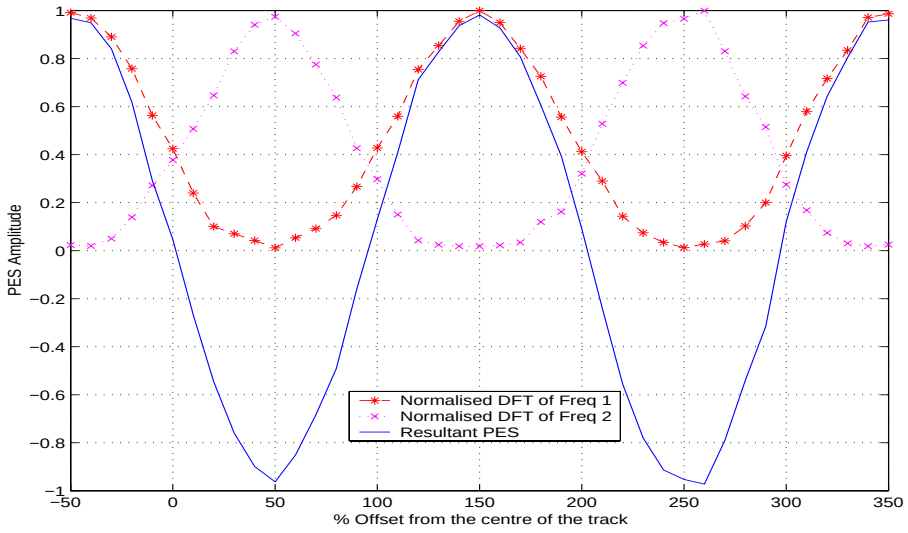


Figure 3.24: Resultant DFT-based PES of servo frequency pattern (ratio 1:4).

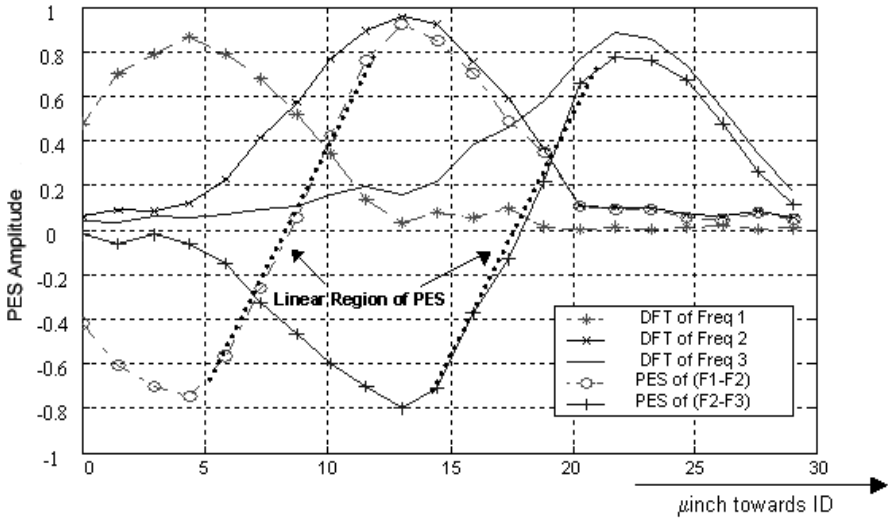


Figure 3.25: Experimental PES generation of multiple-frequency servo pattern.

are computed using (3.24)-(3.28) and as shown in Figure 3.25. With the different frequency components at the adjacents tracks, the drifting direction can be can be

identified easily. The linear portion of the two computed cross-track PES functions are combined to get the position error between the head and media.

It can be seen that the experimental PES functions are similar to that of the simulated PES functions in Section 3.3. However, due to the vibrations within the experimental setup and writing process, there are some variations in the width of the written tracks. Thus, the zero crossing points indicating the centers of the tracks are not at exactly 10 $\mu$inch apart. This necessitates to the improvement of the spin stand which is the subject of next chapter.

## 3.5 Summary

Frequency-encoded servo pattern (FESP) allows the reduction of servo pattern overhead by 50% and more tracks to be squeezed within the same disk space. The results also indicate that 100 kTPI (with a track width of 0.254 $\mu m$) FESP can be written using the partial erasure method. Digital demodulation of the FESP technique is used to decode the PES. From the simulation and experiments conducted, the Fourier transform algorithm is found to work reasonably better as compared to digital area demodulation and CD techniques. The PES processing based on the simplified DFT algorithm has higher noise immunity as compared to the digital area demodulation method [10] and effect of synchronization error has less impact on the computation error. In addition, by getting only the fundamental harmonics of the FESP, it is more computation efficient than the conventional DFT/FFT

algorithms. Thus, combination of FESP and the simplified DFT-based detection scheme allows computation efficiency and high flexibility in signal processing, together with reducing the position sensing noise in terms of additive noise and synchronization error.

# Chapter 4

# Implementation of Reader Servo System on a Spin Stand

For the demonstration of achieving ultra-high recording density, highly precise and efficient servomechanism is needed to position the transducer with respect to the media on the commercial spin stand. In this chapter, improvement of the capability of an existing spin stand is performed by implementing an external servo system on a Personal Computer (PC) to achieve higher accuracy and disturbance rejection for precise tracking. A combined multiple frequencies servo encoding and simplified DFT-based decoding scheme is used to generate the PES which is fed back to the servo controller for real-time track following operation. A modified head cartridge base with a sub-nm resolution piezo actuator is used as the positioning device to support higher track density demonstration on the spin stand.

## 4.1 Implementation Setup

Combined efforts from the mechanical structure and electronics system are required to support the heads and media on the commercial spin stand for demonstration of higher TPI [72]. The latest model of Guzik system (Model S1701B) [29] is used for the demonstration of DSI's heads and media capabilities. The Guzik system provides the ease of writing different frequencies servo pattern on the media and measurement of the various properties of the read/write heads and media.

In the servo system, the measured PES is the only feedback to the servo controller to indicate the displacement of the read/write heads with respect to the track on the disk, from which a corrective signal is generated to minimize the error. In this implementation setup, the servo control system consists mainly of a personal computer (PC), a high sampling rate digitizer card (Acqiris DP210) [8] and a multi-functional I/O card (PCI NI-MIO 16E1) [48], which are used for the signal processing of the servo information and reader servo controlling. The block diagram of the system architecture is as shown in Figure 4.1. The processing of the position signal is performed on the digitized readback signal from the pre-amplified transducer in real-time using the PC, and the computed measurement is then fed to the servo controller for thermal drift elimination and track following operation.

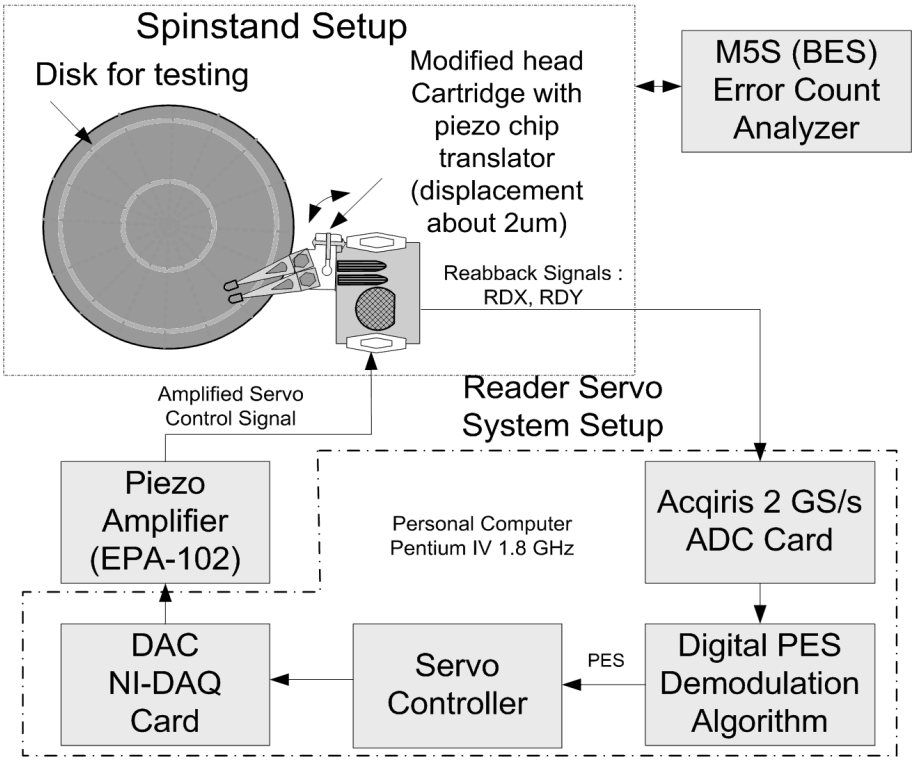


Figure 4.1: Reader servo system architecture.

## 4.2 PES Formulation

In this implementation, frequency-encoded servo scheme, as shown in Figure 4.2, is used for the servo pattern layout on the spin stand.

With the proposed servo pattern, the readback servo signal is a linear combination of the series of dipulses at two different frequencies at any one time, assuming a linear readback process and the transducer is less than 2 times the width of the servo track. Simplified DFT algorithm as discussed in the previous chapters is used in this setup to extract the amplitude of each of these frequency components and generate the PES.

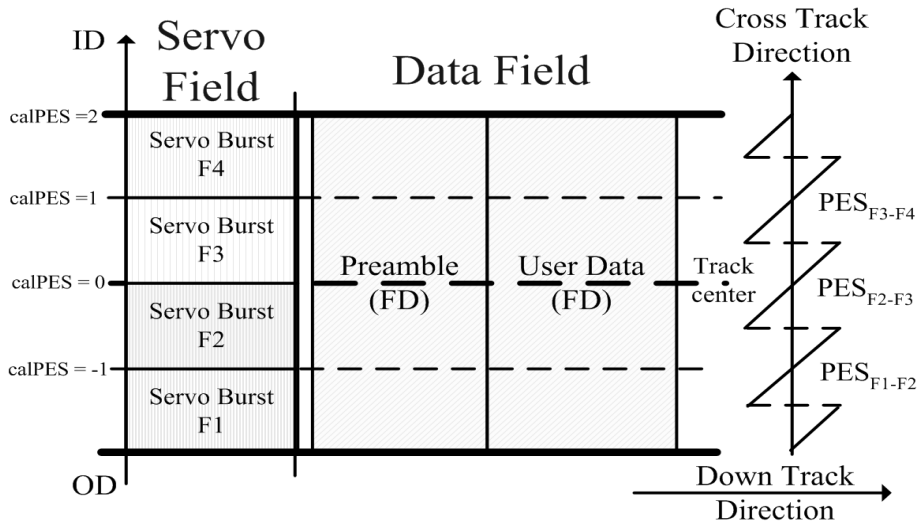


Figure 4.2: Multiple frequencies servo burst pattern.

### 4.2.1 Calibration of PES

To overcome the inability to write quadrature servo pattern at half-track using the current setup, multiple frequencies servo pattern written at narrower track pitch is suggested. With more frequencies written, the linear portion of each individual position signal can be combined to make the linear servo control range wider and decrease the mis-positioning due to overshooting at the final access stage.

In this setup, due to the maximum displacement provided by the modified head cartridge with piezoelectric (PZT) element, which is about 140 $\mu$inch and system limitations, servo patterns of four different frequencies are written on the 2.5" magnetic disk to represent four servo tracks of 10 $\mu$inch for demonstration of track following operation. These frequency servo patterns are selected based on the investigation and analysis of computation noise which will be discussed in the

next section.

Each of the individual servo frequency components is extracted using (3.24) and (3.25) to form the individual $D_x$ of frequency $x$ components.

However, due to the difference in sensitivity of the read head at the different burst frequencies, the maximum magnitude of each individual $D_x$ are not necessarily same. In addition, the resultant waveform is affected by ISI, a well-known phenomenon contributed by close proximity of adjacent transitions on the disk. The effect of the ISI is manifested in reduction of burst amplitude. The resultant waveform may also appear as a sinusoid instead of the usual train of Lorentzian pulses for closely spaced transitions. These effects are more severe for the burst of higher frequency, resulting in different maximum amplitudes for the two bursts. The ISI also modifies the harmonic content of the burst waveform. The burst of higher frequency has less number of high frequency harmonics compared to the burst of lower frequency. The proposed detection method using DFT estimates the amplitude of the fundamental only, and the changes in the magnitude of the harmonics are considered negligible. Therefore, the magnitudes of each individual fundamental frequency components need to be calibrated and normalized to overcome the problem associated with ISI and frequency dependence of head-sensitivity.

$$
\begin{aligned}
D_{n1} &= \frac{|D_1|}{(|D_1| + |D_2| + |D_4|)} \\
D_{n2} &= \frac{|D_2|}{(|D_1| + |D_2| + |D_3|)} \\
D_{n3} &= \frac{|D_3|}{(|D_2| + |D_3| + |D_4|)} \\
D_{n4} &= \frac{|D_4|}{(|D_3| + |D_4| + |D_1|)}
\end{aligned} \tag{4.1}
$$

Another method is based on off-line calibration of the detection gains at the different frequencies, one frequency at a time. The calibration process starts with a pattern generated using a square wave write current of frequency equal to one of the burst frequencies. The read head is then placed at the center of the pattern so that the maximum amplitude is seen for the burst waveform. At this location, the amplitude is maximum for the frequency at which calibration is being carried out. The amplitude of the fundamental component is thus estimated from the samples of readback waveform using (3.24).

$$
\begin{aligned}
D_{n1} &= \text{max of } |D_1| \text{ for burst signal with frequency F1} \\
D_{n2} &= \text{max of } |D_2| \text{ for burst signal with frequency F2} \\
D_{n3} &= \text{max of } |D_3| \text{ for burst signal with frequency F3} \\
D_{n4} &= \text{max of } |D_4| \text{ for burst signal with frequency F4}
\end{aligned} \tag{4.2}
$$

Using (4.1) or (4.2), each individual frequency components, $|D_x|$ where x = 1,2,3,4, is normalized and Figure 4.3 shows the individual normalized frequency components, $D_{n1}$ of F1, $D_{n2}$ of F2, $D_{n3}$ of F3 and $D_{n4}$ of F4 using DFT detection technique.

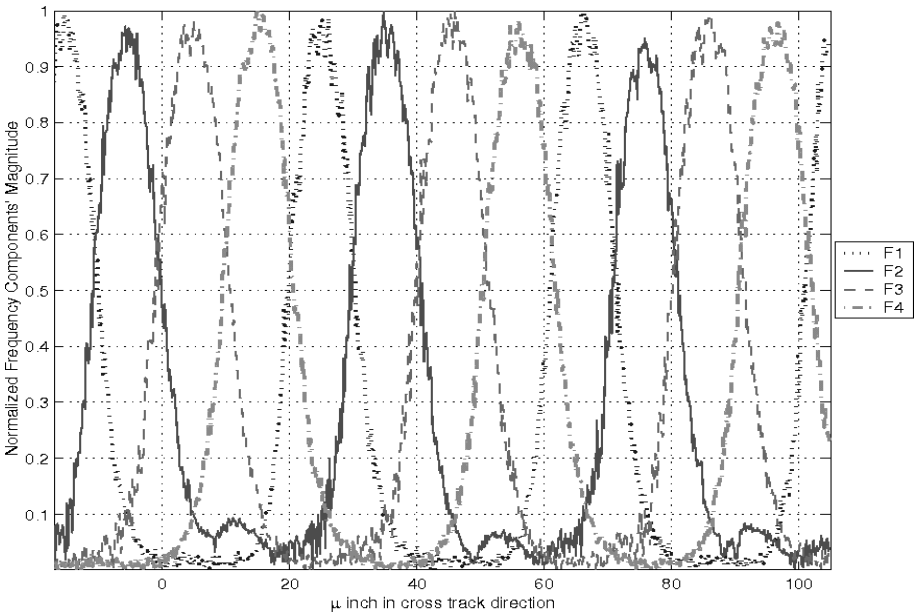


Figure 4.3: Normalized DFT of servo pattern F1, F2, F3 and F4.

These individual DFT components of the servo pattern are calibrated and combined to determine the position offset error and fed into the servo controller. The calibrated PES, $P_{cal}$ is formed by combining the valid region of each individual dual frequency PES, $P_{nf}$ where f = 1,2,3,4 as follows:

$$\begin{aligned} P_{n1} &= \frac{(D_{n1} - D_{n2})}{(D_{n1} + D_{n2})} \\ P_{n2} &= \frac{(D_{n2} - D_{n3})}{(D_{n2} + D_{n3})} \\ P_{n3} &= \frac{(D_{n3} - D_{n4})}{(D_{n3} + D_{n4})} \\ P_{n4} &= \frac{(D_{n4} - D_{n1})}{(D_{n4} + D_{n1})} \end{aligned} \tag{4.3}$$

$$P_{cal} = \begin{cases} -sP_{n1} - s1; & C_1 \text{ satisfies} \\ -sP_{n2} + s2; & C_2 \text{ satisfies} \\ -sP_{n1} - s1; & C_3 \text{ satisfies} \\ -sP_{n2}; & C_4 \text{ satisfies} \\ -sP_{n2}; & C_5 \text{ satisfies} \\ -sP_{n3} + s1; & C_6 \text{ satisfies} \\ -sP_{n4} + s2; & C_7 \text{ satisfies} \\ -sP_{n3} + s1; & C_8 \text{ satisfies} \\ invalid & \text{none of the above} \end{cases} \tag{4.4}$$

where $s1 = 1$ and $s2 = 2$ are the PES values with respect to the track center for calibration. Since 1 unit is chosen to correspond to 1 track width, the *scale* factor, $s$ is set to be 0.5 as the individual PES ranges from -1 to 1. The conditions are given as

$$C_1 = (D_{n1} > (D_{n2} \& D_{n3} \& D_{n4})) \& (D_{n2} > D_{n4}) \tag{4.5}$$

$$C_2 = (D_{n1} > (D_{n2} \& D_{n3} \& D_{n4})) \& (D_{n2} < D_{n4}) \tag{4.6}$$

$$C_3 = (D_{n2} > (D_{n1} \& D_{n3} \& D_{n4})) \& (D_{n1} > D_{n3}) \tag{4.7}$$

$$C_4 = (D_{n2} > (D_{n1} \& D_{n3} \& D_{n4})) \& (D_{n1} < D_{n3}) \tag{4.8}$$

$$C_5 = (D_{n3} > (D_{n1} \& D_{n2} \& D_{n4})) \& (D_{n2} > D_{n4}) \tag{4.9}$$

$$C_6 = (D_{n3} > (D_{n1} \& D_{n2} \& D_{n4})) \& (D_{n2} < D_{n4}) \tag{4.10}$$

$$C_7 = (D_{n4} > (D_{n1} \& D_{n2} \& D_{n3})) \& (D_{n3} > D_{n1}) \tag{4.11}$$

$$C_8 = (D_{n4} > (D_{n1} \& D_{n2} \& D_{n3})) \& (D_{n3} < D_{n1}) \tag{4.12}$$

For example, in condition, $C_1$, if the $D_{n1}$ value is greater than $D_{n2}$, $D_{n3}$, and $D_{n4}$

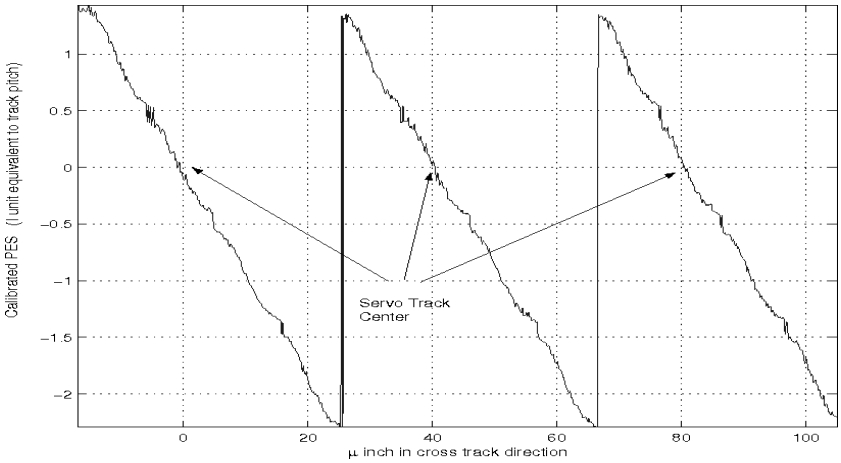


Figure 4.4: Normalized PES profiles.

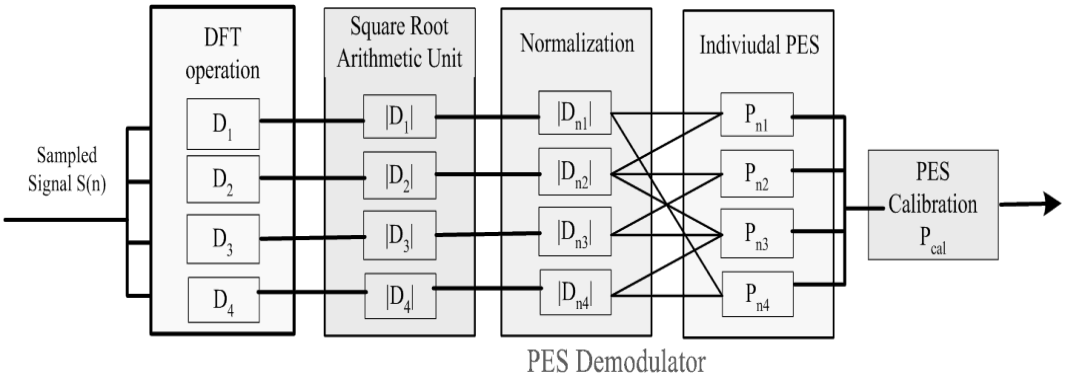


Figure 4.5: Block diagram of PES generation and calibration process.

values and the value of $D_{n2}$ is also greater than $D_{n4}$ value, then the offset position of the head with respect to the track center (between servo tracks of F2 and F3) is in the range of 1.5 track to 0.5 track in the OD direction.

Based on (4.4), the extended PES is as shown in Figure 4.4. An overview of the PES demodulation process is as shown in Figure 4.5

### 4.2.2 Computation Speed and PES Noise Analysis

To get the optimal demodulation results, the sensing noise needs to be minimized. There are several components that can contribute to the computation noise, namely (1) quantization, (2) truncation error, (3) computation algorithm and (4) implementation of averaging. In the following subsections, each of these contributing factors is investigated to determine an optimal servo pattern and computation method for satisfactory PES generation.

#### ADC Quantization Error

The ADC requirements are different in data and servo fields. The data detectors usually demand for higher sampling clock rate, whereas the PES estimators demand finer ADC resolution to minimize the quantization error. However, in the implementation, the digitizer card that is being currently used is an ADC system with only 8 bits of vertical resolution (256 levels) in which the dynamic range of the ADC covers the Full Scale Range (FSR) of the input voltage setting. As can be seen from Figure 4.6, for different FSR setting, the $3\sigma$ error increases proportionally as the FSR is increased. In other words, as the ADC resolution decreases, the effect of quantization noise increases.

For example, if the input voltage is set to 1 V, the ADC resolution is equivalent to 3.9 mV. Given that the magnitude of the pre-amplified readback signal from the current media and head used is usually about 100 mV - 300 mV, to obtain the

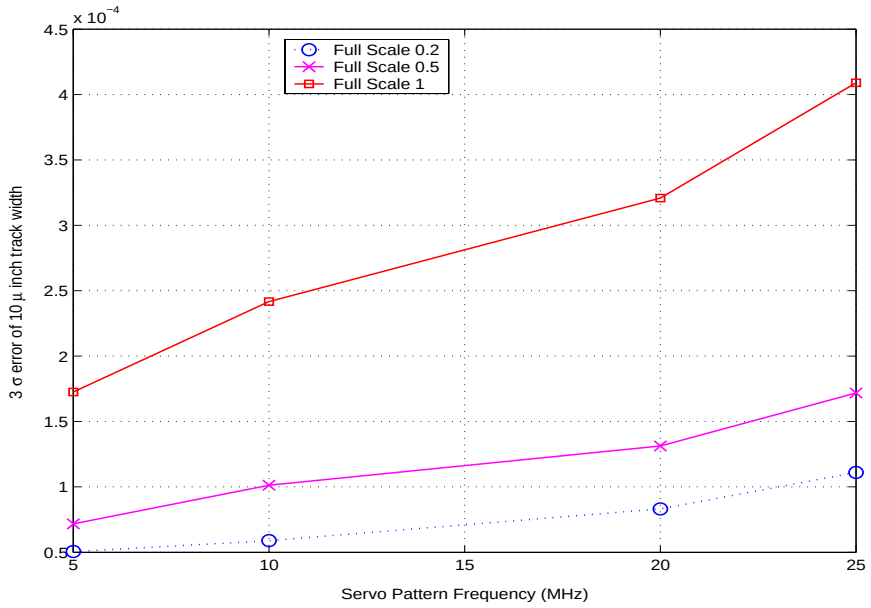


Figure 4.6: Computational noise due to quantization errors (Full Scale Range).

best dynamic range from the ADC, the FSR is set at 0.5 V (that is $\pm$ 0.25V) with the ADC resolution equivalent to 2 mV.

### Servo Burst Frequency and Magnitude

Four different frequencies of 25 MHz, 20 MHz, 10 MHz and 5 MHz are written on the media and sampled at 0.5 GS/s. The readback digitized servo signal is processed by the simplified DFT-based algorithm to determine the PES. The $3\sigma$ error is computed and as can be seen from Figure 4.6, higher $3\sigma$ error is measured from servo signal of higher frequency.

The main reasons are the ISI effect and superposition principle of the magnetic written data as discussed previously. The frequency chosen for writing the

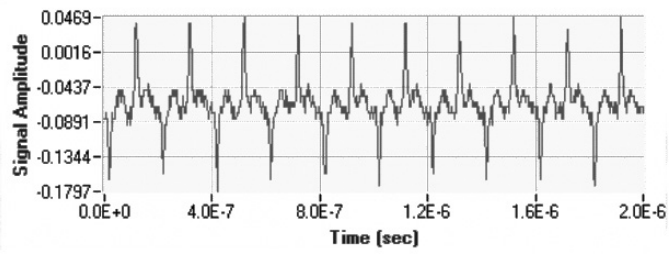


Figure 4.7: Readback signal of 5 MHz servo pattern.

servo pattern will also affect the computation noise. Figure 4.7 and Figure 4.8 show the readback signals of servo pattern with frequencies 5 MHz and 25 MHz, respectively. Depending on the parameters of the head gap, flying height, spacing between the head disk interface (HDI) and type of transducer and media used, the $PW_{50}$ is different. The amplitude of the output signal will begin to decrease due to ISI, at a transition density (directly related to linear recording density) which is inversely proportional to the pulse width. For the given $PW_{50}$, the transition density increases with increase in frequency. Thus, ISI increases leading to reduction in SNR as frequency increases. In the experiment setup, the $PW_{50}$ is found to be 50 ns. The track average amplitude (TAA) and the resolution between low frequency (LF) and high frequency (HF) burst waveform against the written transition density are as illustrated in Figure 4.9.

### Computation Cycle and Time Delay

The effect of using different number of cycles for computation is studied. Figure 4.10 shows the PES $3\sigma$ error versus the cycles taken for computation for four

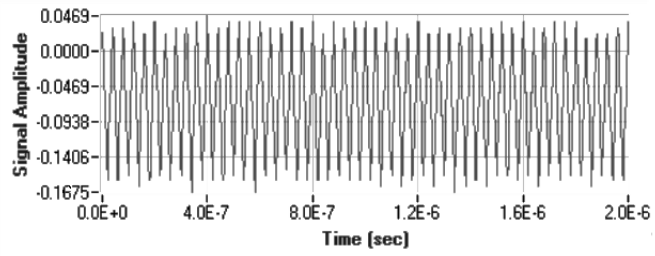


Figure 4.8: Readback signal of 25 MHz servo pattern.

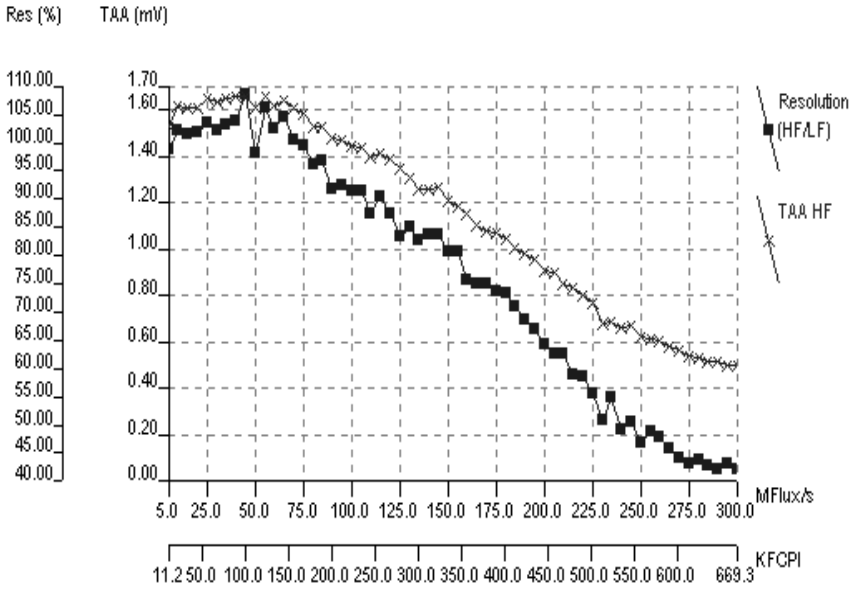


Figure 4.9: Signal amplitude and resolution plot as a function of signal frequency.

different servo frequencies of 5, 10, 20 and 25 MHz. As can be seen, the $3\sigma$ computation noise on a blank media is less than about 0.065 $\mu$inch for frequency less than 25 MHz with respect to track pitch of about 10 $\mu$inch. With the trade-off between $3\sigma$ error and cycles of servo burst needed for PES detection, optimal TMR can be achieved at the tangents of the slopes which are about 10 cycles of servo bursts and the resultant $3\sigma$ error is about 0.025 $\mu$inch.

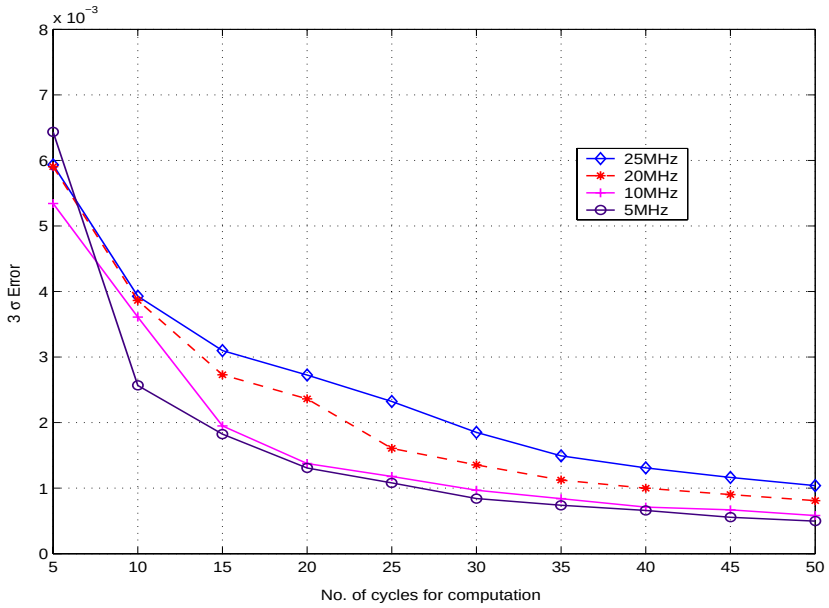


Figure 4.10: PES $3\sigma$ computation noise due to DFT computation.

The increase in the computation cycle for averaging will result in lower demodulation noise. However, there is a tradeoff to the minimization of demodulation noise, that is the additional time taken. This additional time taken to reduce the demodulation noise will add up to the total computation delay.

The computation delay is the time that it takes to process the PES, perform any necessary checks, calculate the desired control signal and output to the actuator to adjust the head's position. This will result in lower PES sampling rate and in turn create difficulty in designing and implementing a higher bandwidth servo controller due to loss of phase margin [67]. However, for initial controller design, since the specification for sampling frequency can be lower, the number of computation cycles can be slightly increased to 20 cycles to further reduce the sensing noise.

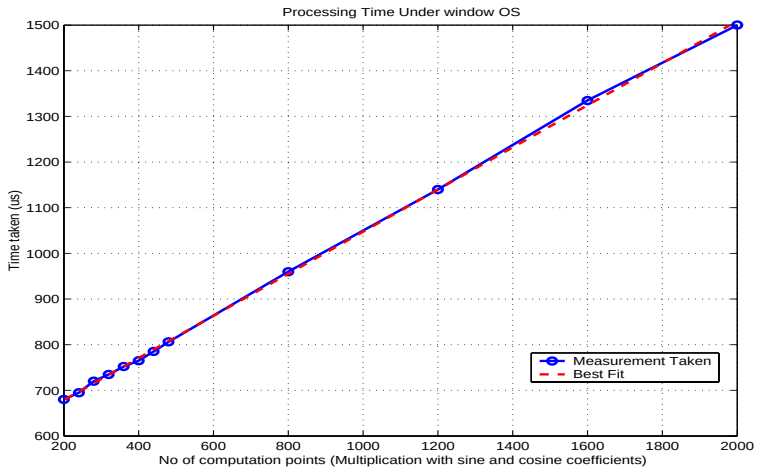


Figure 4.11: Overall execution time for DFT-based PES detection under Windows OS platform.

### Algorithm Optimization

The simplified DFT-based PES demodulation algorithm is a computationally intensive task as it consists of additions, multiplications and square root operations for the computation of each frequency magnitude, although the sine and cosine coefficients are computed and tabulated as a look-up table beforehand. For each additional frequency servo pattern needed for decoding, the amount of processing time taken increases proportionally as shown in Figure 4.11. More computationally efficient method of generating PES based on the Fourier Transform Theorem is needed, especially for more than three frequencies servo pattern.

The overall execution time includes the analog to digital conversion and acquisition time, PES demodulation algorithm, control algorithm and control signal output time. The processing time for the PES generation is proportional to the

number of data points taken for computation. Under Windows OS platform (Windows 98), each computation point, consisting of multiplication with cosine and sine coefficients, takes about 0.45 $\mu s$, whereas under Linux OS platform (Redhat Linux 7.2, Kernel 2.4.16), each computation point takes about 35 ns. Table 4.1 shows the breakdown of the approximate time taken for each component in the whole process.

The processing time is given by

$$T_p = S_{pts} * C_p * N_F * T_{mul} \tag{4.13}$$

where $S_{pts}$ is the number of samples in each period of servo frequency burst, $C_p$ is the number of period taken for computation, $N_F$ is the total number of servo frequencies pattern and $T_{mul}$ is the time taken for the multiplication of the exponential term per data point. In the implementation, this accounts for 1/3 of the overall execution time, for $S_{pts} = 10$, $C_p = 20$, $N_F = 4$ and $T_{mul} = 37.5$ ns under Linux OS, Pentium IV 1.8 GHz PC. With the current PC setup, the overall acquisition and execution time takes slightly about 85 $\mu s$ with $\pm 15$ $\mu s$ jitter. Thus, a maximum closed-loop feedback rate of 12 kHz can be attained.

## 4.3 System Integration

Due to the fix digitization rate provided by the digitizer card, precaution is taken to reduce the errors in sampling process. In the implementation, the acquisition rate is selected to be 0.5 GS/s, and the four different servo frequencies are chosen

Table 4.1: Breakdown of individual reader servo control program timing.

| **Sequence** | **Timing** ($\mu sec$) **in Window 98** | **Timing** ($\mu sec$) **in Linux** | **Remarks** |
|---|---|---|---|
| Start Acquisition | Don't care | Don't care | First Data |
| Readout | Don't care | Don't care | Transfer data |
| While(){ | | | |
| Read control parameters | $< 1$ | $< 1$ | For control |
| Read setpoint | 100 | 20 | For control |
| DFT Computation | 320 | 30 | For 20 cycles |
| calPES | 5 | $< 1$ | PES Calibration |
| Control | $< 1$ | $< 1$ | Controller |
| PES Output | 10 | 5 | PES Calibration |
| Control Signal Output | 10 | 5 | Controller |
| while(!done) | - | - | Wait Next sector |
| Readout | 310 | 15 | Data Transfer |
| } | | | Repeat Loop |
| Total | $880 \pm 50$ | $85 \pm 15$ | Total Time |

to be 31.25 MHz (62.5 MFlux/s), 25 MHz (50 MFlux/s), 20 MHz (40 MFlux/s) and 12.5 MHz (25 MFlux/s), which are divisors of the acquisition rate (500 MS/s). Additionally, as can be seen from the plot of signal amplitude against signal fre-

quency for the current setup in Figure 4.9, signals with frequency below 75 MFlux/s (or 37.5 MHz) have reasonably high and constant amplitude. As the current spin stand setup is required to support higher track density and speed is of less importance, more sampling points are taken for computation to minimize PES sensing noise and reduce the effect of quantization error. In addition, the main focus is to study the effect of varying sampling points and effectiveness of the PES generation scheme.

**Remarks:** Flux/s is the measurement unit for the number of transitions per second and Hertz is the measurement unit for the number of periodic waveform per second, which is also known as dipulse. The measurement of transitions in Flux is double the measurement in Hertz.

Using the Guzik spin stand, sets of FESP are written on the media, following which the user data are also written at the track center after a short time gap. The waveform of the servo and preamble signal is as plotted in Figure 4.12. The servo signal consists of two fundamental servo frequencies, whereas the data channel portion contains single frequency preamble signal for synchronization at the beginning of each data field. The spindle speed is set at 4000 RPM, that is 15 ms per revolution. The sampling interval is about 120 $\mu$s and there are 125 sectors per revolution. An external clock generator is used to trigger the PC-based reader servo system to acquire the servo signal and compute the PES at every sector.

Various parameters are configured and tuned to obtain an optimal servo frequency pattern and computation of parameters for a satisfactory reader servo con-

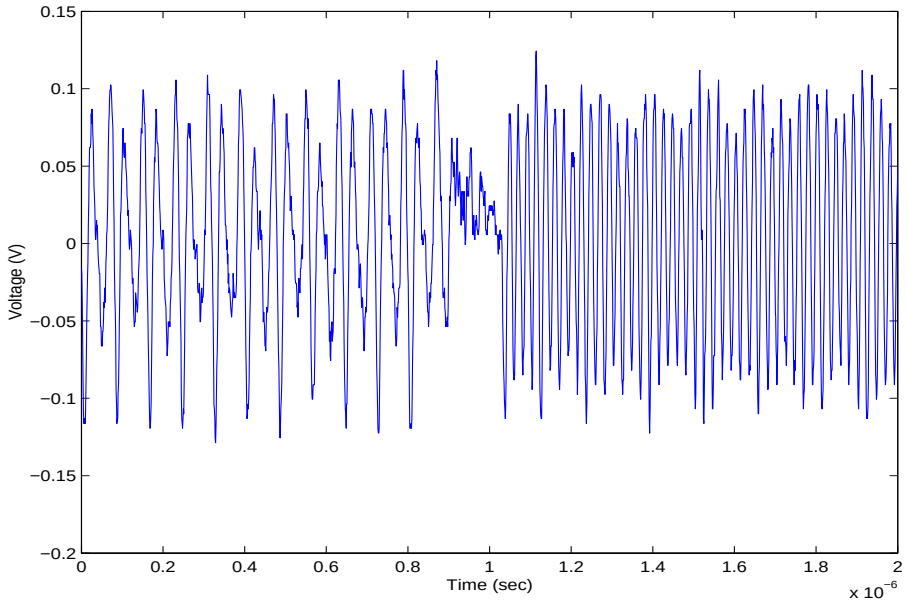


Figure 4.12: Readback signal of servo pattern and preamble.

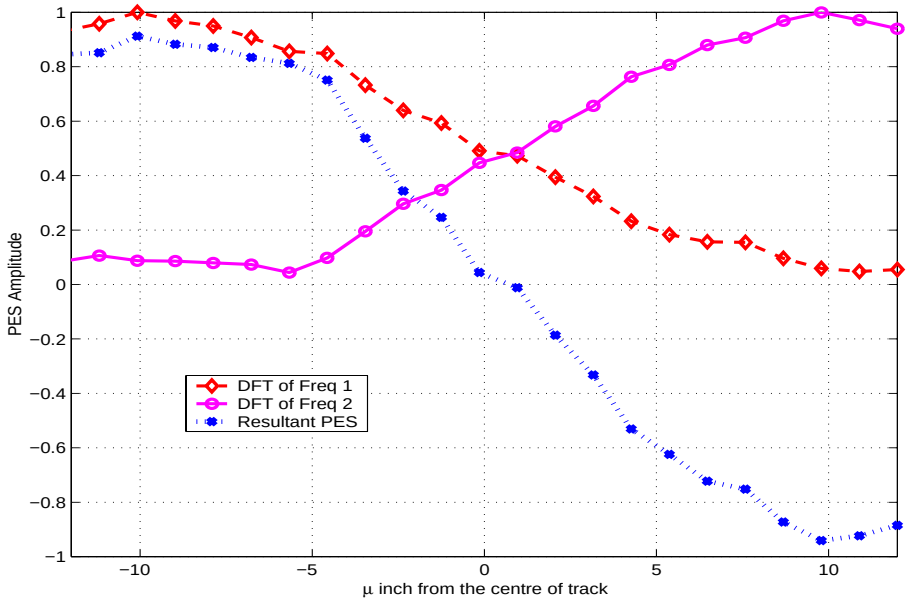


Figure 4.13: PES detection of servo pattern.

trol. The resultant cross-track PES function is as shown in Figure 4.13.

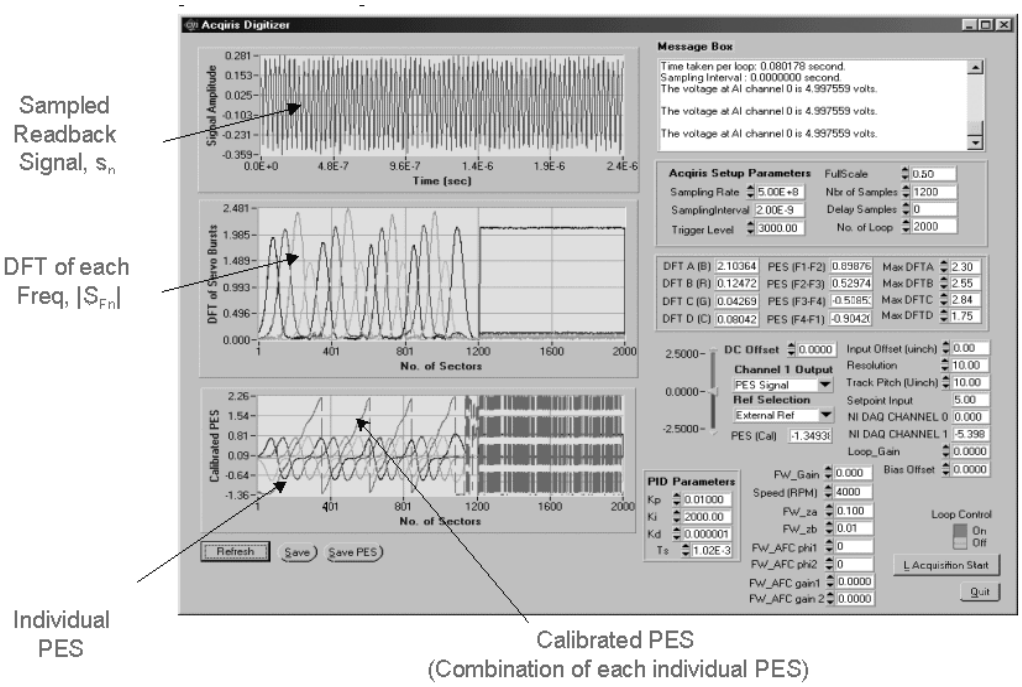


Figure 4.14: Screenshot of the reader servo GUI program.

The reader servo program is written using Labwindow CVI development software (Version 4.01) under Windows. Figure 4.14 shows the screenshot of the graphical-user-interface (GUI) of the program. This GUI allows the ease of viewing the readback signal, the individual DFT result of each frequency component and the calibrated PES, which is to be fed into the servo controller for positioning reference.

The read/write head used for experiment is a 40 $Gbit/in^2$ commercial head and as can be seen from Figure 4.15, the write head's width is about 12.5 $\mu$inch and the read head's width is about 8.2 $\mu$inch.

Figure 4.15 shows three sets of track profile tests taken at different times.

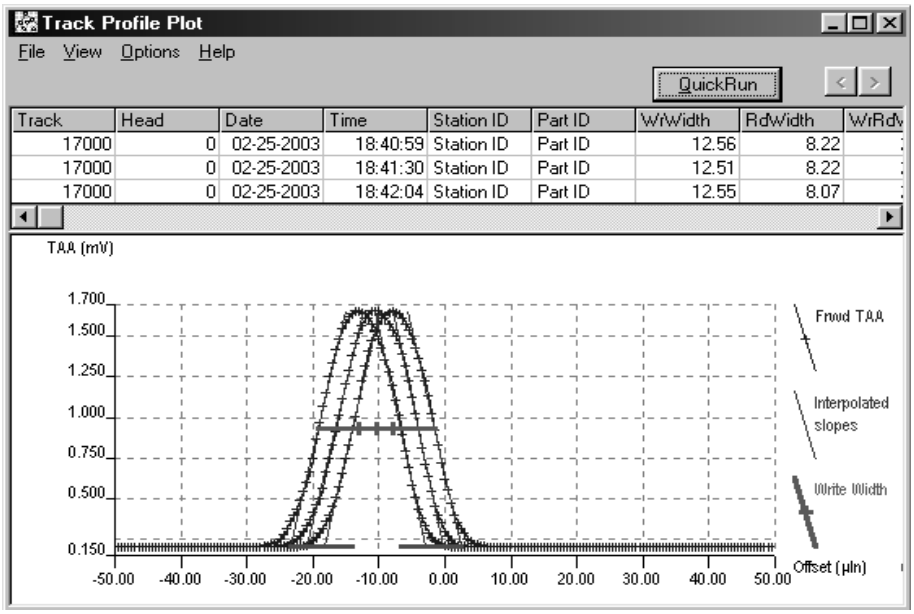


Figure 4.15: Track profiles plot of head and media.

The track profile test is used to characterize the performance of head and medium at different offsets. The track-average amplitude (TAA) of the readback signal is measured and plotted against the read head center offset from the track center.

The $PW_{50}$ is also found to be about 9.5 ns from the Saturation test provided by Guzik system with the spinning speed of the spin stand at 4000 RPM. Thus after some trial and errors, the track width is chosen to be 10 $\mu$inch based on the partial erasure method mentioned previously in Section 3.4.1.

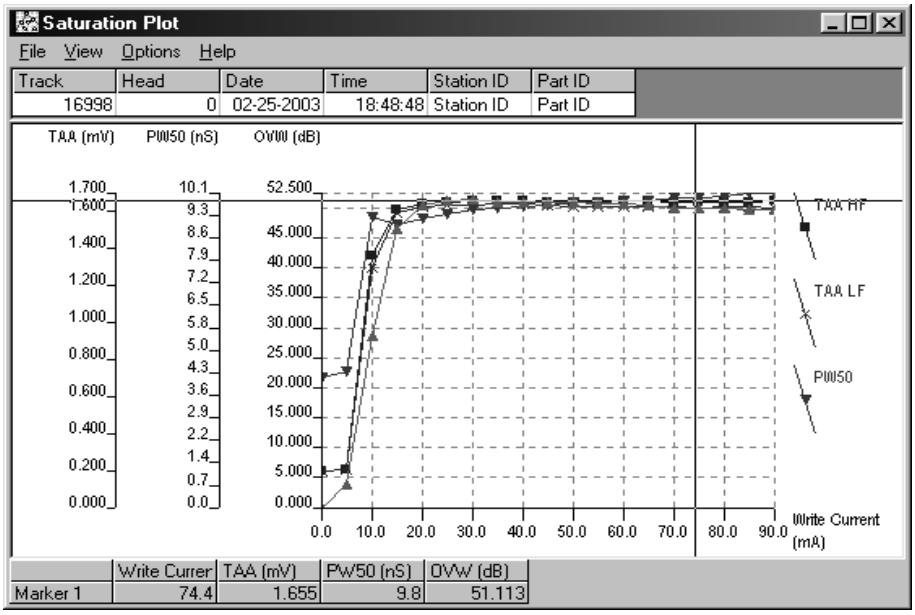


Figure 4.16: Write current saturation plot.

## 4.4 Servo Control Implementation

The Guzik head cartridge is modified and a PZT is inserted within a small gap to provide the sub-nanometer movement for servo control. A low voltage piezo chip translator (LVPZT) (Model No. PL033) [54], which is shown in Figure 4.17, is used for the precise positioning of the read/write head. This PZT provides a displacement range of about 2 $\mu$m and sub-nanometer resolution of 0.02 nm.

Figure 4.18 shows the modified head cartridge which includes the piezo chip translator for precise positioning.

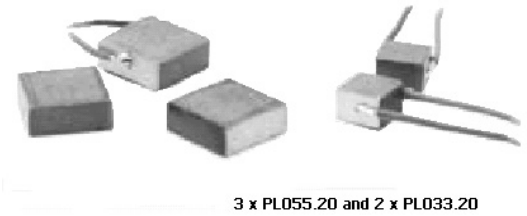


Figure 4.17: Images of LVPZT translator chips (Model No. PL055 and PL033).

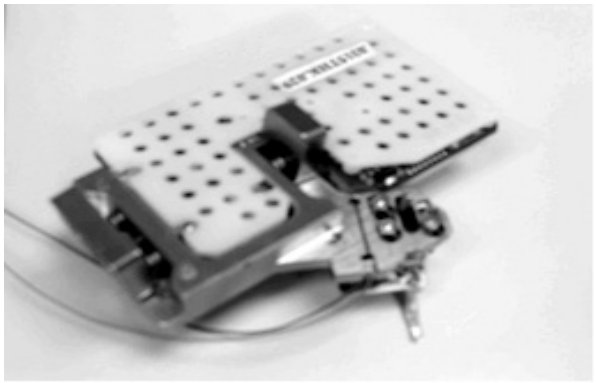

Figure 4.18: Modified head cartridge with PZT chip translator.

### 4.4.1 Modeling of Piezo Actuator

Before designing a controller for servo control, an accurate model of the plant needs to be obtained. In this case, the plant will include the piezo amplifier and the modified head cartridge with the PZT chip translator. The gain provided by the piezo-amplifier, which is 20 times amplification, is also included in the model.

Figure 4.19 shows a Lissajous plot of a ±50 V, DC offset at 50 V (which is after amplification of 20 times by the piezo amplifier), 500 Hz driving signal and the corresponding head displacement. The range of movement at ±50 V is ±1.8

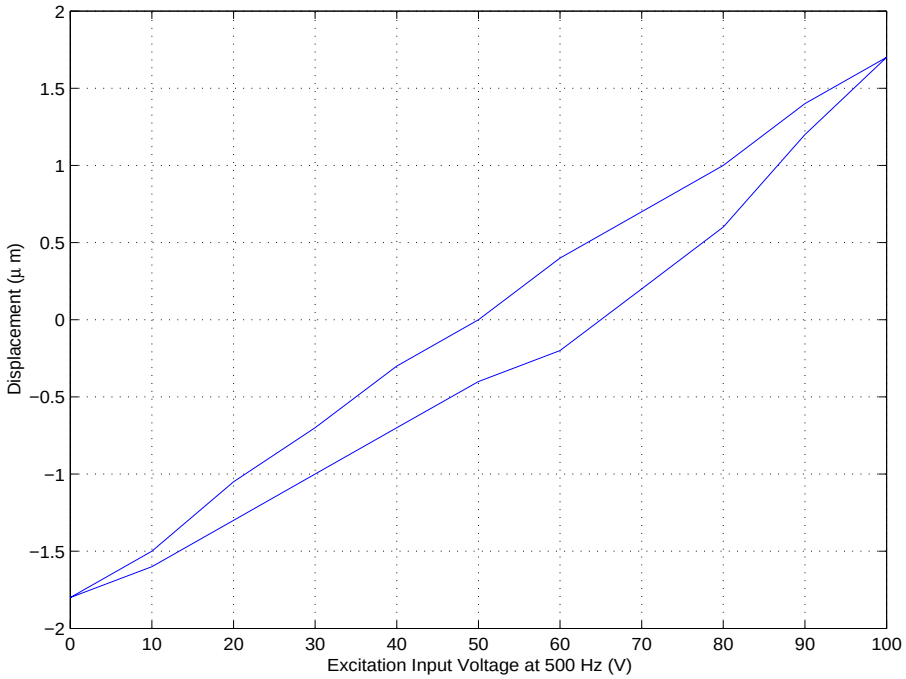


Figure 4.19: Hysteresis loop of modified PZT head cartridge (Excitation input: sinewave of 100 $V_{p-p}$ at 50 V DC Offset and frequency of 500 Hz).

$\mu m$. The hysteresis observed in the figure causes the phase lag in the open loop frequency response. Although this is not a fatal fault, it is one of the factors that can reduce the control performance.

The Dynamic Signal Analyzer (DSA) (Model:HP 35670A) is used to provide swept sine from 5 Hz to 10 kHz for the frequency response measurement of the modified PZT head cartridge. Laser Doppler Vibrometer (LDV) from Polytec [55] is used to measure the absolute displacement of the PZT, for given excitation input.

The resolution of LDV is set at 2 $\mu$m/V with the amplitude of excitation input 1 $V_{p-p}$ and DC offset at zero. The frequency response of the modified head

cartridge with PZT chip translator plant and the identified model are as shown in Figure 4.20.

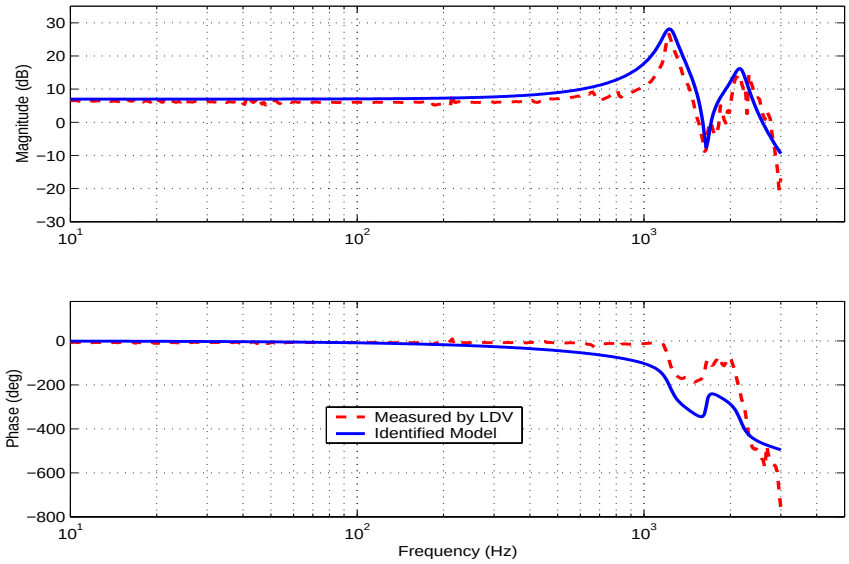


Figure 4.20: Open loop frequency response of the modified PZT head cartridge plant model.

As can be seen from the measured frequency response, the modified PZT head cartridge plant including the read/write head can be modeled as a pure gain up to around 1.32 kHz where the first structural resonant mode occurs.

Generally, the modified PZT plant in $s$-domain can be modeled and expressed as a constant and with resonant peaks as

$$\begin{aligned} G(s) &= k_g H_d(s), \\ &= k_g \prod_{i=1}^{n} \frac{s^2 + 2\zeta_{zi}\omega_{zi}s + \omega_{zi}^2}{s^2 + 2\zeta_{pi}\omega_{pi}s + \omega_{pi}^2} \end{aligned} \tag{4.14}$$

where

$H_d(s)$ is the resonance transfer function defined as in (4.14),

$k_g$ is the plant gain,

$\omega_{zi}$ $(i = 1, \cdots, n)$ are the natural frequencies for zeros,

$\zeta_{zi}$ $(i = 1, \cdots, n)$ are the corresponding damping ratios for zeros,

$\omega_{pi}$ $(i = 1, \cdots, n)$ are the natural frequencies for poles, and

$\zeta_{pi}$ $(i = 1, \cdots, n)$ are the corresponding damping ratios for poles.

For the plant as shown in Figure 4.20, the plant model is identified through trial and errors based on the peaks and frequencies of the resonance modes. The parameters of up to third resonance modes are given in Table 4.2.

### 4.4.2 Design of Servo Controller

The control law is designed to minimize the effects of internal and external disturbances on the PES. As stated in Chapter 1, the internal disturbances are caused by spindle motion, the airflow over the disk and heads, the noise in sensing the PES and the reactions from seeks. The external disturbances are largely due to shock and vibration.

As the main focus of this thesis is not advanced control design, the specifications for the controller system can be less stringent. The design specifications are summarized in Table 4.3. Thus the reader servo system is being implemented using a simple proportional-plus-integral-plus-derivative (PID) controller.

Table 4.2: Parameters of the modified PZT head cartridge model.

| Parameters | Symbol | Value |
|---|---|---|
| DC Gain (dB) | $k_g$ | -4 |
| First Pole Freq (Hz) | $\omega_{p1}$ | 1230 |
| First Pole Damping | $\zeta_{p1}$ | 0.055 |
| First Zero Damping | $\zeta_{z1}$ | 0.2 |
| Second Pole Freq (Hz) | $\omega_{p2}$ | 1650 |
| Second Zero Freq (Hz) | $\omega_{z2}$ | 1570 |
| Second Pole Damping | $\zeta_{p2}$ | 0.2 |
| Second Zero Damping | $\zeta_{z2}$ | 0.015 |
| Third Pole Freq (Hz) | $\omega_{p3}$ | 2170 |
| Third Zero Freq (Hz) | $\omega_{z3}$ | 2170 |
| Third Pole Damping | $\zeta_{p3}$ | 0.05 |
| Third Zero Damping | $\zeta_{z3}$ | 0.2 |

Table 4.3: Specifications for modified PZT head cartridge control design

| | |
|---|---|
| Settling Time (ms) | $\geq 5$ |
| Peak of sensitivity function (dB) | $< 10$ |
| Servo Bandwidth (Hz) | $\geq 200$ |

The time domain relation of a PID controller is

$$u(t) = K_p e(t) + K_i \int_0^t e(t)dt + K_d \frac{de(t)}{dt}. \tag{4.15}$$

Laplace transformation of (4.15) yields

$$C(s) = \frac{U(s)}{E(s)} = \frac{K_d s^2 + K_p s + K_i}{s}, \tag{4.16}$$

where the choice of $K_p$, $K_d$ and $K_i$ will be determined by the system dynamics.

The PID transfer function can be approximated using the bilinear transformation [34] as in (4.17). Other approximations will yield different algorithms for the digital controller.

$$C(z) = G\frac{(K_p + \frac{K_i T_s}{2} + \frac{K_d}{T_s})z^2 + (\frac{K_i T_s}{2} - K_p - \frac{2K_d}{T_s})z + \frac{K_d}{T_s}}{z^2 - z} \tag{4.17}$$

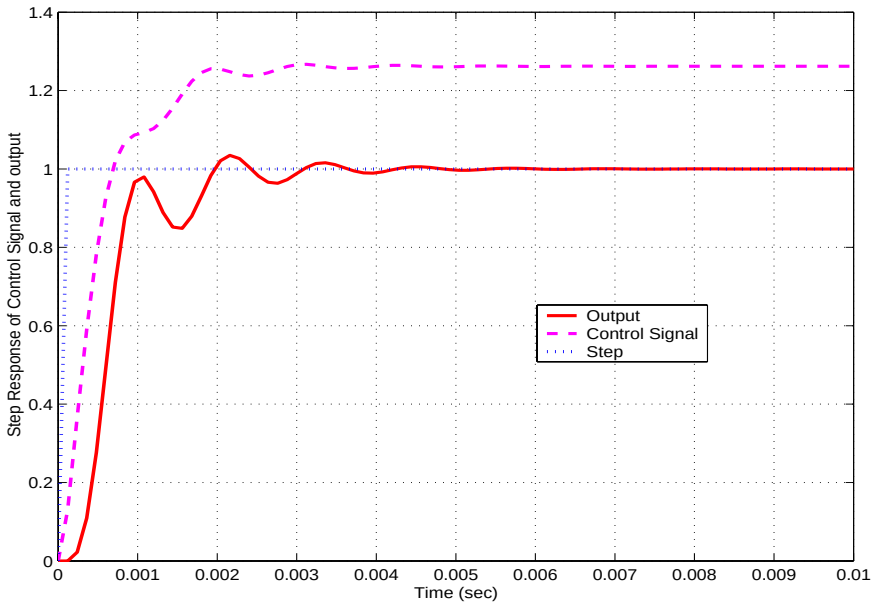


Figure 4.21: Step response of the servo control signal and output (in Volts).

Since the proportional and integrative constants are most important, they have received the more attention. The design portion of this problem is in the selection of the coefficients $K_i$ and $K_p$. With the presence of the proportional and

integral action, the compensator $C(z)$ will have a pole at $z = 1$, which is the image of the continuous-time integrator pole in relation to (4.16).

It is the integration portion of the PID that gives the closed-loop control a pole at DC, so this is reflected in the value chosen for $K_i$. It is also observed that a higher gain assigned to $K_p$ seems to increase the servo bandwidth. A controller gain, G is added to the controller for ease of tuning. As the gain, G is increased, the effective noise transfer function is decreased. However, any further increase in the controller gain (G = 0.4) will result in an unstable controller. It appears from the simulation that the integration constant has the most influence on noise control. A trial-and-error design gives a settling time of about 5 $ms$ for a controller gain G of 0.4, with $K_d = 0.000001$, $K_i = 2000$, and $K_p = 0.01$. The step response to the servo control signal and output with respect to the step input is simulated and as shown in Figure 4.21.

### 4.4.3 Reader Servo System Performance

Figure 4.22 shows the frequency response of the modified PZT head cartridge based on the relative displacement of the head and disk (computed PES). The amplitude of excitation input is 1 $V_{p-p}$ and DC offset 0 V from frequency range of 10 Hz to 3 KHz. The frequency response based on the generated PES signal matches the measurement taken by the high precision LDV especially in the lower frequency range ($<$ 2 kHz). With the sampling rate of about 8.3 kHz, the 1st few resonance modes of less than 4 kHz can be captured. However, due to the limited servo

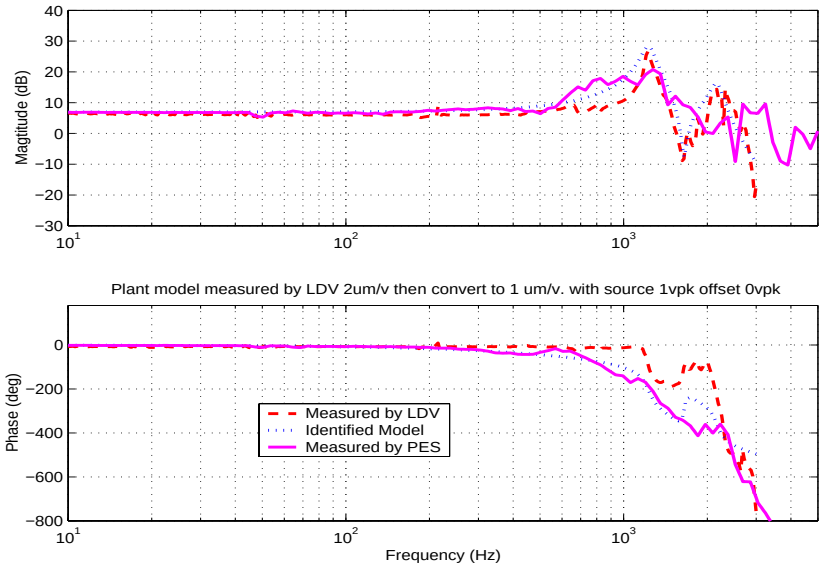


Figure 4.22: Plant model from LDV measurement, identified model and PES measurement at sampling frequency of 8.3 kHz.

information range, the actual resonant peak may not be measured accurately by the generated PES signal.

Experiments were conducted with the PC implementing various PID sets to make comparisons between simulations and experiments. The target of the track following controller is to maintain the PES to a minimum level in the presence of all the existing disturbances and measurement noises. A closed-loop bandwidth of 300 Hz is obtained with a controller gain of 0.4, $K_d = 0.000001$, $K_i = 2000$ and $K_p = 0.01$. The designed controller is implemented and the closed-loop response of the reader servo system is as shown in Figure 4.23.

Complementary sensitivity transfer function measures how the system re-

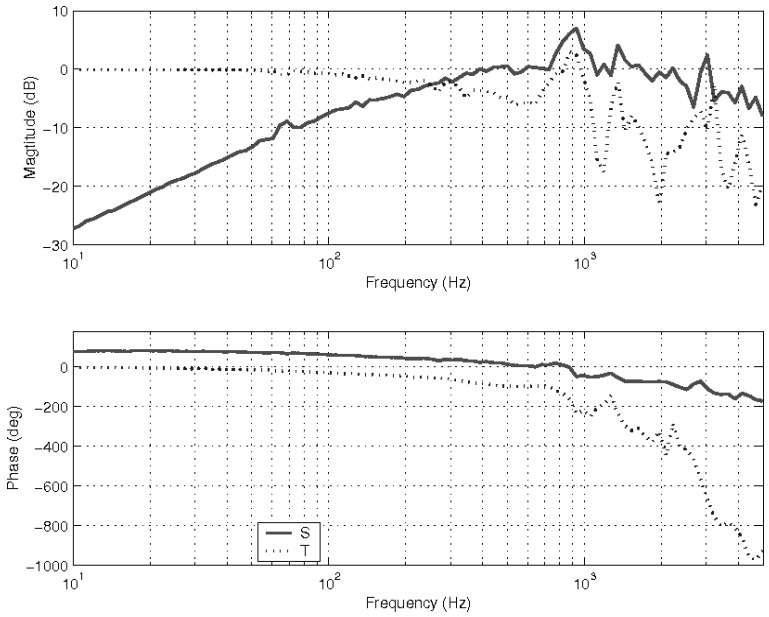


Figure 4.23: Sensitivity and complementary sensitivity transfer functions.

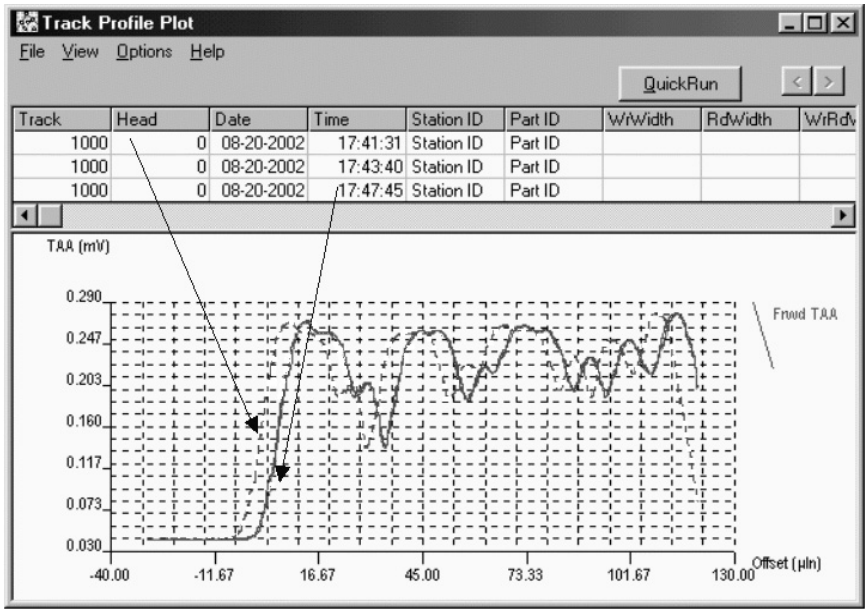


Figure 4.24: Track profiles taken with and without servo.

sponds to reference input and also the measurement noise, whereas the sensitivity transfer function measures how much the system rejects vibrations.

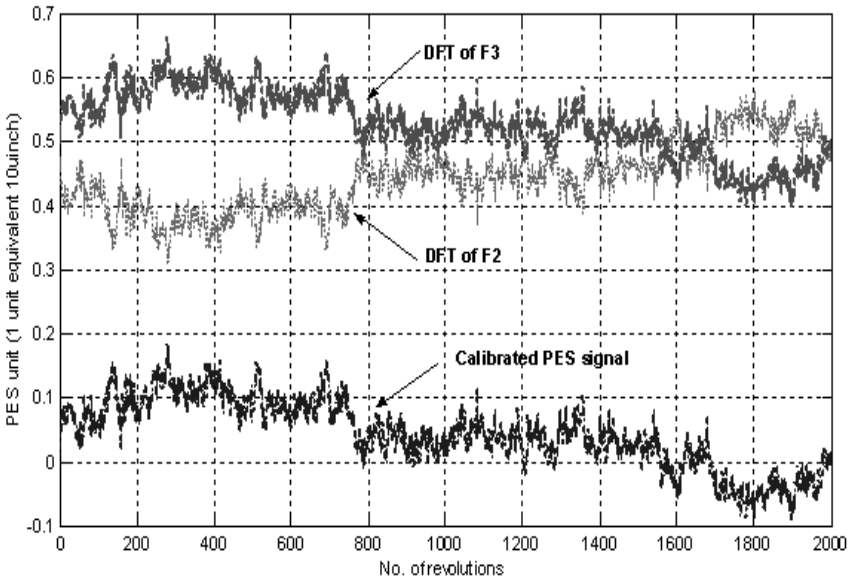


Figure 4.25: Time domain PES without servo control.

The track profile screenshot in Figure 4.24 shows the amount by which the head drifted away from the disk media at different times. The tracks are written at 10 $\mu$inch apart from each other. With the servo control and the new digital PES generation scheme, the track profiles taken at 4 minutes apart, show similar results.

Figure 4.25 and Figure 4.26 show the position error signal (where $1/\sqrt{2}V_{rms} \equiv$ 1 track width) for every revolution in time domain with and without closing the servo. With the servo control, the drifting of the head's position can be greatly sensed. Linear averaging method in time domain is used to separate PES into PES RRO and PES NRRO [68]. Assuming the average of PES NRRO converges to

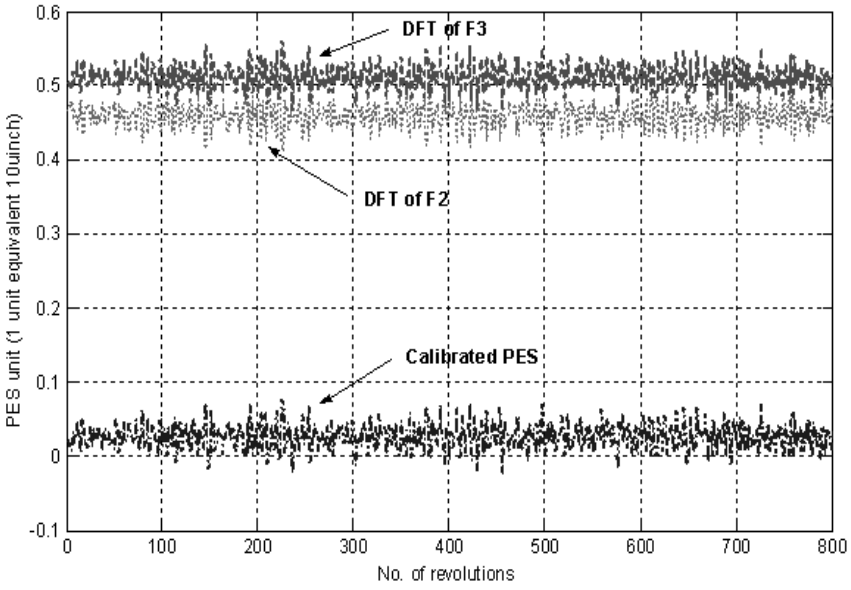


Figure 4.26: Time domain PES with servo control.

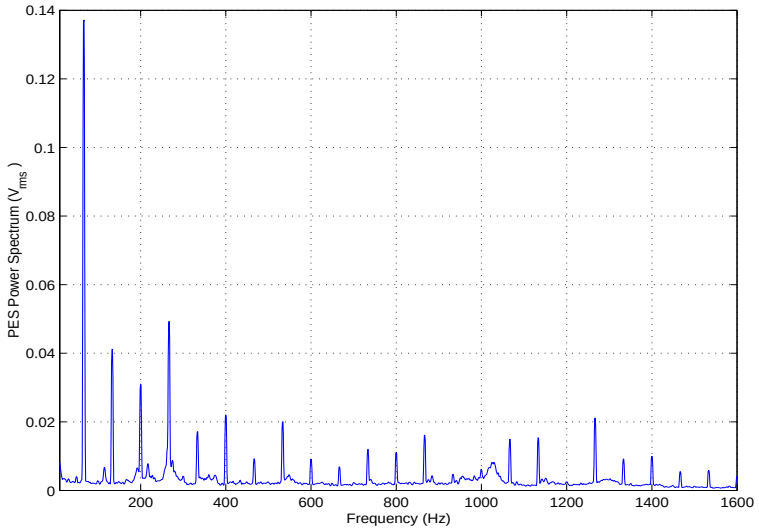


Figure 4.27: Power spectrum of PES without PID controller.

zero, the PES RRO and NRRO can be calculated as

$$PES(k)_{RRO} = \frac{1}{N}\sum_{i=1}^{N} PES_i(k), \tag{4.18}$$

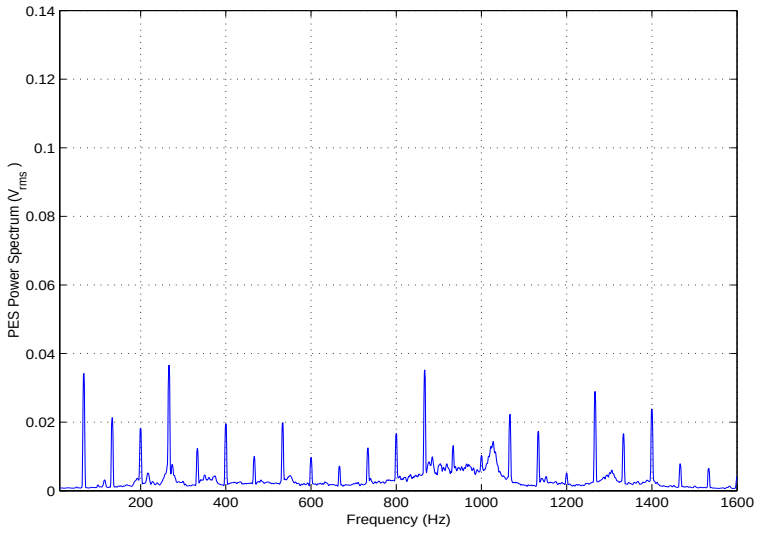


Figure 4.28: Power spectrum of PES with PID controller.

$$PES_i(k)_{NRRO} = PES_i(k) - PES(k)_{RRO}. \tag{4.19}$$

where $PES_i(k)$ is the PES value at the $k$ sectors of $i$ revolutions. The total number of revolutions (or spindle index) is N. The RRO and NRRO before using the controller can be seen from time domain PES signal in Figure 4.29 over a number of revolutions. The RRO component can be clearly seen as a periodic signal in Figure 4.29 and its fundamental frequency of 67 Hz corresponds to the rotation speed of the spin stand which is 4000 RPM. The $3\sigma$ RRO error is found to be about 1 $\mu$inch and $3\sigma$ NNRO error is about 0.55 $\mu$inch.

With the servo controller activated, the $3\sigma$ PES error including RRO and NRRO components is reduced by 18.7% as compared to without using any controller. The improvement is mainly by the suppression of the first 5 RRO components as can be seen from the power spectra plots of PES without and with

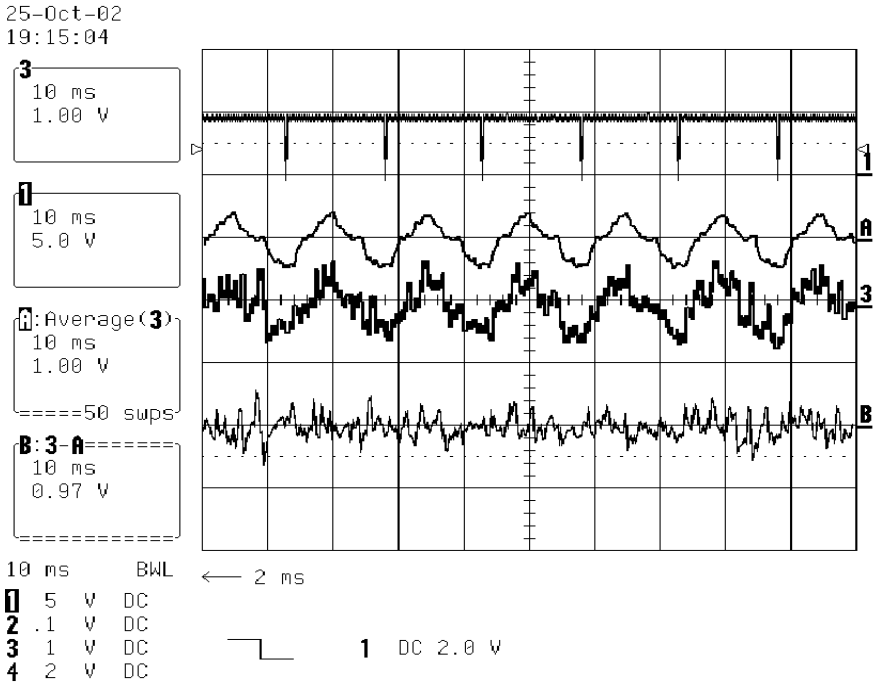


Figure 4.29: (a) Channel 1 displaying spindle index, (b) Channel A shows RRO components, (c) Channel 3 displaying computed PES retrieved from DAQ analog output channel, and (d) Channel B shows NRRO components.

controller as shown in Figure 4.27 and Figure 4.28, respectively. However a few higher frequency RRO components ($13^{th}$, $14^{th}$, $15^{th}$) are also amplified which is due to Bode's Integral constraint [4].

Typically, higher TPI drives require higher servo bandwidth to reject disturbances such as windage, electro-magnetic noise, disk fluttering, external vibration etc, so that effective track following can be guaranteed. However, in servo control of the piezo head cartridge, one of the factors that limits the achievable closed-loop bandwidth is the uncertainty of the modified head cartridge resonance [19].

A comparison between the Guzik servo controller and reader servo controller is summarized in Table 4.4. However due to the different servo patterns used for PES demodulation and the hardware limitations to the modification of the reader servo to the Guzik spin stand, the comparison is only based on the specification given by the Guzik company [29]. The TMR, or $3\sigma$ PES error, with and without the reader servo controller are summarized in Table 4.5.

Table 4.4: Comparison of system specifications

| System specification | Guzik spin stand | PC-based servo system |
|---|---|---|
| Track position repeatability ($\mu$in.) | $< 0.3$ | 0.25 |
| Servo Bandwidth (Hz) | 50 | 300 |

Table 4.5: PES $3\sigma$ error with and without controller

| Measurement | Without controller ($\mu$in.) | With controller ($\mu$in.) | Improvement (%) |
|---|---|---|---|
| PES $3\sigma$ | 1.07 | 0.87 | 18.7 |

### 4.4.4 Discussion

Large measured PES error ($3\sigma = 1.07$ $\mu$inch) has been observed especially at track center where lies the two different frequency servo components.

One of the reasons is the track-edge effect. As in the case for partial erasure method, when a new pattern is written, the track edges of the old information are erased incompletely. The track-edge effect is frequency-dependent, the higher the ratio between the frequencies of the old and the new data patterns, the stronger the residual signal from the track edges [66]. Thus, the ratio of servo frequencies written are selected to be small to alleviate the track-edge effect which is particularly a problem for the partial erasure method used in this research for servo writing. However, in practice, the partial erasure method is not used and the write head used during the servo writing manufacturing process is smaller than the actual write head in the HDDs. Hence, in actual implementation, the track-edge effect will not be that prominent.

Another reason is the written-in RRO which is a repeatable periodic signal and phase-locked to the spindle rotation. It is caused by NRRO while servo writing, disk warping, disk slip and thermal expansion of the disk etc. Although NRRO may also look like a periodic signal, it is not phase-locked to the spindle rotation. As in the case of the open loop servo-writing process in the use of the spin stand, written-in RRO can be observed easily. According to internal mode principle, only RRO and NRRO within the servo bandwidth can be attenuated. A special controller, called run-out compensator, may be used for the cancellation of RRO and NRRO, especially for those close to or beyond the bandwidth [58].

The target of the track following controller is to maintain the PES to a minimum level in the presence of all the existing disturbances and measurement noises.

Obviously, the sensitivity and complementary sensitivity transfer functions satisfy $S(s) + T(s) = 1$. That is if a higher bandwidth servo is designed, it will have better rejection of the disturbances with a higher measurement noise level in PES. However, if the servo bandwidth is lower, although there is less measurement noise, the PES will be dominated by various disturbances. Thus the challenge of tracking controller design is to pick the controller structure and parameters to balance the impact of various disturbance sources and measurement noise given the piezo chip translator bandwidth limitations and sampling frequencies of the PES.

To have a better rejection of disturbances and faster response, a higher bandwidth servo is required. However, the design of higher bandwidth servo is usually limited by the sampling rate of the PES and the resonance mode of the actuator. For future work, multi-rate servo control will be designed to improve the servo performance. In addition, patterned servo media can be used to create advanced PES patterns, which is difficult to achieve in conventional servo writing techniques and eliminate track edge noise. Different PES schemes can be designed and compared using the same platform.

To further reduce the disk vibration and disturbances, active feed-forward control proposed in [68] can be used to reduce high frequency RRO components. In future, for real-time operation, an embedded system consisting of dedicated high speed DAC, digital signal processing (DSP) system and Fuse Programmable Gate Array (FPGA) devices can used for the actual prototyping of the advanced servo positioning system.

## 4.5 Summary

A PC-based servo control system allowing flexibility, fast implementation and programming ease, has been implemented successfully on Guzik spin stand. Several components that can contribute to the computation noise, namely quantization, truncation error, computation algorithm, and implementation of averaging have been analyzed and tuned to obtain an optimal servo frequency pattern and computation parameters for a satisfactory reader servo control. Demodulation noise on a blank media is less than about 0.065 $\mu$inch for frequency less than 25 MHz with respect to servo track pitch of about 10 $\mu$inch.

Total PES computation and processing time, which is about 85 $\mu$s ($\pm$15 $\mu$s due to non-real time PC setup), has been attained. With 125 servo sectors per revolution and spindle speed at 4000 RPM, the PES sampling rate is 8.3 kHz. Error of 1.07 $\mu$inch ($3\sigma$ PES) has been observed especially at servo track center where lie the two different frequency servo components, which is due to the RRO and NRRO components. Together with the PES demodulation, a high closed-loop servo bandwidth of 300 Hz can be attained for spin stand servo control and an improvement of 18.7% in reduction of disturbances has been achieved as compared to without servo control.

To further improve the servo bandwidth, higher PES sampling rate is required. Thus the next chapter will present a method to measure the head's position while reading the user data and in turn increase PES sampling rate.

# Chapter 5

# Position Error Signal Generation using User Data

To meet the required positioning accuracy for robust and higher density data storage system, reduced position sensing noise or higher sampling rate of PES are required. This chapter will focus on a way to increase PES sampling rate by measuring the position of the read/write head while the head is reading the user data information.

## 5.1 Review of Advanced Servo Methods for Higher Feedback Rate

To achieve better servo performance, higher closed-loop servo bandwidth is desired. However, to achieve the desired specifications for the servo system, the sampling rate need to be about ten times greater to minimize the loss of phase margin [23]. With the current trend of servo bandwidth pushing above 5 kHz, PES sampling rate of more than 50 kHz is needed to further improve the servo performance. Although high sampling rate is desirable, care must also be taken to consider the high frequency resonance mode which is usually ignored in the low bandwidth servo control design [67].

In embedded servo systems, the rate at which the servo controller reads the PES measurements is proportional to the number of the servo burst sectors present on the disk and the spinning speed of the disk. The spinning speed of the disk cannot be increased arbitrarily, else it will result in increased mechanical disturbances from spindle motor, such as NRRO and other noise issues. Increasing the number of servo sectors will reduce the amount of storage space. Therefore for a given disk drive, the frequency of the PES measurement is bounded by these two factors.

The drawback of embedded system is that position error signal is only available when the head is reading the servo sector. No additional positioning information is available until the next servo sector passes by the head. Thus, if the position

information can also be obtained within the data block, a higher sampling rate can be achieved. Several researchers have proposed methods to improve the rate of PES measurements.

1. The use of a dual-stripe MR heads for the estimation of track mis-registration, as disclosed in [30], was based on the assumption that the signal waveform changes only in amplitude as the head moves off track. The differences between the MR elements' output envelopes are demodulated by a peak value detection circuit and the sum of the two element signals is considered as a position error signal. However, the use of MR head is not the current industry standard for magnetic storage systems, which are currently based on the GMR head. With the increasing demand for higher density and the peak detector becoming obsolete, this method is not feasible anymore.

2. A novel data servo method has been proposed in [31], such that the head position error signal can be directly extracted from the data sequences encoded by a modified Group Inter-Track Orthogonal Coding (GITOC). In this method, the original data sequences are divided into a series of 2-bit groups and further coded to eight code bits using eighth-order Hadamard matrix coding rules. However, this will limit the number of bit cells reserved for user data bits.

3. Gaines and Despain from Acorn Technologies [25] have patented several methods that can also increase the sampling rate. One of the methods is to make use of the synchronization pattern, which is meant for clock syn-

chronization within each data block, to include servo information for position estimation. However, the adjustment of read head relative to the data tracks occurs only after each synchronization blocks which is still not on a continuous basis.

4. Another method by Despain and Gaines [22] is to use information about the extent of errors in sensed data to perform a control function for reproducing the data stored in predetermined storage locations in a storage media. In one of the embodiments, the apparatus includes a first transducer positioned for sensing predetermined storage locations and generating a first signal representing data containing at least one constraint from the predetermined storage locations and any errors introduced into the sensed data during sensing. In another embodiment, the apparatus may include a transducer with two or more sensors. Although the error rate can be used to reflect the off-track status, the use of error rate for feedback control and the requirements of PES scheme are not addressed. In addition, it may take too long to get the information on the extent of errors to react to the track mis-registration.

5. Ioannou and Despain [33] also presented an algorithm that can generate estimates of the PES during reading process at high sampling rates by processing the dedicated servo burst measurements and the measurements of a non-linear function of PES obtained from the data sectors. The non-linear function of PES is generated from the Mean Square Error (MSE) path metric data used to choose the correct bit sequence using Viterbi algorithm in the PRML decoding process. Similar to the previous method, the estimator re-

quires sufficient system evolution to select either the positive or negative displacement estimators to determine the off-track direction.

The bit error rate (BER) can be used to reflect the off-track error, however the determination of off-track direction as proposed by the Despain and Ioannou [25] [22] [33], are neither cost-effective because they use more than one transducer nor accurate as estimators are used. In this thesis, a novel method, which allows measurement of the position of the read head while the head is reading the user data information for embedded servo system will be presented next. The method will allow the off-track direction to be easily determined and PES in servo and user data sectors to be measured quickly and accurately.

## 5.2 Frequency-Encoded Servo and User Data

The proposed new scheme writes user data at different frequencies and phases. As illustrated in Figure 5.1, FESP is used in conjunction with user data of multiple frequencies, $F_N$ ($N$ is 1,2,3...) representing the different frequencies. The method provides different frequencies in the servo and data sectors of adjacent tracks. The user data information can be written at different bit intervals by adjusting the timing in a programmable clock generator such that the written data information has a readback signal with either its frequency or phase differing from a readback signal in its adjacent tracks. This can be achieved by an increase or decrease in the time interval to change the frequency of the data information signal during the

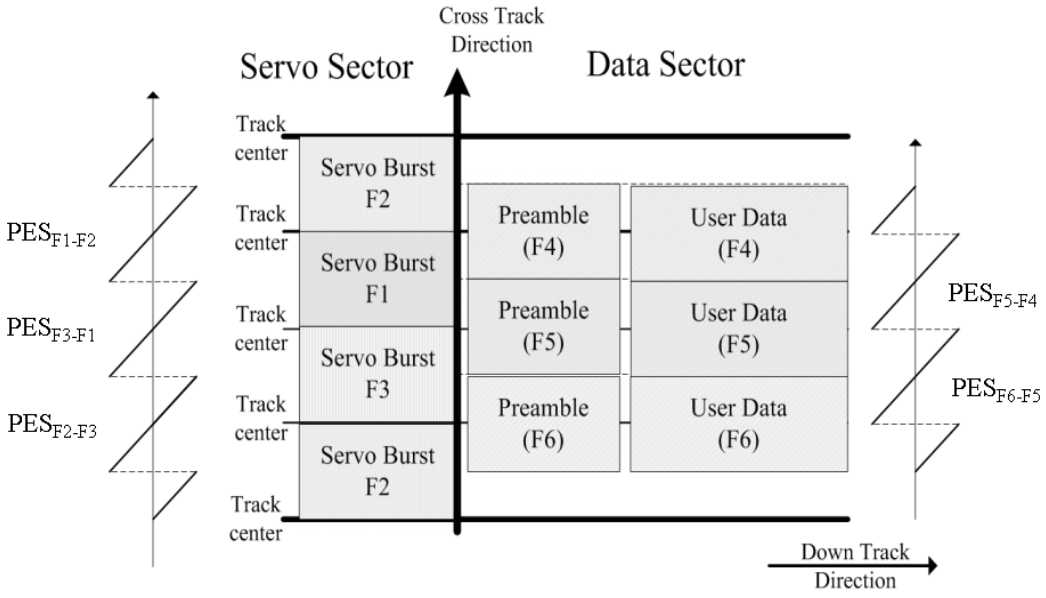


Figure 5.1: Multiple frequencies servo and data sectors layout.

writing process or by a shift in the time interval through starting the write process at a different phase of the same signal frequency.

By having different phase shifts or frequencies of encoding data on each adjacent track, each track information can be extracted accordingly. For different servo or data track centers, the readback signal consists of different frequency components as compared to its adjacent tracks which can be seen in Figure 5.2. Based on this information, the position of the head, the drifting direction can be determined easily.

To extract the position information, one way is by getting the sine and cosine coefficients of the specific data pattern, which is the DFT-based decoding algorithm. One preferred detected data pattern is one or more continuous dipulses

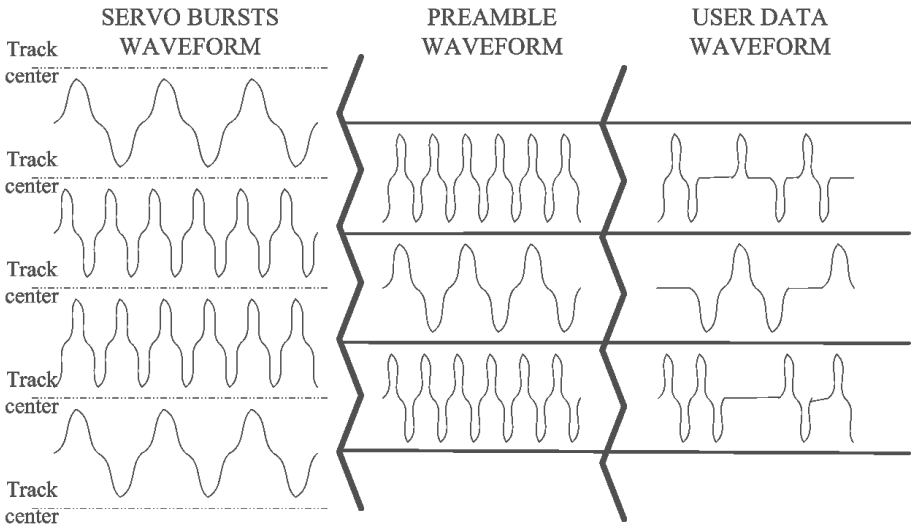


Figure 5.2: Illustration of multiple frequencies readback servo and user data signals.

with alternating transitions, since the dipulse utilizes a pattern with a known fundamental frequency. In this way, high frequency noise can be eliminated. Based on the characteristics of the specific data pattern, it can be analyzed by extracting the frequency component of the data, and the result be used to estimate the relative head's position.

A combination of FESP and DFT-based demodulation technique is used for PES generation during the servo sector which had been discussed in the earlier chapters. As for the estimation of the position information from the frequency-encoded user data sectors, firstly, an ideal Lorentzian waveform (5.1) or similar model like sinusoidal waveform of the readback signal with frequencies $Freq_{m+1}$, $Freq_m$, $Freq_{m-1}$ is pre-defined. By mixing the noise-free pre-defined signal, large amount of noise and other non-idealities like baseline shift, thermal asperities, and baseline popping in the input signal spectrum can be masked off, thus resulting in

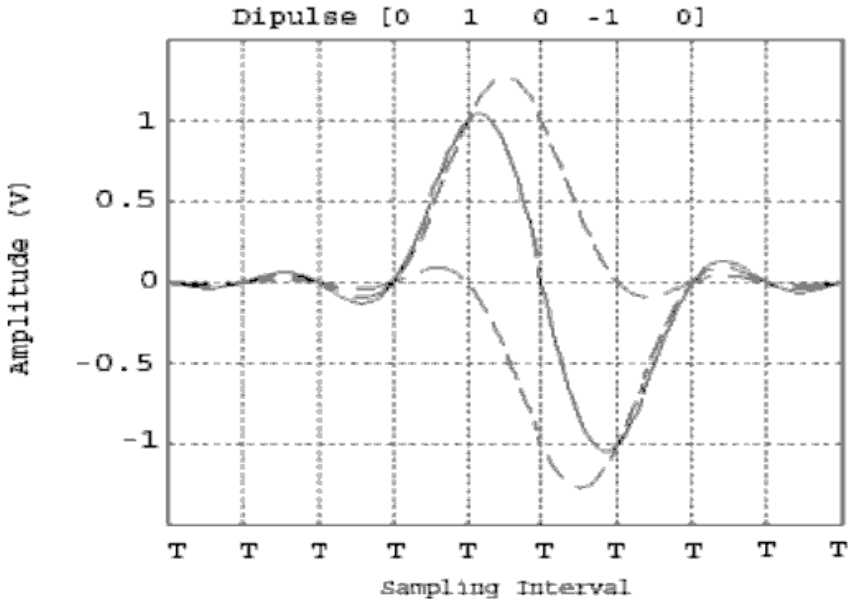


Figure 5.3: A dipulse of data sequence (0 1 0 -1 0 ) due to two sequential transition in PR Class IV (PR4) channel.

a higher SNR signal [2]. As for the case of the pre-selected pattern to be dipulse, consisting of two transitions written at a spacing of $B_m$ and phase shift $\Theta_m$, the mixing signal is

$$R_m(t) = V_{sp}^{peak}[\frac{(PW_{50}/2)^2}{(t - B_m/2 - \Theta_m)^2 + (PW_{50}/2)^2} - \frac{(PW_{50}/2)^2}{(t - B_m/2 - \Theta_m)^2 + (PW_{50}/2)^2}], \tag{5.1}$$

where $V_{sp}^{peak}$ is the peak amplitude of the single pulse, $PW_{50}$ is the amplitude at 50% of the maximum amplitude. Bit interval, $B_m$ is inversely proportional to 2 times the dipulse frequency, $f_m$ and $T$ is the sampling interval. For example, the dipulse is detected as a sequence of 0 1 0 -1 0 in a PR4 channel as shown in Figure 5.3.

Based on the previous estimation of the head position, the read back signal, $d(n)$ is mixed with a series of predetermined and generated sample values $R(n)$. The modulated signals, $D(n)$ for track $m-1$, $m$ and $m+1$ are

$$D_{m-1}(n) = d(n)R_{m-1}(n), \tag{5.2}$$

$$D_m(n) = d(n)R_m(n), \tag{5.3}$$

$$D_{m-1}(n) = d(n)R_{m-1}(n), \tag{5.4}$$

where $R_m(n)$ has frequency $f_m$ and phase shift, $\Theta_m$, and are different from $R_{m-1}(n)$ and $R_{m+1}(n)$ where the adjacent tracks are of different frequencies or phase shifts.

Next, by using digital maximum likelihood detector (MLD) based on PRML system, whenever a desired data sequence is decoded, the magnitude of the frequency component, $Y_{DFT}$ of each dipulse found within the specified window $T_w$ is computed. Magnitudes of the $k^{th}$ dipulse is obtained as

$$Y_{DFT_k} = \sum_{n=1}^{N} D_m(n)e^{-j2\pi(n-1)/N}, \tag{5.5}$$

$$|Y_{DFT_k}| = \sqrt{(Y_{DFT_k\_real})^2 + (Y_{DFT_k\_imag})^2}. \tag{5.6}$$

Following this, the system will search for the data sequences and compute the DFT magnitude repeatedly until the end of the specified window $T_w$, consisting of $q$ bits of user data. The average DFT magnitude, $Y_{ave}$ of all the decoded data sequences $(say, K)$ within the window opened is obtained as

$$Y_{ave} = \frac{\sum(|Y_{DFTk}|)}{K}. \tag{5.7}$$

For better accuracy, smooth averaging of the DFT magnitudes within the same sector can be used. A simple 1st order filter is given as

$$DFT_{ave} = \alpha DFT_{ave} + (1-\alpha)Y_{ave}, \qquad 0 < \alpha < 1, \tag{5.8}$$

where $\alpha$ is a weighting factor. The relative head's position is estimated based on the resultant $DFT_{ave}$, and together with the track number, it can be used for precise track following. Flow diagram illustrating the simplified DFT-based PES demodulation process is as shown in Figure 5.4. With the PES generation from user data as shown in Figure 5.5, PES can be generated from the servo and data sector in time-multiplexed mode.

The resultant $DFT_{ave}$ and the servo PES value from the same sector are normalized and used to estimate the read head position. As the servo PES and the track number are retrieved at every sector, the servo PES is sent to the servo controller for track seeking and coarse positioning operation. Similarly, the user data position indicator value, as shown in Figure 5.6, can be fed to the servo controller for precise track following, especially within the user data block. An overview of both the PES generation and servo system is as shown in Figure 5.7.

## 5.3 Simulation and Experimental Results

The method proposed has been simulated using MATLAB. The user readback signal is modeled based on Lorentzian equation and generated randomly at frequencies of 20 MHz and adjacent tracks at frequencies of 30 MHz.

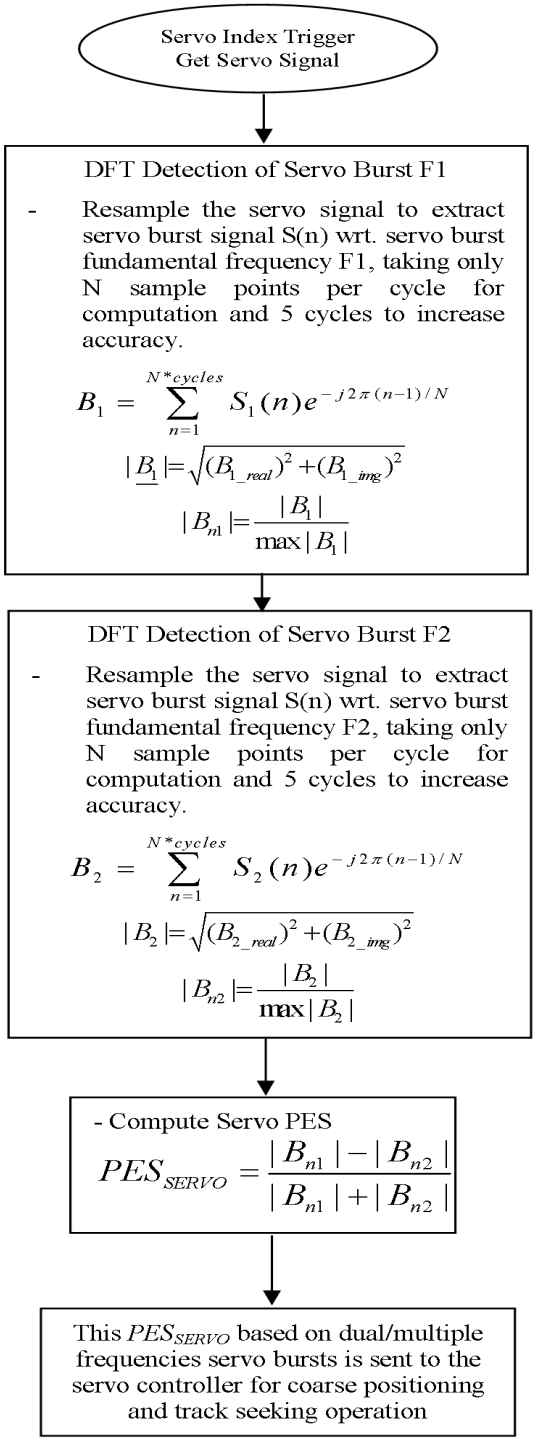


Figure 5.4: PES generation from servo sectors.

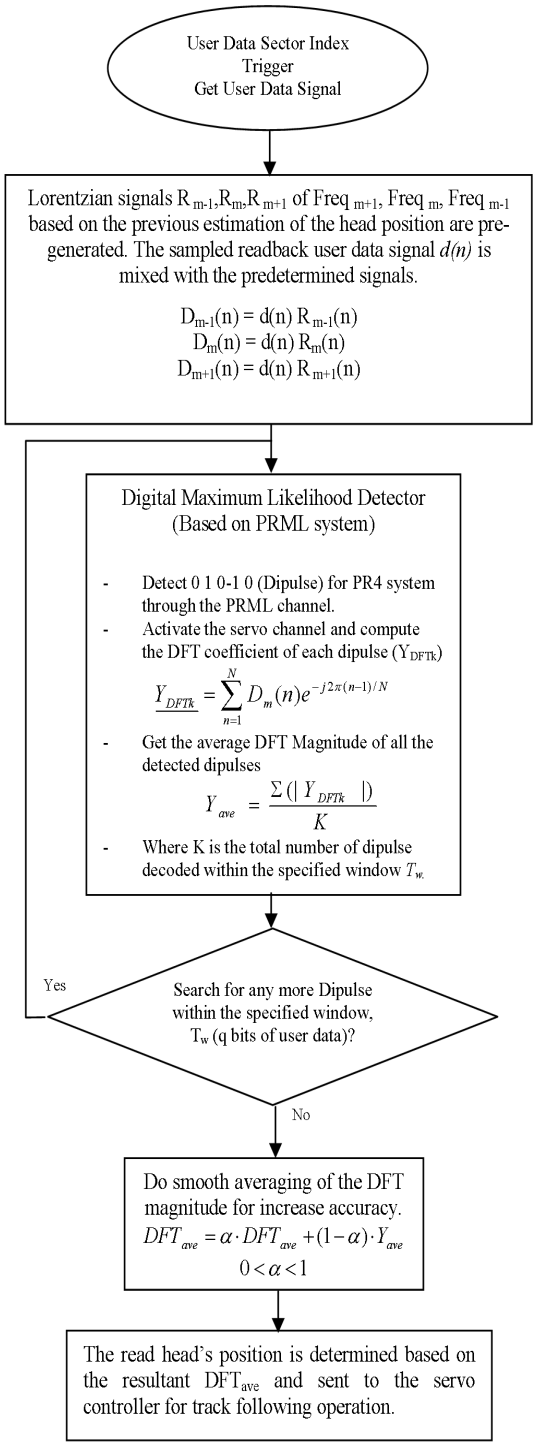


Figure 5.5: Flowchart of PES generation from user data.

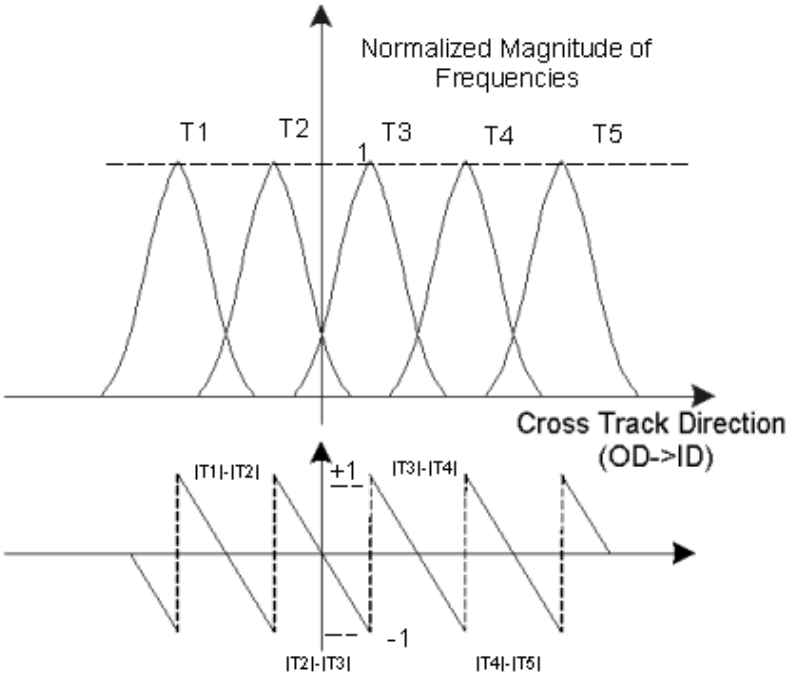


Figure 5.6: Track profile generated from PES of user data.

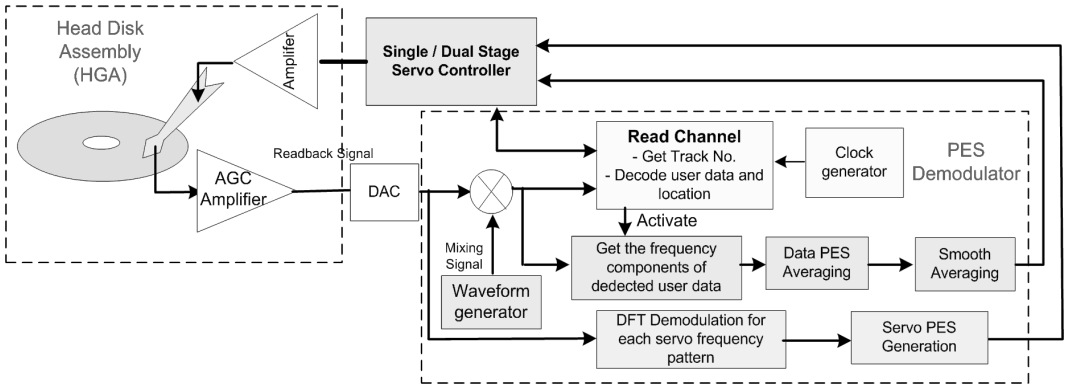


Figure 5.7: Block diagram of servo control system with advanced PES generation from user data.

A simple maximum likelihood algorithm [66] is used to emulate the PRML channel to detect the desired dipulse pattern and its location. Figure 5.8 shows a set of the generated random user data. Whenever the desired dipulse sequence

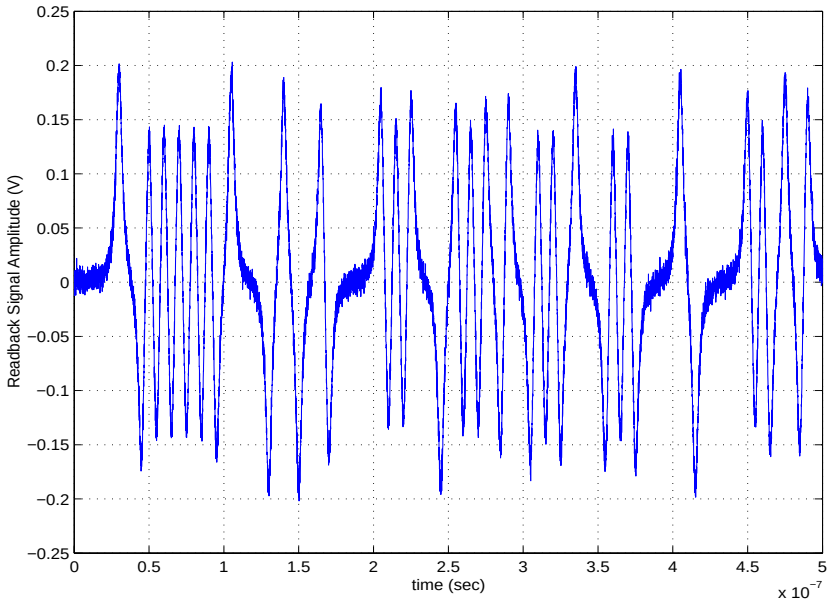


Figure 5.8: Readback signal of random user data.

is found, the magnitude $|Y_{DFT_k}|$ of the frequency component of the dipulse data is computed using (5.5) - (5.6). Assuming a window length of 50 dipulses, the average DFT magnitude of all the decoded data sequences ($K$) within the window, $Y_{ave}$, is obtained as in (5.7). The first $DFT_{ave}$ is obtained from the $PES_{SERVO}$ and the $Y_{ave}$ is in turn filtered with the previous $DFT_{ave}$ to obtain the smoothed averaged PES as in (5.8) where $\alpha$ is chosen to be 0.5. After smooth averaging for 5 times, the resultant data PES is as shown in Figure 5.9.

As for the experimental setup, the Falkon Fluid Bearing Spindle (FBS) servo test stand [27] [68] developed by the Mechatronics and Micro-systems group in DSI, is used because it provides precise timing needed to write the magnetic data, which is currently not available on the Guzik spin stand. Thus a set of random user data of two different frequencies 10 MHz and 15 MHz is written using the

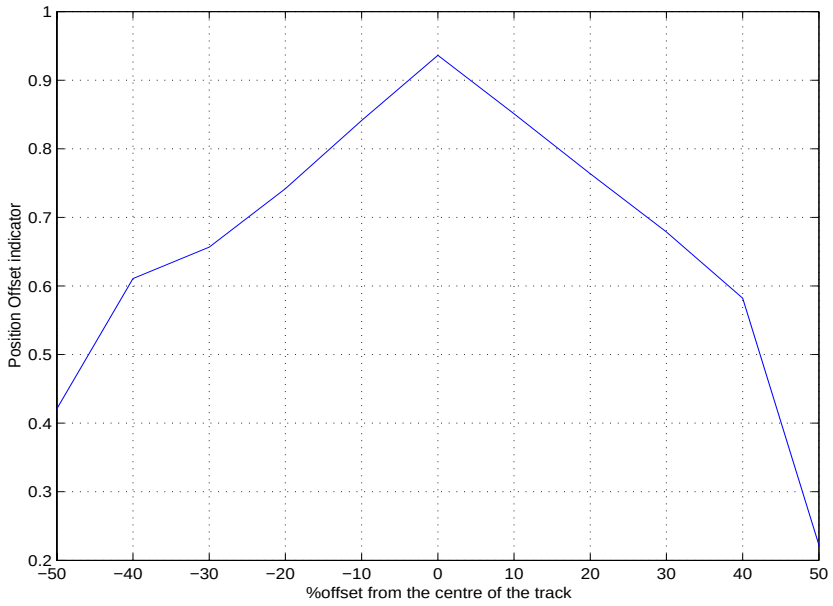


Figure 5.9: PES detection from simulated random user data.

setup with spindle speed at 5400 RPM. The write element is of 0.42 $\mu$m wide and the width of the read element is 0.25 $\mu$m. The raw readback signal is collected off-line using the Lecroy digital oscilloscope from -50 % to +50 % of the track at an interval of 10 % which is about 40 nm. These recorded data are computed off-line using (5.2) - (5.8) under MATLAB and the resultant data PES is as shown in Figure 5.10. From Figure 5.10, we can see that the gradient of the smoothed PES with respect to the position from track center exhibits a linear relationship when the transducer deviates from the track center. This observation is due to the overlap of the signals of adjacent tracks and the decreasing signal strength of the user data in the track at that particular frequency. However, the linearity of the gradient of the user data PES diminishes progressively towards the track center, which is due to the difference in the reader/writer track widths. The width of

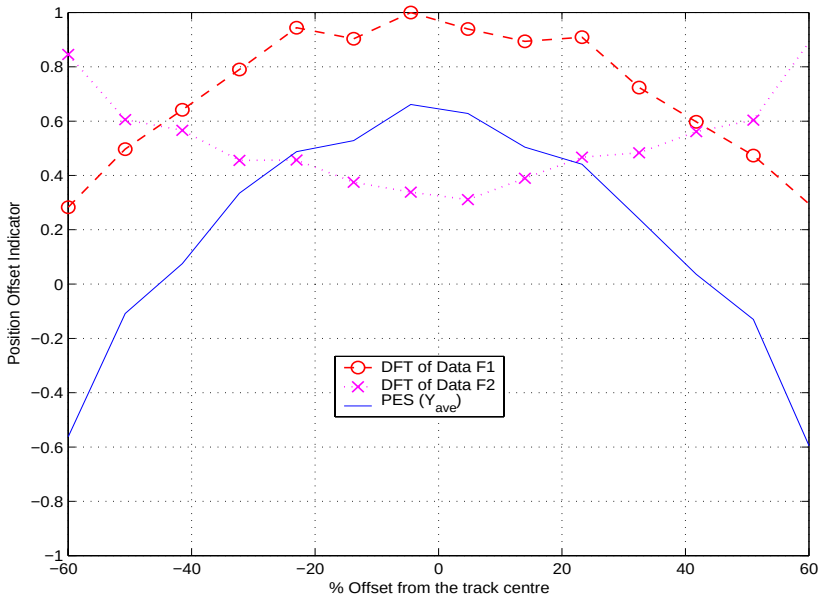


Figure 5.10: PES detection from experimental random user data.

write head element is normally wider than the width of the read head element in current hard disk drive technology. This leads to saturation over the peak of the data PES around the center of the track when the read head element retrieves information written by a wider write head. This saturation gives rise to difficulty in determining the direction of displacement between the read/write head and the track center of the medium.

However, this can be resolved by encoding different frequencies or phase shifts for adjacent tracks as can be seen from Figure 5.6. Conversely, for a given track width, the proposed scheme provides better PES linearity with a relatively wider reader and thus results in better servo to position the head.

The method provides a direct measurement of the head position with respect

to the track and ease of displacement direction determination by relying on different frequency components from the readback signal.

Although the preliminary aim of the frequency-based user data coding scheme is to enable the extraction of servo information from the user data and improve performance of servo control, this scheme may also allow the read channel to have more freedom in optimization. Supposing that the two neighboring tracks have the same frequency, when off-track head reads a neighboring track, the interference would be random noise. In the case for a neighboring track of different frequency, the interference becomes a colored noise which can be filtered easily. Thus it also enables better decoding performance in the read channel.

Although the servo bandwidth can be increased with a higher PES sampling rate, the disturbance beyond the bandwidth could be amplified by the sensitivity hump due to Bode's Integral Theorem (BIT) [4]. To minimize TMR, the height of sensitivity peak should be as low as possible. In [50], it has shown that the sensitivity limitation from BIT is related to the relative degree of the PZT actuator model. A proper PZT actuator control design may suppress the sensitivity hump approaching to 0 dB. Henceforth, no trade-off of positioning accuracy between the extension of bandwidth and the amplification of disturbance may be needed.

The use of different frequencies in adjacent tracks amounts to changing the recording density in each track. It may make the system more complicated and does not make full use of the bit storage capacity. However, with the reduction in the inter-track interference effects, more tracks can be packed on the same area,

thus the increase in track density can compensated for the loss in bit density.

## 5.4 Summary

A novel method to detect the position of the read head position during reading the user data sectors is presented. The idea of having frequency-encoded user data sectors and an algorithm for the extraction of the frequency components allows the direct measurement of PES within data sector, unlike the methods proposed by Despain et al [25] [22] [33], which are based on the use of extra transducers and the displacement estimation from the BER. Simulation and experimental results show that the relative head position can be obtained from the random user data. This additional position measurement retrieved from the user data sectors allows the servo controller to get updated error information and act accordingly while the read channel is decoding the user data, thus providing immediate track-following accuracy. The proposed scheme can increase the sampling of the position information, which allows the design of servo controller with an increase in the servo bandwidth and positioning accuracy, especially for dual-stage servo system.

# Chapter 6

# Conclusion and Future Work

The demands for larger capacity and faster access speed have increased in magnetic hard disk drives. Aggressive growth in areal densities in magnetic disk storage requires increasing accuracy in the tracking control system. To provide fast movement and precise positioning, various attempts to improve the servo control of the hard disk drive have been done. This thesis investigates and develops digital PES demodulation methods for frequency-encoded servo pattern to reduce the position sensing noise for ultra-high track density recording system. Several observations from the simulation and experimental results are made. The following summarizes the contributions made in this research.

1. Detailed background knowledge of PES generation methods, especially on the conventional amplitude servo pattern are presented. Digital servo demodulation techniques on frequency-encoded servo pattern have been studied.

We show that the frequency-encoded servo pattern will result in reduced servo overhead, ease of determining off-track direction and minimized track interferences. The PES generated using CD method of single harmonics has poorer performance in terms of linearity. In terms of SNR, it is followed by area demodulation together with FIR filters and the Fourier transform methods.

In terms of code efficiency, the discrete Fourier transform algorithm is more computational intensive as compared to FFT algorithm. A computationally less intensive and simplified DFT approach using the fundamental frequencies of the servo patterns is proposed. The method has almost the same performance as the FFT algorithm with windowing. In addition, this approach requires less data points for computation, thus reducing the amount of processing time.

2. Experimental data is used to verify the simulation results and performances of different detection methods. Frequency-encoded servo pattern can be easily created on the disk surface and a high track density of 100 kTPI (track width $= 0.254$ $\mu$m) has been written. The experimental results showed similar PES as compared to the simulations. DFT method is found to be less susceptible to noise and synchronization error has less effect as compared to the CD method.

3. A simple reader servo control system is implemented on a commercial spin stand using an external PC as the digital PES generation and servo control system. A modified PZT head cartridge base is used as the positioning actuator. The PC-based servo system performed a simplified DFT-based PES detection algorithm on the sampled data to generate PES for real-time servo control. A maximum PES sampling rate of 12 kHz can be attained. At a spindle speed of 4000 RPM and 125 servo sectors resulting in 8.3 kHz closed-loop frequency, a high closed-loop servo bandwidth of 300 Hz has been attained with a simple PID controller. In addition, a reduction of low frequency disturbances by 18.7% have been achieved as compared to without servo control on the spin stand.

4. In addition, digital servo demodulation methodology based on frequency detection of the frequency-encoded user data is presented. Simulation results verified the possibility of embedded frequency-encoded user data scheme, which allows the minimization of inter-track interferences as well as retrieving additional position information within the user data sectors.

In view of the results obtained, the following directions are emphasized for future research :

1. Frequency-based servo encoding and digital decoding schemes have been studied in this thesis. The coherent demodulation method in this thesis used only the fundamental harmonic of the burst signal which uses either the sine or cosine as the mixing signal. If synchronization can be done, other cases such as using the first, third and fifth harmonics of the burst can be applied for demodulation of the multiple frequency servo encoding pattern. Another method would be to use all the harmonics in the nominal burst for comparison.

2. Due to the limited 8-bit digitization level, quantization has a large impact on the resultant PES since the smallest change in the servo signal corresponds to the sensitivity of the head's displacement with respect to the track center. In this thesis, only the FSR is set to minimize the quantization error. To further overcome the effect of quantization noise, a technique which involves over-sampling, followed by a lowpass filter and sub-sampling [46] can be applied.

3. The technique of retrieving PES within the user data sector based on the detected frequency components allows the increase of PES sampling rate. Currently, only preliminary results of dual-frequency user data are obtained. More research and efforts are needed for the methodology to become implementable in feedback control of different reader/writer and actuator combinations. In addition to reading PES within user data sector, other detection

methods which provide higher SNR for detection of PES during the writing process, as opposed to the reading process, need to be investigated.

4. Patterned media has been regarded as the next direction to increase areal density [38] [66]. By patterned media technology, servo patterns such as null and phase patterns can be created easily and with the advantage of no edge erase band noise, better performance of position detection can be achieved [39]. Thus significant research efforts can be focused on servo patterning methodology to increase the accuracy of servo writing and search for a low-cost pattern generation technology.

5. Future research can also be in the area of servo pattern and demodulation for perpendicular recording in which the bits are stored by arranging magnets vertically, with opposite poles facing each other and is thermally more stable at high storage densities [16].

# Bibliography

[1] A. A. Abidi, "Integrated circuits in magnetic disk drives," *Proc. of* $20^{th}$ *European Solid-State Circuits Conf.*, pp. 48-57, Sep. 1994.

[2] D. Abramovitch, "Customizable coherent servo demodulation for disk drives," *IEEE/ASME Trans. Mechatronics*, Vol. 3, No. 3, pp. 184-193, Sep. 1998.

[3] D. Abramovitch and G. Franklin, "A brief history of disk drive control," *IEEE Control Systems Magazine*, Vol. 22, No. 3, pp.28-42, Jun. 2002

[4] D. Abramovitch, T. Hurst, and D. Henze, "The PES Pareto method: Undercovering the strata of position error signals in disk drives," *Proc. American Control Conf.*, Vol. 5, pp. 2888-2895, Jun. 1997.

[5] D. Abramovitch, T. Hurst, and D. Henze, "Measurements for the PES pareto method of identifying contributors to disk drive servo system errors," *Proc. American Control Conf.*, Vol. 5, pp. 2896-2900, Jun. 1997.

[6] D. Abramovitch, T. Hurst, and D. Henze, "Decomposition of baseline noise sources in hard disk position error signals using the PES Pareto method," *Proc. American Control Conf.*, Vol. 5, pp.2901-2905, Jun. 1997.

[7] D. Abramovitch, T. Hurst, and D. Henze, "An overview of the PES Pareto method for decomposing baseline noise sources in hard disk position error signals," *IEEE Trans. Magn.*, Vol. 34, No. 1, pp.17-23, Jan. 1998.

[8] Acqiris Company Website [Online], Products Information, *http://www.acqiris.com/*.

[9] K. Aikawa, "Method for digitally demodulating position signals recorded on recording media," U.S. Patent 6,122,117, 2000.

[10] A. Al-Mamun, T.H. Lee, and G.H Tay, "Efficient position encoding in hard disk drive using dual frequency servo bursts," *Proc. 27th IECON Conf.* Vol. 1, pp. 609 - 614, Nov. 2001.

[11] H.S. Ang, *Advanced burst patterns for servo encoding in high track density hard disk drive*, B.Eng. Thesis, National University of Singapore, Department of Electrical and Computer Engineering, Jun. 2002.

[12] K. Aruga, "3.5-inch high-performance disk drives for enterprise applications: AL-7 series," *Fujitsu Sci. Tech. Journal*, Vol. 37, No. 2, pp. 126-139, Dec. 2001.

[13] R.C. Barrett, E.H. Klaassen, and T.R. Albrecht, "Timing-based track following servo for linear tape systems," *IEEE Trans. Magn.*, Vol. 34, No. 4, pp. 1872-1877, Jul. 1998.

[14] K.A. Belser and W.L. Cheung "Two-frequency servo PES pattern," U.S. Patent 5,966,264, 1999.

[15] H.N. Bertram, *Theory of magnetic recording*, Cambridge, New York, Cambridge University Press, 1994.

[16] H.N. Bertram and M. Williams, "SNR and density limit estimates: A comparison of longitudinal and perpendicular recording," *IEEE Trans. Magn.*, Vol. 36, No. 1, pp. 4-9, Jan. 2000.

[17] W.G. Bliss, L. Du, and M. Karasanbhai, "Digital servo demodulation in a digital read channel," *IEEE Trans. Magn.*, Vol. 34, No. 1, pp. 13-16, Jan. 1998.

[18] W.L. Cheung, "Digital demodulation of a complementary two frequency servo PES pattern," U.S. Patent 6,025,970, 2000.

[19] K.K. Chew, "Control systems challenges to high track density magnetic disk storage," *IEEE Trans. Magn.*, Vol. 32, No. 3, pp. 1799-1804, Jan. 1996.

[20] J.W. Cooley and J.W. Tukey, "An algorithm for the machine computation of the complex Fourier series," *Mathematics of Computation*, Vol. 19, pp. 297-301, Apr. 1965.

[21] E. Cooper and R. Hampshire, "Adaptive compensation for position error signal nonlinearity," *IEEE Trans. Magn.*, Vol. 38, No. 3, pp. 1593-1602, May 2002.

[22] A.M. Despain and R.S. Gaines, "Apparatus for developing a dynamic servo signal from data in a magnetic disc drive and method," Patent WO/0028540, 2000.

[23] G.F. Franklin, J.D. Powell, and M. Workman, *Digital control of dynamic systems*, Addison Weasley, $3^{rd}$ edition, 1997.

[24] M. Frigo and S.G. Johnson, "FFTW: an adaptive software architecture for the FFT," *Proc. Int. Conf. Acoustics, Speech, and Signal Processing*, Vol. 3, pp. 1381-1384, May 1998.

[25] R.S. Gaines and A.M. Despain, "Data storage system using synchronization signals incorporating servo information," Patent WO/0145092, 2001.

[26] A. Ganapathiraju, M. Balducci, A. Choudary, J. Hamaker, J. Picone, and A. Skjellum, "Benchmarking of serial and parallel FFT algorithms," *Proc. IEEE Southeastcon*, pp. 328-330, Blacksburg, VA, Apr. 1997

[27] G. Guo, T. Huang, K.M. Tay, S. Weerasooriya, and A. Al-Mamun, "A DSP based hard disk servo test stand," *IEEE Trans. Magn.*, Vol. 34, No. 2, pp. 480-483, Mar. 1998.

[28] G. Guo, Q. Hao, and T.S. Low, "Dual-stage control design for high track per inch hard disk drives," *IEEE Trans. Magn.*, Vol. 37, No.2,p.860-865, Mar. 2001.

[29] Guzik Company Website [Online], Spin Stand Products Information, *http://www.guzik.com.*

[30] L.N. He, Z.G Wang, B. Liu, D.J. Mapps, P. Robinson, W.W. Clegg, D.T. Wilton, and Y. Nakamura, "Estimation of track misregistration by using dual-

stripe magnetoresistive head," *IEEE Trans. Magn.*, Vol. 34, No. 4, pp. 2348-2355, Jul. 1998.

[31] L.N He, N. Honda, and K. Ouchi, "A novel data servo method," *IEEE Trans. Magn.*, Vol. 32, No. 5, pp. 3896-3898, Sep. 1996.

[32] IBM Corporation Website [Online], Limits of magnetic recording, *http://www.almaden.ibm.com/st/projects/limits*, May 2002.

[33] P.A Ioannou, "Servo control apparatus and method using absolute value input signals," Patent WO 01/35176, ACORN Technologies Inc., 2001.

[34] R.G. Jacquot, *Modern digital control systems*, Marcel Dekker, Inc, $2^{nd}$ edition, 1995.

[35] D. Janz, "Tri-phase servo pattern for providing position information in a magentic disk drive." U.S. Patent 5,095,393, 1992.

[36] Z. Jin and H.N. Bertram, "Simulation of the effect of medium noise on servo PES detection in longitudinal recording," *IEEE Trans. Magn.*, Vol. 36, No. 6, pp. 4011-4018, Nov. 2000.

[37] M. Kryder, "Achieving 100 Gb/sq. in.: Barriers and opportunities," *Presentation at Toyota Technical Institute*, Japan, Mar 1998.

[38] X. Lin, J.G. Zhu, and W. Messner, "Spin stand study on density dependence of switching properties in patterned media," *IEEE Trans. Magn.*, Vol. 36, No. 5, pp. 2999-3001, Sep. 2000.

[39] X. Lin, J. G. Zhu, and W. Messner, "Investigation of advanced position error signal patterns in patterned media," *Journal of Applied Physics*, Vol. 87, No. 9, pp. 5117-5119, May 2000.

[40] R.G. Lyons, *Understanding digital signal processing* Addison Wesley, $1^{st}$ edition, 1996.

[41] K.K.A. Makinwa, J.W.M. Bergmans, and J.O. Voorman, "Analysis of a biphase-based servo format for hard-disk drives," *IEEE Trans. Magn.*, Vol. 36, No. 6, pp. 4019-4027, Nov. 2000.

[42] R. Moistad, D. Langiois, and D. Johnson, "Linear tape servo writing enables increased track density," *http://www.tapecouncil.org/increasingTrack.pdf.*

[43] C. Marven and G. Ewers, *A simple approach to digital signal processing*, Wiley-Interscience, $1^{st}$ edition, 1996.

[44] C. Mee and E. Daniel, *Magnetic storage handbook*, McGraw-Hill, New York, $2^{nd}$ edition, 1996.

[45] Y. Miura, "Information storage for the broadband network era - Fujitsu's challenge in hard disk drive technology," *Fujitsu Sci. Tech. J.*, Vol. 37, No. 2, pp. 111-125, Dec. 2001.

[46] D. Morgan, *Numerical methods for DSP systems in C*, John Wiley and Sons, Inc., New York, $1^{st}$ edition, 1997.

[47] H. Nakanishi and M. Mizukami, "High track density head positioning using sector servos," *IEEE Trans. Magn.*, Vol. 19, No. 5, pp. 1698-1700, Sep. 1983.

[48] National Instrument Company Website [Online], NI DAQ Products Information, *http://www.ni.com/*.

[49] F. Nekoogar and G. Moriarty, *Digital control using digital signal processing*, Prentice Hall PTR, $1^{st}$ edition, 1999.

[50] C. K. Pang, *Vibration analysis and control in hard disk drive servo systems*, M.Eng. Thesis, National University of Singapore, Department of Electrical and Computer Engineering, 2003.

[51] A. Patapoutian, "Optimal burst frequency derivation for head positioning," *IEEE Trans. Magn.*, Vol. 32, No. 5, pp. 3899-3901, Sep. 1996.

[52] A. Patapoutian, "Signal space analysis of head positioning formats," *IEEE Trans. Magn.*, Vol. 33, No. 3, pp.2412-2418, May 1997.

[53] A. Patapoutian, "Analog-to-digital convertor algorithms for position error signal estimators," *IEEE Trans. Magn.*, Vol. 36, No. 1, pp. 395-400, Jan. 2000.

[54] Physik Instrumente (PI) Company Website [Online], Piezo Products Information, *http://www.physikinstrumente.com/*.

[55] Polytec Company Website [Online], Laser Dopple Vibrometer Products Information, *http://www.polytec.de/polytec-com/de/index.html*.

[56] D.E. Reed, W.G. Bliss, and R.T. Behems, "Detecting servo data and servo bursts from discrete time samples of an analog read signal in a sampled amplitude read channel," U.S. Patent 6,144,513, Nov. 2000.

[57] A.H. Sacks, *Position signal generation in magnetic disk drives*, Ph.D. Thesis, Carnegie Mellon University, DSSC, Department of Electrical and Computer Engineering, Sep. 1995.

[58] A.H. Sacks, M. Bodson, and W. Messner, "Advanced methods for repeatable runout compensation (disk drives)," *IEEE Trans. Magn.*, Vol. 31 No. 2, pp. 1031-1036, Jun. 1994.

[59] L.J. Serrano, "Multiple servo track types using multiple frequency servo patterns," U.S. Patent 6,034,835, 2000.

[60] K. Stoev, F. Liu, Y. Chen, X. Dang, P. Luo, J. Chen, J. Wang, K. Kung, M. Lederman, M. Re, G. Choe, J. N. Zhou, and M. Yu, "Demonstration and characterization of 130 Gb/in2 magnetic recording systems," *Journal of Applied Physics*, Vol. 93, No. 10, pp. 6552-6554, May. 2003.

[61] Y. Uematsu and M. Fukushi, "Servo track writing technology," *Fujitsu Sci. Tech. J.*, Vol. 37, No. 2, pp. 220-226, Dec. 2001.

[62] A.M. Taratorin, *Characterization of magnetic recording systems: A practical approach*, Guzik Technical Enterprises, $1^{st}$ edition, 2000.

[63] G.H. Tay, *Dual frequency servo burst for encoding position information in hard disk drives*, B.Eng. Thesis, National University of Singapore, Department of Electrical and Computer Engineering, Jun. 2001.

[64] A. Tewari, *Modern control design with MATLAB and Simulink*, John Wiley & Sons, Ltd, $1^{st}$ edition, 2002.

[65] F. Tomiyama, H. Ide, T. Hamaguchi, H. Takano, T. Yamaguchi, and N. Kodama, "Optimal track-width design of AMR/GMR Heads for high-track-density disk drives," *IEEE Trans. Magn.*, Vol. 34, No. 4, pp. 1970-1972, Jul. 1998.

[66] S.X. Wang and A.M. Taratorin, *Magnetic information storage technology* Academic Press, $1^{st}$ edition, 1999.

[67] M.T. White and W. Lu, "Hard disk drive bandwidth limitations due to sampling frequency and computational delay," *Proc. IEEE/ASME International Conference*, pp. 120-125, Sep. 1999.

[68] S. Weerasooriya, T.S. Low, and J.L. Zhang, "Efficient implementation of adaptive feedforward runout cancellation in a harddisk drive," *IEEE Trans. Magn.*, Vol. 32, No. 5, pp. 3920-3922, Sep. 1996.

[69] W.E. Wong, *Digital detection of position error signal in hard disk drive*, B.Eng. Thesis, National University of Singapore, Department of Electrical and Computer Engineering, Jun. 2001.

[70] T. Yamaguchi, K. Usui, and H. Hirai, "Modeling and TMR (track misregistration) budget design for head-positioning of high track-density disk drives," *IEEE Trans. Magn.*, Vol. 35, No. 2, pp. 892-897, Mar. 1999.

[71] T.H. Yip, M.A. Suriadi, E.H Ong, and G. Guo, "Numerical simulation of air flow in a near-HDD configuration," *Proc. Asia Pacific Magnetic Recording Conference*, pp. TU-P-01, Aug. 2002.

[72] Z. Zhang, Y.C. Feng; T. Clinton, G. Badran, N.H. Yeh, E. Girt, S. Harkness, M. Munteanu, H.J. Richter, R. Ranjan, S. Hwang, G.C. Rauch, M. Ghaly, D. Larson, E. Singleton, V. Vas'ko, J. Ho, F. Stageberg, V. Kong, K. Duxstad, and S. Slade, "Magnetic recording demonstration over 100 Gb/in$^2$," *IEEE Trans. Magn.*, Vol. 38, No. 5, pp. 1861-1866, Sep. 2002.

# Curriculum Vitae

**Wai Ee Wong** was born in Singapore. She received the B.Eng. (Hons) degree in Electrical and Computer Engineering from National University of Singapore (NUS) in 2001. From 2001 to 2003, she was a Research Scholar in A*STAR, Data Storage Institute (DSI), pursuing the Master of Engineering Degree by research in NUS. Currently, she is working for A*STAR, Data Storage Institute, Singapore, as a Research Engineer. Her research interests include PES generation methods in data storage channels, servo track writing and patterning for future storage devices.

Her research works related to this dissertation resulted in the following publications:

1. W.E. Wong, G. Guo, A. Al-Mamun, W. Ye, and J. Zhang, "A position encoding and decoding scheme for ultra high density magnetic recording," *Proc. of Asia Pacific Magnetic Recording Conference*, pp. WE-P-08, Aug. 2002.

2. W.E. Wong, L. Feng, G. Guo, W. Ye, and A. Al-Mamun, "Implementation of a servo positioning system on spin stand," *Proc of 29th Annual Conf. of the IEEE Industrial Electronics Society, IECON*, pp. 2114-2119, Nov 2-6 2003.

3. W.E. Wong, G. Guo, W. Ye, A. Al-Mamun, and J. Zhang, "Detection of track misregistration within user data channel," (Chapter 5 of the thesis), Singapore Patent Application No.: 200304108-4, Jul. 2003.

4. J. Liu, W.E. Wong, L. Feng, and G. Guo, "Implementation of a high performance multirate control system using PC," *Proc. of IEEE Int. Conf. on Power Electronics and Drive Systems, PEDS,* pp. 636-641, Nov. 2003.

5. Z. He, G. Guo, L. Feng, and W.E. Wong, "Design of a head carrying cartridge with micro actuation for high density magnetic recording," *Proc. of 2nd Int. Conf. on Computational Intelligence, Robotics and Autonomous Systems, CIRAS*, Dec. 2003.

6. A. Al-Mamun, T.H. Lee, G. Guo, W.E. Wong, and W. Ye, "Measurement of position offset in hard disk drive using dual frequency servo bursts," *IEEE Trans. Instrumentation and Measurement*, Vol. 52, No. 6, pp 1870 - 1880, Dec 2003.

7. W.E. Wong, G. Guo, A. Al-Mamun, W. Ye, and J. Zhang, "PES Generation using User Data Channel for Embedded Servo System," *submitted to the IEEE/ASME Trans. on Mechatronics*, Dec. 2003.